University of Southampton

Faculty of Environmental and Life Sciences

Ocean and Earth Science

Carbon – Trace Metal Interactions in the Oceanic Twilight Zone

by

Joanna Jane Ainsworth

Thesis for the degree of Doctor of Philosophy

May 2022

University of Southampton

Abstract

Faculty of Environmental and Life Sciences

Ocean and Earth Science

Doctor of Philosophy

Carbon – Trace Metal Interactions in the Oceanic Twilight Zone

by

Joanna Jane Ainsworth

Marine microbes are an important control on carbon (C) sequestration depth and biogeochemical cycling of nutrients and trace metals in the global ocean. The biological carbon pump (BCP) is the set of processes by which inorganic carbon (CO_2) (along with nutrients and trace metals) is fixed into organic matter via photosynthesis by autotrophic phytoplankton and the C, nutrients and trace metals sequestered away from the atmosphere generally by transport into the deep ocean. Most (~80 %) of the organic C produced by autotrophic phytoplankton is remineralised (returned to the dissolved inorganic inventory from the particulate organic form) in the surface ocean and the inorganic CO_2 is available for release back into the atmosphere. The depth at which remineralisation occurs is important, as the deeper the remineralisation depth of the C the increased likelihood of long term storage in the deep water and sediment. The sequestration of C is primarily dependent on flux attenuation and remineralisation of organic matter in the mesopelagic or 'twilight' zone (100-1000 m), where much of the downward particle flux is attenuated via zooplankton and bacterial respiration, replenishing dissolved nutrients and trace metals back into the water column. Understanding the controls on the BCP in the twilight zone is important to understand the transfer efficiency of C sequestration and the regulation of atmospheric CO_2.

Oceanic regions such as the Southern Ocean have inefficient BCPs as the phytoplankton are unable to fully utilise available nutrients, restricting their growth and drawdown of C due to limited access to micronutrients such as iron (Fe). Iron is a scare resource in these regions and low concentrations of bioavailable Fe exert significant controls on global phytoplankton productivity, species composition and therefore ecosystem structure and the C cycle. Iron is not only an important micronutrient for phytoplankton growth but also for heterotrophic bacteria, limiting bacterial secondary production and abundance.

Two focused and inter-related processes which influence Fe cycling and consequently C cycling in the mesopelagic were investigated. Firstly, differentiating the biotic and abiotic factors on Fe cycling in the twilight zone and the (de-) coupling of Fe and macronutrients at depth. Secondly, to investigate Fe and C (co-) limitation of mesopelagic bacteria.

This researched performed shipboard experiments and subsequent laboratory work to evaluate the relative remineralisation rates of C, Fe and silica (Si) from live and detrital phytoplankton cells resuspended in upper mesopelagic waters. Iron consistently transferred from the particulate fraction into the dissolved fraction from both live and detrital cells, this transfer was dominated by the abiotic movement of extracellular adsorbed particulate iron into the dissolved fraction (de-

absorption). The live phytoplankton cells remained viable throughout the incubations and continued to respire C whilst the detrital cells potentially leaked dissolved organic C which was subsequently taken up and respired by bacteria with minimal secondary bacterial production. Limited dissolution of Si occurred from the live viable cells with the detrital cells showing more Si dissolution potential. The remineralisation length scales of Fe, C and Si were thus decoupled in the upper mesopelagic as Fe resulted in the shortest remineralisation length scale due the abiotic transfer of extracellular Fe into the dissolved pool, which could resupply biota potentially alleviating Fe limitation. Intracellular pools of Fe (along with C and Si) would be exported to deeper depths with a slow remineralisation rate if processes such as grazing or cell lysis do not act to break cells up and speed up remineralisation processes.

Heterotrophic bacterial production was Fe and C (co-) limited in the mesopelagic above the ferricline. An increase in cell abundance of very large high nucleic bacteria when combined Fe and C were added to mesopelagic waters from 150 and 500 m supported a large (1-2 order of magnitude) increase in bacterial production indicating the (co-) limitation of a sub-population of the free-living bacteria at depth. The controls on ferricline depth and mesopelagic standing stocks of Fe (from winter mixing, scavenging, Fe associated with sinking material and the de-absorption of Fe into the water column) will be important in determining the extent of ocean Fe C (co-) limitation of mesopelagic bacterial growth and production and will be a driver in bacterial community composition at depth. Nutrient limitation in the mesopelagic bacteria has potentially important consequences if it also reduces the overall rate of remineralisation and thus both generates a potential reinforcing feedback on the maintenance of a deep ferricline and increases the remineralisation depth and hence long-term storage of carbon in the ocean.

Table of Contents

Table of Tables

Table of Figures

Table of Figures

Research Thesis: Declaration of Authorship

Print name: Joanna Jane Ainsworth

Title of thesis: Carbon – Trace Metal Interactions in the Oceanic Twilight Zone

I declare that this thesis and the work presented in it are my own and has been generated by me as the result of my own original research.

I confirm that:

1. This work was done wholly or mainly while in candidature for a research degree at this University;
2. Where any part of this thesis has previously been submitted for a degree or any other qualification at this University or any other institution, this has been clearly stated;
3. Where I have consulted the published work of others, this is always clearly attributed;
4. Where I have quoted from the work of others, the source is always given. With the exception of such quotations, this thesis is entirely my own work;
5. I have acknowledged all main sources of help;
6. Where the thesis is based on work done by myself jointly with others, I have made clear exactly what was done by others and what I have contributed myself;
7. None of this work has been published before submission

Signature: ..... Date: 18th May 2022

Acknowledgements

I have many people to thank for their help and support over the last 4 years in the research for and production of this thesis. Special mention must go to my supervisors Mark Moore and Alex Poulton for their guidance and teaching, especially on the cruises as for the first expedition I was a complete newbie to working in labs, let alone on the Southern Ocean and with radio-isotopes! Marks constant support and depth and breadth of knowledge has been inspiring and helped keep this research focused.

I have been lucky enough to go on 3 research cruises and a huge thanks must go to every single person who helped make each one such a success. Interacting with so many different people with interests and specialisms in different areas has helped put my research in context and their help on board was invaluable. They also took my Euphonium practice with good humour!

Special mention is needed for those who collected and analysed contextual data alongside my research. Mark Stinchcombe and Katsia Pabortsava for providing the inorganic nutrients. Mark Stinchcombe and Helge Winklebauer for help in collecting Fe samples on DY086 and DY090, Antony Birchill for collecting and analysing DY111 dFe samples. Alastair Lough, Maeve Lohan and Koko Kunde for helping me analyse my DY086 trace metal samples. Neil Wyatt, Mark Moore and Hannah East for analysing the DY086 and DY111 POC data. Rachel Rayne, Millie Goddard-Dwyer and Claire Evans for showing me the flow cytometer ropes.

Some of the figures have been produced by people with greater plotting skills than me. Thanks to Nathan Briggs and Filipa Carvalho for collecting, calibrating and processing the COMICS I *in-situ* chlorophyll-*a* time series (Figure 4) (funded through a European Research Council Consolidator grant (GOCART, agreement 724416, PI: Stephanie Henson), Elisa Lovecchio for providing the Benguela currents Figure 5a, Mark Moore for all the chlorophyll-*a* climatology figures and Adrian Martin for the contextual water mass Figure 6a and c.

Outside of the oceanography world I must thank two very important people. My sister, Kate, who has been my inspiration to study the natural world and who continually astounds me with her knowledge and enthusiasm. And my husband, Paul, who has encouraged and supported me every step of the way to follow my dream and importantly who looked after our cats while I was away!

This work was supported by the Natural Environment Research Council grant for the COMICS project. Grant codes: NE/M020835/1, NE/M020835/2 (AJP), NE/M02072X/1 (CMM), Studentship (1942696).

Definitions and Abbreviations

AABW ..... Antarctic Bottom Water

AAIW ..... Antarctic Intermediate Water

Abiotic ..... A non living factor in an ecosystem

AOU ..... Apparent Oxygen Utilisation

BCP ..... Biological Carbon Pump

BGE ..... Bacterial Growth Efficiency

Biotic ..... An ecosystem factor produced by the action of living organisms

BN ..... Benguela North, site designator for the DY090 COMICS cruise

BP ..... Bacterial Production (production of new bacterial biomass)

BR ..... Bacterial Respiration

BS ..... Benguela South, site designator for the DY090 COMICS cruise

$bSiO_2$ ..... Biogenic Silica

C ..... Carbon

$CaCo_3$ ..... Calcium Carbonate

Cd ..... Cadmium

CDW ..... Circumpolar Deep Water

Chl-a ..... Chlorophyll-*a*

Co ..... Cobalt

Colloidal Fe ..... Iron particles of the size fraction 0.02 to 0.2 µm - equal to the difference between dissolved Fe and soluble Fe

COMICS ..... Controls over Ocean Mesopelagic Interior Carbon Storage, the cruise designated DY086 and DY090

Corg ..... Organic Carbon

CO_2 ..... Carbon Dioxide

CTD ..... Conductivity, Temperature and Depth

Cu ..... Copper

CUSTARD..... Carbon Uptake and Seasonal Traits in Antarctic Remineralisation Depth, the cruise designated DY111

Diazotrophs..... A microorganism that can fix molecular nitrogen (N_2)

DIC..... Dissolved Inorganic Carbon

Dissolved iron (dFe) ..... Inorganic iron particles in the water column of the size fraction <0.2 µm.

DNA..... Deoxyribonucleic Acid, organic chemical of complex molecular structure that is found in all prokaryotic and eukaryotic cells and in many viruses. DNA codes genetic information for the transmission of inherited traits.

DOM..... Dissolved Organic Matter

DPM ..... Disintegration Per Minute; the output count of the scintillation counter that detects the presence of each isotope decay.

dTM..... Dissolved Trace Metal

DVM ..... Diel Vertical Migration

Endocytosis ..... A cellular process in which substances are brought into the cell, the material to be internalized is surrounded by an area of cell membrane which then buds off inside the cell to form a vesicle containing the ingested material.

Eukaryotes ..... Organisms characterized by the presence of a nucleus, a number of chromosomes in which DNA is organized in the form of nucleoproteins, and by a number of membrane-bound organelles.

Extracellular iron..... Iron associated/bound to the surface of a particle (cell)

Fe ..... Iron

HCl..... Hydrochloric Acid

HNLC ..... High Nutrient Low Chlorophyll

HNO_3 ..... Nitric Acid

HR-ICP-MS..... High Resolution Inductively Coupled Plasma Mass Spectrometry

Intracellular iron ..... Iron retained within a cell which cannot be removed using the Ti-EDTA citrate solution.

LHNA ..... Large High Nucleic Acid

Ligand ..... A substance that forms a complex with a biomolecule to serve a biological purpose.

Limitation/co-limitation ..... The term (co-) limitation can be interpreted in many ways, but for the purposes of this study we refer to two types of resource (co-) limitation. Firstly, when two or more nutrients are present at concentrations too low to support microbial requirements and secondly, the enhanced concentrations of one limiting nutrient may facilitate the uptake of another. For this study, a population is described as nutrient limited if addition of the nutrient stimulated a positive cellular response.

LPDE ..... Low-Density Polyethylene

Mn ..... Manganese

N ..... Nitrogen

NEP ..... Net Export Production

OOI ..... Ocean Observatories Initiative and site designator for the DY111 CUSTARD cruise

P3A, P3B, P3C ..... Site occupation designators for the South Georgia COMICS DY086 cruise

P ..... Phosphorus

Particle associated (PA) Fe ... Iron associated intra and extracellular with particles

PF ..... Polar Front

PFA ..... Paraformaldehyde

PFe ..... Particulate iron of the size fraction > 0.2 µm

POC ..... Particulate Organic Carbon

POM ..... Particulate Organic Matter

PON ..... Particulate Organic Nitrogen

POP ..... Particulate Organic Phosphorus

PTFE ..... Polytetrafluoroethylene

Prokaryotes ..... A type of cell that does not have a true nucleus or membrane-bound organelles, bacteria are prokaryotes.

Remineralisation..... The breakdown of organic matter (particles from a biological source) into its simplest inorganic forms (dissolved phase).

RLS ..... The remineralisation length scale (the vertical distance over which organic particle flux declines by 63%, affected by particle respiration, fragmentation and sinking rates, (Boyd and Trull, 2007; Cavan et al., 2017b))

RRS ..... Royal Research Ship

SAF ..... Sub Antarctic Front

SAMW ..... Sub-Antarctic Mode Water

Seawater (SW) associated Fe Iron not associated with the particles so are within the seawater (dissolved + wall washed cells)

SG..... South Georgia

Si ..... Silica

Siderophores..... The largest class of known compounds that can bind and transport Fe.

SLNA..... Small Low Nucleic Acid

Soluble Fe ..... Iron of the size fraction <0.02 µm

SSC ..... Side Scatter

SS ..... Stainless Steel

TDTM ..... Total Dissolvable Trace Metals

TEP ..... Transparent Exopolymer Particles

Ti-EDTA ..... Titanium – Ethylenediaminetetra acetic acid; the wash used to bind Fe to allow determination of intra-cellular iron

TM..... Trace Metal

TN..... Transect North, site designator for the DY111 CUSTARD cruise

TS ..... Transect South, site designator for the DY111 CUSTARD cruise

vLHNA ..... very Large High Nucleic Acid

Zn ..... Zinc

Chapter 1 Introduction

1.1 The carbon cycle

The carbon (C) cycle is a key determinant of planetary climate. Ninety-two percent of the C on our planet that is not locked up in geological reservoirs (such as rocks, coal, oil and gas) resides in the ocean (Sarmiento and Gruber, 2002). The majority of this C is stored in the ocean through a series of physical and chemical processes which have been collectively termed 'carbon pumps' (Volk and Hoffert, 1985), which have played a key role in the natural C cycle over a range of geological timescales, significantly influencing atmospheric C variability (Sundquist and Visser, 2003). Moreover, human activities have the potential to directly and indirectly influence the oceanic C cycle. The Intergovernmental Panel on Climate Change (IPCC) report (2021) states that it is unequivocal that the growth in CO_2 in the atmosphere since 1750 is due to the direct emissions from human activities. During the last decade (2010–2019), average annual anthropogenic CO_2 emissions reached the highest levels in human history at 10.9 ± 0.9 PgC yr^{-1} (IPCC report, 2021). Of these emissions, 46 % accumulated in the atmosphere (5.1 ± 0.02 PgC yr^{-1}), 31 % (3.4 ± 0.9 PgC yr^{-1}) was removed by terrestrial ecosystems and 23 % (2.5 ± 0.6 PgC yr^{-1}) was taken up by the ocean (IPCC report, 2021). The increasing concentrations of anthropogenic atmospheric CO_2 and associated impacts on our climate are a constant concern and heavily studied.

The world's oceans absorb atmospheric CO_2 through physico-chemical processes related to solubilisation (the so-called solubility pump) and biological processes starting with photosynthetic production of organic material (the so-called biological pump) (Volk and Hoffert, 1985). Passow and Carlson (2012) suggested that approximately two-thirds of the vertical gradient in C in the sea is due to the biological pump, with the remainder due to the solubility pump. The solubility pump is a physical process where gases and heat are exchanged between the surface ocean and the lower atmosphere (Volk and Hoffert, 1985). At colder temperatures more CO_2 can be solubilised, thus high latitude colder oceans adsorb more CO_2 resulting in a substantial pool of dissolved inorganic carbon (DIC) (Volk and Hoffert, 1985). The colder denser waters generated by heat and hence buoyancy loss to the atmosphere at high latitudes sink into the interior entraining the DIC into deeper waters where the colder DIC rich waters travel along the thermohaline circulation to be upwelled and returned to the surface where the water warms and the CO_2 is released back into the atmosphere (Volk and Hoffert, 1985).

The oceanic Biological Carbon Pump (BCP) starts with photosynthesis by phytoplankton converting dissolved CO_2 (DIC), nutrients and water, using energy from the sun, into particulate organic matter

and oxygen in the surface waters (Volk and Hoffert, 1985). This particulate organic matter (algal cells) comprises of particulate organic carbon (POC) and particulate forms of the nutrients such as nitrogen (PON) and phosphorus (POP) as well as particulate forms of other trace elements such as iron (Fe) (Volk and Hoffert, 1985; Longhurst and Harrison, 1989; Longhurst, 1991; Ducklow et al., 2001). Most (~80 %) of the organic C produced by phytoplankton is respired (remineralised; returned to the dissolved inorganic inventory from the particulate organic form) in the surface ocean and the inorganic CO_2 is available for release back into the atmosphere while the majority of the remaining fraction which leaves the surface is remineralised at relative shallow depths in the upper ~1000 m (Eppley and Peterson, 1979). Approximately one-sixth of the C that is fixed by phytoplankton is directly utilised by bacteria in the surface ocean (Ducklow et al., 1993; Cole et al., 1988; Boyd et al., 2019), the remaining C either enters the classic marine food web or is transported as sinking particles to the deeper ocean, generating long-term storage via the BCP (Eppley and Peterson, 1979). The depth at which remineralisation occurs is important, as the deeper the remineralisation depth of the C the increased likelihood of long-term storage in deep water and sediment rather than being released back into the atmosphere (Kwon et al., 2009). The sequestration of C appears to be primarily dependent on this flux attenuation and the remineralisation of organic matter in the mesopelagic zone (Passow and Carlson, 2012). Buesseler and Boyd (2009) succinctly note that, ‘‘the surface ocean’’ is ‘‘where the ‘strength’ of the biological pump is set’’ whereas ‘‘the subsurface ocean’’ is ‘‘where the ‘efficiency’ of the biological pump is determined.’’ Understanding the controls on the depth of C remineralisation is thus important for understanding the efficiency of the BCP and the regulation of atmospheric CO_2 (Kwon et al., 2009; Weber et al., 2016).

The ‘efficiency’ of the BCP can be considered in a number of ways, the strength or overall efficiency of the BCP is set in the surface as the proportion of inorganic macronutrient (carbon, nitrate or phosphate) which is converted to organic material while the transfer efficiency is the proportion of exported material that gets to a given depth (Buesseler and Boyd, 2009). The strength or overall efficiency of the BCP, in part, can depend on the availability of the key nutrients needed for phytoplankton cell health and growth which can limit biomass and hence drawdown of CO_2. The Redfield ratio describes the stoichiometric coefficients of the primary elements (C, nitrogen (N), phosphorus (P)) within phytoplankton, which as a first order average around $C_{106}N_{16}P_1$ (Redfield, 1934). However, the stoichiometry of organic materials is known to vary considerably between taxa and with cell physiology (Geider and Roche, 2002; Martiny et al., 2013) and is particularly variable if extended to include the micronutrients also needed by the phytoplankton for correct cell function, $(C_{106}N_{16}P_1)_{x1000}Fe_8Mn_4Zn_{0.8}Cu_{0.4}Co_{0.2}Cd_{0.2}$ (Morel et al., 2003, Moore et al., 2013), see Table 1 for the cell function of each metal and Twining and Baines, (2013) for more information.

Table 1: Common metals and their functions within marine phytoplankton, adapted from Twining and Baines, (2013).

Metal	**Functions**
Iron (Fe)	Electron transport in photosynthesis and respiration
	Electron transport in photosynthesis and N fixation
	Conversion of nitrate to ammonia
	N fixation
	Conversion of hydrogen peroxide to water
	Reduction of reactive oxygen species
Manganese (Mn)	Oxidation of water during photosynthesis
	Disproportionation of superoxide to hydrogen peroxide and O_2
	Hydrolysis of arginine to ornithine and urea
Zinc (Zn)	Hydration and dehydration of carbon dioxide
	Hydrolysis of phosphate esters
	Nucleic acid replication and transcription
	Synthesis of tRNA
	Synthesis of single-stranded DNA from RNA
	Hydrolysis of peptide bonds
	Disproportionation of superoxide to hydrogen peroxide
Copper (Cu)	Photosynthesis electron transport
	Cytochrome oxidase Mitochondrial electron transport
	Ascorbate oxidase Ascorbic acid oxidation and reduction
	Superoxide dismutase Disproportionation of superoxide to hydrogen peroxide and O_2
	High affinity transmembrane Fe transport
Cobalt (Co)	Vitamin B12 carbon and hydrogen transfer reactions
Cadmium (Cd)	Hydration and dehydration of carbon dioxide

These trace metals are required in much smaller concentrations than the macronutrients and out of these trace metals, Fe is required in the greatest abundance but is found in limiting concentrations in some oceanic regions (e.g., Martin et al., 1990). There are 2 main nutrient limitation regimes that dominate between the low latitude and high latitude oceans (Moore et al., 2013). The macronutrients of N and P are vital for phytoplankton growth and can be limiting in low and mid latitude oceans (Moore et al., 2013) where warm and sunlit surface waters are heavily stratified restricting mixing with the cold nutrient rich interior water and thus reducing nutrient supply to phytoplankton in the surface ultimately limiting their growth and production. At these latitudes, nutrient limitation can be eased by upwellings at eastern ocean margins and at the equator where the wind and Ekman transport moves the surface nutrient deficient waters aside to allow the nutrient rich deep waters to upwell (Chavez and Toggweiler, 1995). Any Fe deficit can also be alleviated through Aeolian dust supply to allow full consumption of the macronutrients after which N and P can become limiting (Sigman and Hain, 2012).

In high latitude oceans where the surface water is cold there is not the same strong density gradient allowing the vertical mixing of the deeper nutrient replete waters. There is then the potential for key micronutrients such as Fe to be limiting, restricting the drawdown of N and P and resulting in a weak or overall inefficient BCP in regions such as the Southern Ocean (Martin et al., 1990). Such regions that have excess macronutrients with low productivity are termed high nutrient low chlorophyll regions (HNLC: Chisholm and Morel, 1991). An exception is the macronutrient silicic acid, which displays a strong meridional concentration gradient across the polar frontal zone (Tréguer and van Bennekom, 1991). Silicic acid is required by diatoms for shell formation and its availability to the north of the Polar Front can be reduced to growth limiting concentrations (<2.5 μM) (Nelson and Tréguer, 1992; Brzezinski et al., 2000). Any excess nutrients from a weak inefficient BCP can then be supplied to the low latitude oceans via subduction and the thermohaline circulation. Figure 1 shows how the biogeochemical cycles of the macronutrients of N, P and the micronutrient of Fe are coupled and influence the CO_2 sequestered by the BCP (Sigman and Hain, 2012; Moore et al., 2013).

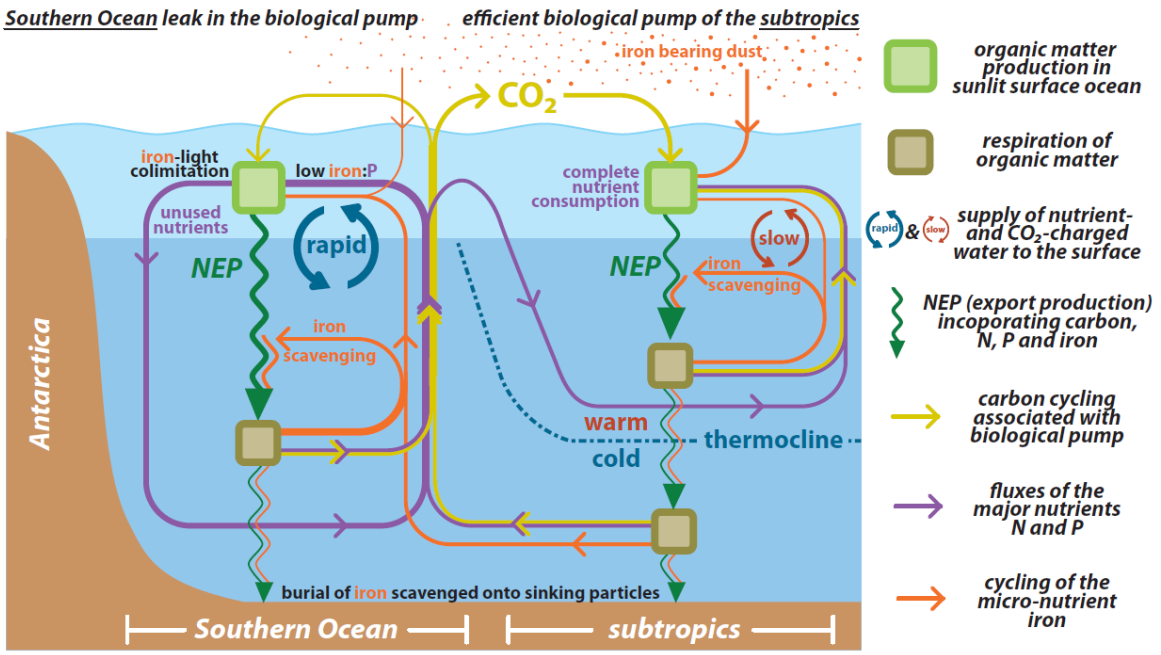

Figure 1: Coupled Fe, N and P biogeochemical cycles in high and low latitude oceans. From Sigman and Hain, (2012).

A number of hypotheses exist that investigate the controls on the transfer efficiency of the sinking C and other elements out of the surface ocean and into the deep ocean and sediments for long term storage. Remineralisation depth may be influenced by temperature which influences respiration rates (Laws et al., 2000) with colder environments having deeper remineralisation depths (Marsay et al., 2015, Weber et al., 2016). Temperature variation with global warming predictions is continuously being researched and the potential for a non-uniform microbial response to ocean warming across the globe has important implications for biogeochemical cycles and our ability to model and predict (Cavan et al., 2019a). Varying temperature sensitivity affects heterotrophic microbial respiration and hence future POC export (Cavan et al., 2019a). Dissolved oxygen also influences respiration rates (Devol and Hartnett, 2001) with reduced remineralisation at sufficiently low dissolved oxygen concentrations (2-5 µmol kg^{-1}; Cavan et al., 2017b).

A further broad topic studied is to investigate the role of ecosystem structure on remineralisation depth. Within this topic there is the ballast hypothesis that suggests that phytoplankton species (such as coccolithophores and diatoms) that produce dense biominerals (such as $CaCO_3$ and opal) increase the density and thus the rate of the sinking particles (Armstrong et al., 2002; Klaas and Archer, 2002), diatoms are ubiquitous phytoplankton and are responsible for one-fifth of the photosynthesis on Earth (Amin et al., 2012). Also the role of zooplankton grazers within the ecosystem can affect the transfer efficiency of the BCP, the grazing and fragmentation of large particles into smaller slower sinking particles reduces the depth of remineralisation reducing the

transfer efficiency (Cavan et al., 2017a). The diel vertical migration (DVM) of the zooplankton themselves can also transfer C from the surface to depth where they produce faecal pellets or themselves die and sink thus increasing the remineralisation depth and BCP transfer efficiency (Wilson et al., 2013). The depth to which the zooplankton travel could be affected by dissolved oxygen concentrations, with low concentrations being avoided by zooplankton (Bianchi et al., 2013, Cavan et al., 2017b), thus the many aspects controlling remineralisation depth are coupled when considering the transfer efficiency of the BCP.

Since remineralisation depth is a key factor in the transfer efficiency of the BCP (Kwon et al., 2009), the mesopelagic zone (100 – 1000 m depth) and the understanding of the processes that occur in this depth region are critical in determining C budgets and fluxes to the deep ocean. The mesopelagic zone is the depth region where much of the downward particle flux is attenuated via zooplankton and bacterial respiration (Ducklow et al., 2001) replenishing dissolved nutrients and trace metals back into the water column. Different nutrients are remineralised at different depths, for example the remineralisation length scale for C is longer than that for N as heterotrophic bacteria preferably act upon N over the C (Smith et al., 1992). Biogenic silica ($bSiO_2$) generally has a longer remineralisation length scale (the depth at which particles are remineralized and returned to the dissolved inventory), than both C and N (Denman and Pena, 2000) as the frustules possess organic C coatings that have to be removed (by bacteria) before the $bSiO_2$ can be dissolved (Bidle and Azam, 1999).

Heterotrophic bacteria play a key role in controlling the transfer efficiency of the BCP through respiration of organic material (DOC and POC) both in the surface prior to export and at depth. Any nutrient limitation of bacterial production and growth could influence the rate of remineralisation of organic carbon (DOC or POC) and thus the export depth and long-term sequestration of biologically stored C in the oceans. Heterotrophic bacterial production and growth can be limited by Fe and organic carbon (Obernosterer et al., 2015 and references therein) as considerable Fe is required within the cellular respiratory chain, which can represent more than 90 % of the intracellular Fe pool in bacteria (Tortell et al., 1999; Andrews et al., 2003). In oligotrophic regions where macronutrients are scarce, bacteria can also be limited by Nitrogen (N), which is used for building proteins and nucleic acids (Mills et al., 2008).

Heterotrophic bacteria perform two major functions in the transformation of phytoplankton derived organic matter: they produce new bacterial biomass (bacterial secondary production), and they respire organic C to inorganic C (bacterial respiration). Taxa can be adapted based on resource exploitation strategies (Lauro et al., 2009) either associated with particles or free-living in the water column (Duret et al., 2019). Prokaryotic communities associated with particles generally show

higher concentrations, growth rates, enzymatic activities and metabolic diversity than their free-living counterparts (Grossart et al., 2007; Ganesh et al., 2014; Satinsky et al., 2014; Dang and Lovell, 2016). Taxa can also be characterised by their ecological behaviour with *K*-strategist (specialist) prokaryotes thriving on suspended particles and *r*-strategists (generalists) being observed in high proportions on sinking particles (Duret et al., 2019). In the surface the non-sinking prokaryotic community can be dominated by *Rhodobacteraceae* and *SAR11 Clade 1* as well as *Flavobacteriaceae*, and the prokaryotic community attached to fast-sinking particles can be dominated by *Flavobacteriaceae*, *Rhodobacteraceae*, *Saprospiraceae* and the *SAR11 Clade 1* with community composition changing with depth (Baumas et al., 2021).

It is now well established that limited Fe availability lowers phytoplankton pigment content and light harvesting capabilities, hinders photosynthesis and growth rates, so reduces the production of POC, PON, POP and biogenic minerals ($CaCO_3$ and opal) in different oceanic regions (Boyd et al., 2007). The diminished CO_2 drawdown and nutrient assimilation in Fe limited regions will also affect the C and nutrient concentrations in the thermohaline circulation, impacting global supply (Boyd et al., 2007). This is particularly apparent across the south Pacific Ocean, where transport by sub-Antarctic mode water (SAMW) and Antarctic Intermediate water (AAIW) plays a key role in setting thermocline nutrient levels (Sarmiento et al., 2004).

1.2 The biogeochemical cycle of iron in the oceans

Iron is recognised as a key micronutrient influencing the BCP (Martin et al., 1990) and the biogeochemical cycle of Fe involves complex interactions between lithogenic inputs (atmospheric, continental, or hydrothermal), internal cycling (dissolution, precipitation, scavenging, biological uptake and remineralisation) and sinks of sedimentation processes, subduction and transport (Gledhill and Buck, 2012; Tagliabue et al., 2017), Figure 2.

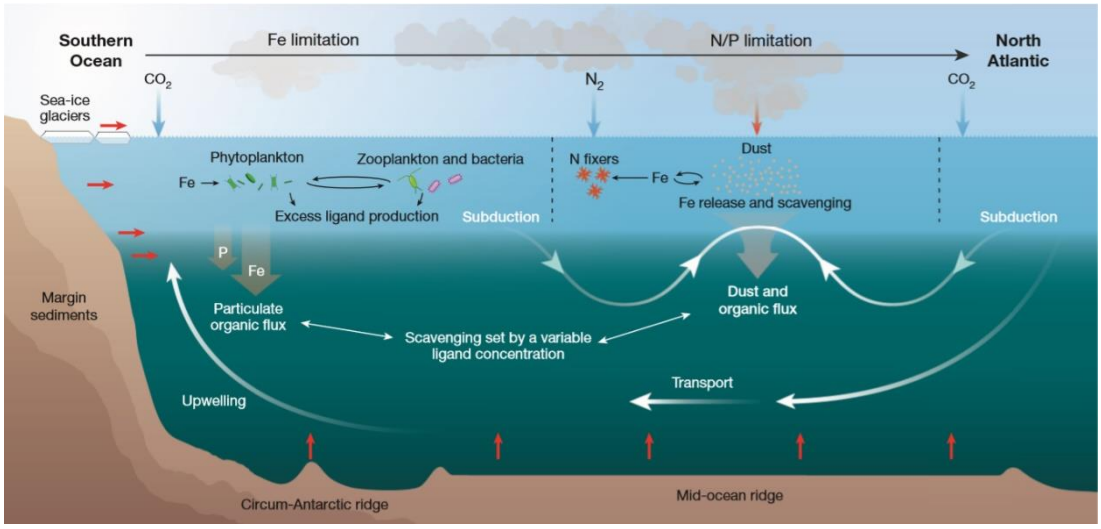

Figure 2: Major processes (focussing on the Atlantic sector) of the oceanic iron cycle showing contrast between the iron limited Southern Ocean and major nutrient limited low latitude ocean. Sources of iron (red arrows) from dust in the low latitudes to ice, shelf sediments and upwelled hydrothermal sources in the Southern Ocean. Biological cycling and production of excess ligands dominate the Southern Ocean cycling of Fe while nitrogen fixation occurs in the low latitudes. Iron can be scavenged and subducted and transported to influence the interior ocean and global oceans, (from Tagliabue et al., 2017)

All the main redox states of iron, Fe(0), ferrous Fe(II) and ferric Fe(III), are able to persist as solids almost indefinitely with low solubility in oxygenated marine environments which limits their bioavailability (Raiswell and Canfield, 2012). Iron is also particle reactive so rapidly scavenged from the water column on to sinking particles (Goldberg et al., 1954). Both of these factors make Fe a rare resource for ocean biota in the modern oxic ocean with surface waters bearing picomolar to nanomolar concentrations of dissolved unchelated inorganic iron, Fe' (Johnson et al., 1997), the most readily available form of Fe to phytoplankton (Morel et al., 2008). These low concentrations of bioavailable Fe exert significant controls on global phytoplankton productivity, species composition and therefore ecosystem structure and the C cycle. Nevertheless, substantial concentrations of dissolved Fe (dFe) persist in seawater through being organically complexed by colloidal material or truly soluble ligands, which bind more than 99% of dissolved Fe (Gledhill and

Buck, 2012). This organic complexation, systematically increases Fe solubility and bioavailability (Boyd and Ellwood, 2010; Caprara et al., 2016) as soluble Fe (<0.02 μm) is one of the most directly available for phytoplankton uptake (Raiswell and Canfield, 2012; Hassler et al., 2020).

The bioavailability of Fe is dependent on the physicochemical speciation of dissolved Fe (Hutchins et al., 1999). The majority of Fe in oceans exists in the form of dissolved nanoparticles (<0.2 μm) and particulate biogenic and lithogenic colloids (>0.2 μm). This particulate-bound Fe constitutes as much as 65 to 85 % of the total dissolvable Fe fraction in the mixed layer of the Southern Ocean (Chever et al., 2010; Nishioka et al., 2005). Dissolved Fe includes both small soluble Fe species and larger colloidal Fe forms. The occurrence of Fe in colloidal particles may decrease Fe bioavailability and increase Fe removal through colloid aggregation into larger particles, which then settle from the water column (Wu et al., 2001).

1.2.1 Iron sources to the ocean

Prior to the GEOTRACES (www.geotraces.org) suite of global cruises there was a view that Aeolian dust was the major external source of iron to the ocean, and deep Fe concentrations were reasonably constant due to organic Fe binding ligands that protected the dissolved Fe from being scavenged onto particles (Tagliabue et al., 2017).

From a greater observational dataset the sources of Fe are now better understood across different ocean basins and from different depths (Tagliabue et al., 2017). For high latitude regions such as the Southern Ocean the multiple sources of Fe include resuspension of coastal and shallow sediments, glacial/iceberg melt, seasonal sea-ice retreat, dust, hydrothermal activity, eddy shedding/sediment interactions, island wakes, vertical diffusive flux, volcanism and the interaction between the bathymetry and currents (Boyd and Ellwood, 2010). The Fe inputs to the Southern Ocean also potentially influences the supply to the low latitude oceans via the thermohaline circulation (Tagliabue et al., 2017). Intra basin variability of dissolved Fe concentrations reflects the different sources of new Fe such as coastal sediments in the Pacific (Anderson et al., 1982), hydrothermal inputs to mid water along mid ocean ridges (Atlantic (Saito et al., 2013), Pacific (Resing et al., 2015), Southern Ocean (Klunder et al.,2011) and Arctic Ocean (Klunder et al., 2012)) and dust to the surface of the Atlantic (Conway and John, 2014). Contrary to major nutrients that show enrichment in deep older waters the residence time of the Fe is short (10s – 100s years) relative to characteristic ocean circulation timescales (1000s years) with older waters having lower concentrations of dissolved Fe due to the conversion of soluble Fe to particulate Fe by adsorption, precipitation and aggregation processes, collectively known as scavenging (Boyd and Ellwood,

2010). Iron supply terms can be divided into new (that is, adding to the oceanic inventory) and recycled (turnover of the inventory) (Boyd and Ellwood, 2010).

1.2.2 Internal processes

Internal cycling of Fe is driven by biotic and abiotic transformations, from Fe uptake by both phytoplankton and bacteria and subsequent remineralisation, to the abiotic physical and chemical transformations of dissolution, precipitation and scavenging.

1.2.2.1 Biotic transformations

1.2.2.1.1 Biological uptake

The soluble Fe size fraction (<0.02 μm) is a major component of the pool available for cellular uptake with different phytoplankton and bacteria species employing differing uptake strategies (Raiswell and Canfield, 2012; Sutak et al., 2020). At the basic level there are two types of cell. Eukaryotes, that contain membrane bound organelles (cell compartments that perform a variety of functions) including a nucleus, and prokaryotes that do not contain organelles or a nucleus. The prokaryotic group are composed of bacteria and archaea, while many of the key oceanic primary producers, particularly those that dominate in high latitude systems are eukaryotic, including diatoms. For organically bound Fe there are generally two uptake strategies, siderophore mediated Fe acquisition (e.g., Goldman et al., 1983; Soria-Dengg et al., 2001) and the reductive Fe uptake pathway (Allnutt and Bonner, 1987; Eckhardt and Buckhout, 1998; Maldonado and Price, 2001; Shaked et al., 2005). Siderophore mediated Fe uptake involves the synthesis and secretion of ferric Fe chelators which are capable of solubilizing, capturing, and delivering Fe(III) to the cell (Kraemer, 2004). A strategy of releasing chelators to access dissolved or solid phase Fe(III) may make little sense for an individual cell, as the cost of generating chelators outweighs the benefit of likely intercepting only a small proportion of the chelated Fe(III), but such a strategy would make sense for a dense population of cells where a higher proportion of the chelated Fe(III) would be intercepted and used (Raiswell and Canfield, 2012). The reductive pathway uses direct take up of Fe either by photochemical reduction (external to the cell) and/or by the reduction of Fe colloids adsorbed onto the cell surface (Atkinson and Guerinot, 2011). There is a prevalent concept that eukaryotic phytoplankton utilise the reductive pathway and prokaryotes excrete siderophores. However, Shaked and Lis (2012) propose that the occurrence of siderophore vs. reductive Fe uptake can be put down to environmental rather than taxonomic considerations. Diatoms (eukaryotes) are

ruthless competitors for iron, often dominating iron-stimulated blooms (Boyd et al., 2007). For some diatom species, such as *Phaeodactylum tricornutum*, siderophores are taken up without previous reduction (Kazamia et al., 2018) via a specific protein (iron starvation-induced protein 1 (ISIP 1)) which is largely diatom specific, playing an important role in the uptake of siderophores (Kazamia et al., 2018) using non-reductive mechanisms such as endocytosis (Gao et al., 2021). Notably, many marine viruses are also capable of chelating iron on their tails and thus may represent a large sink of marine iron (Bonnain et al., 2016)

Bacteria have a wider number of mechanisms for acquiring Fe than algae and with higher surface-to-volume ratios and siderophore production, prokaryotes gain a large advantage over eukaryotes in obtaining Fe at low concentrations in surface waters, providing competition for this scarce resource (Hutchins, 1995).

1.2.2.1.2 Remineralisation

Iron that has been associated to phytoplankton either by uptake or adsorption can be remineralised within the water column as recycled Fe (Boyd et al., 2015). Recycled Fe in the surface ocean can prolong phytoplankton blooms (Boyd et al., 2015) and alter community structure (Twining et al., 2015). Recycling of Fe at depth may ultimately act as a resupply mechanism to the surface, so the processes responsible form an important part of the Fe and hence nutrient and C cycles (Boyd et al., 2015).

Intracellular Fe (largely associated with metalloenzymes and storage proteins (Mackey et al., 2015)) can be released back into the dissolved phase by zooplankton herbivory, bacterivory or algal cell lysis by viruses (Tagliabue et al., 2017). Small cells (such as bacteria) can be lysed by viruses or grazed upon by small bacterivores. The small celled bacteria can accumulate high cellular Fe concentrations (relative to their cell size) and are prone to rapid grazing/lysis, recycling the Fe within hours to days thus resupplying the Fe pool but not exporting the C to depth (Boyd et al., 2015). Larger celled (>50 µm) diatoms, particularly in the Southern Ocean, can have low Fe use (Strzepek et al., 2011) but are bloom formers with substantial biomass. These large cells are more difficult to break down, both in the surface waters and in the mesopelagic by bacteria so the Fe is biologically retained and exported to depth along with the C (Twining et al., 2014).

Trace metal remineralisation rates are harder to determine compared with macronutrient rates in the ocean as these nutrients occur at low dissolved and particulate concentrations, can be contaminated during sampling, and particulates often occur in heterogeneous aggregates in sediment traps making it hard to study individual trace metals (Twining et al., 2014). Most past

research has focused on new Fe (e.g. from dust) rather than recycled Fe and even less focus has been placed on the remineralisation of Fe in mesopelagic waters (Boyd et al., 2010). The mesopelagic remineralisation experiments that have been performed (Frew et al., 2006; Lamborg et al., 2008 and Boyd et al., 2010) tend to agree that there are lower rates of remineralisation of particulate Fe in subsurface waters (150 to 500 m) which contrast with more rapid recycling rates of both particulate Fe (PFe) and particulate organic carbon (POC) in the surface mixed layer. The different forms of Fe itself can also have different remineralisation length scales with biogenic particulate Fe having a short remineralisation length scale resulting in release to the dissolved Fe pool in the mixed layer (Boyd and Ellwood, 2010). Detrital (in aggregates) Fe has a longer remineralisation length scale than the biogenic Fe, so is released over a greater depth range (Boyd and Ellwood, 2010). Finally, lithogenic Fe has an even greater remineralisation length scale and potentially acts as a scavenging agent to remove the biogenic and detrital Fe (Boyd and Ellwood, 2010).

Other studies have investigated multiple trace metal remineralisation length scales, for example Twining et al. (2014) used trace metal clean techniques to study sinking diatoms and measured the remineralisation of trace elements in the suspended and sinking diatoms at 100 m and 200 m (upper mesopelagic) during a spring bloom event in subtropical waters off New Zealand. The study by Twining et al. (2014) found that Fe has longer remineralisation length scales and was retained within sinking diatom cells. Twining et al. (2014) concluded that the long remineralisation length scale for Fe was due to the Fe being retained biologically within the sinking diatoms and not being solubilised.

Abiotic processes such as scavenging resulting in Fe particles being transported through the water column can also increase the remineralisation length scale of Fe (Frew et al., 2006). When calculating trace metal and POC remineralisation length scales using the power law from Martin et al. (1987), metals have smaller exponents (b value) than the POC resulting in less flux attenuation with depth, i.e. a longer remineralisation length scale (Frew et al., 2006). Remineralisation length scales are a complex interplay between biotic and abiotic factors which when studied in the ocean are hard to differentiate (Twining et al., 2014).

1.2.2.2 Abiotic transformations

Abiotic transformations of Fe are less well studied than biotic mechanisms though likely that the processes interact (Boyd et al., 2017). Abiotic processes such as photo-reduction, most likely of the smallest size class of colloidal particles, serves to re-dissolve Fe again in surface waters (Wells and

Mayor, 1991). Whilst scavenging, sorption, desorption (Frew et al., 2006) and the reaction and kinetics of oxidation (De Baar and De Jong, 2001) remove Fe from the dissolved form to the insoluble or particulate form. A recent study by Bressac et al. (2019) looked at the regeneration efficiencies of PFe and found that the dissolution of lithogenic PFe takes place at lower rates than biogenic PFe. Bressac et al. (2019) also found that dust derived lithogenic particles in the upper 100-200 m acted as a scavenging-modulated sink for dFe as well as a ballasting agent which contrasts the view that lithogenic particles are a major pelagic dFe source as they can also be considered a sink.

1.2.3 Iron influences on major nutrient cycling

Phytoplankton have a variety of trace meta quotas which are driven by biochemical demands of different cells (Twining and Baines, 2013). Iron is required for many processes, including C and N fixation, nitrate and nitrite reduction, chlorophyll synthesis, and the electron transport chains of respiration and photosynthesis (Twining and Baines, 2013). Trace metals are consumed in the euphotic zone by phytoplankton as the first stage in the BCP, influencing the abundance and community composition (Twining and Baines, 2013). The trace metals then sink or are transported biologically through and out of the euphotic zone into the mesopelagic zone with the possibility of being remineralised at all stages (Boyd et al., 2017). The interactions between trace metals and phytoplankton are reciprocal: the plankton influence the distributions, chemical speciation, and cycling of these metals through cellular uptake and remineralisation processes (Sunda, 2012). The depth of remineralisation of the trace metals then control either the re-supply to the upper biota (shallow internal recycling of trace metals) or sequestration into deep water and eventual upwelling to support the biota (externally supplied new trace metals) (Boyd et al., 2017).

1.2.3.1 Nitrogen and carbon

The link between Fe and N fixation by diazotrophs has been well studied (Falkowski, 1997; Karl et al., 2002). Nitrogen fixation uses the protein nitrogenase which has a high Fe content, subsequently the Fe quotas of diazotrophs increase when they fix N instead of growing on reduced N sources (Kustka et al., 2003). In regions such as the tropical Atlantic where productivity can be limited by N (Moore et al., 2013), an episodic dust input can fuel the growth of N fixing organisms (Falkowski, 1997), and is thus important to the maintenance of the ocean's fixed N inventory (Weber and Deutsch, 2014). Knowledge of the N cycle can help estimate the amount of photosynthetically fixed

C exported out of the surface ocean via the biological pump (Eppley and Peterson, 1979). Primary production can be subdivided into 'new' and 'regenerated' production depending on the source of N used (Dugdale and Goering, 1967). New production is defined as the fraction of primary production supported by N (such as nitrate) newly injected into the euphotic zone, while regenerated production is that supported by recycled nutrients (such as ammonium and urea) in the euphotic zone (Eppley and Peterson, 1979). The ratio of new (e.g., nitrate based) to total production is termed the f-ratio (Epply and Peterson, 1979). In HNLC areas such as the Southern Ocean the f-ratio is an important tool to assess the strength of export fluxes in the basin (Thomalla et al., 2011).

For the trace metal Fe there exists a similar concept to the f-ratio for N (Zehr and Ward, 2002). New vs. recycled Fe can be defined via the Fe-ratio which describes the contribution of externally supplied Fe to biological uptake relative to that supported by both externally supplied and internally cycled Fe (Boyd et al., 2005). In the low productivity regions of the Southern Ocean recycled Fe is important as the Fe ratio is around 0.1 (Bowie et al., 2009; Boyd et al., 2005), while around naturally Fe fertilised regions such as the Kerguelen Island there is less reliance on recycled Fe as the Fe ratio reaches around 0.5 or greater (Bowie et al., 2015; Sarthou et al., 2008). Different supply methods of Fe are targeted by different phytoplankton species which employ different uptake methods. For example, vertical diffusive supply of new Fe is targeted by phytoplankton species at depth (Hopkinson and Barbeau, 2008) and in sub-Antarctic low-Fe waters approximately 90 % of productivity may be fuelled by internal Fe cycling (Boyd et al., 2005).

1.2.3.2 Silica and carbon

Some species of phytoplankton, such as siliceous diatoms, have adapted to low Fe environments (Kazamia et al., 2018; Gao et al., 2021). For example, by substituting an Fe-containing enzyme in between photosystem II and photosystem I for a copper containing enzyme (Peers and Price, 2006). Trace metal availability not only affects the growth of phytoplankton supporting or limiting biomass accumulation but can also influence community structure which reflect the biochemical demands, nutrient cycles, environmental availability and distribution of trace metals (Twining and Baines, 2013). For example, in the HNLC region of the Southern Ocean an input of Fe can create a greater growth response from the larger phytoplankton (diatoms) in relation to the smaller size classes (Hoffmann et al., 2006). The larger diatoms are not grazed as heavily by the zooplankton, thus altering the size class structure of the community from before the input of Fe (Hoffmann et al., 2006). Diatom species themselves have different Fe storage mechanisms, using the protein ferritin and vacuoles (Lampe et al., 2018). Use of the protein ferritin for Fe storage may be an adaptation

to less frequent, pulsed Fe inputs which may shift diatom species composition in regions with irregular and reduced Fe inputs (Lampe et al., 2018). These species can maintain higher growth rates due to their Fe storage mechanisms, enabling larger and longer blooms until the next Fe deposition event occurs (Lampe et al., 2018). Ferritin using diatoms such as *Fragilariopsis* species in the Southern Ocean are known for high biogenic silica burial which enhances the silica (Si) pump (Assmy et al., 2013), with this community shift in these regions influencing the biogeochemical cycles of Si and POC storage (Lampe et al., 2018). Diatoms with their silicified frustules affect the flux of C to and within the mesopelagic zone as part of the ballast hypothesis by either adsorbing or integrating organic molecules onto and into their structure (Armstrong et al., 2002; Klaas and Archer, 2002) or increase the sinking speed of organic matter (Haake and Ittekkot, 1990; Hamm, 2002; Ramaswamy et al., 1991). For example, the downward flux of particulate organic carbon (POC) during a diatom dominated spring bloom in the North Atlantic mainly comprised of un-grazed diatom aggregates and spores with a high transfer efficiency through the mesopelagic zone thus transporting the Fe, Si and C into the deep sea (Martin et al., 2011).

More recent studies now suggest that it is not the diatoms alone that control the C transport efficiency (which themselves are controlled by trace metal availability, (Boyd et al., 2007)) but the whole plankton community structure, including grazing zooplankton (Gehlen et al., 2006; Guidi et al., 2016) and heterotrophic microbes (Liu et al., 2019). Diatoms, which are influenced by Fe availability, may produce large quantities of dissolved organic matter (DOM) (Biddanda and Benner, 1997; Myklestad, 2000) which in turn affects the heterotrophic microbial community composition as a source of labile C (Landa et al., 2016). In regions such as the Southern Ocean, Fe availability controls phytoplankton and heterotrophic microbial metabolism while the lack of bioavailable organic C represents an additional constraint for heterotrophic microbes (Church et al., 2000; Obernosterer et al., 2015) which could be relieved by phytoplankton derived DOM (Landa et al., 2016). A diatom dominated community that is supported by trace metal availability will also be influenced by grazing pressure, with a shift from small to larger diatoms and an increase in export fluxes (Moriceau et al., 2018). However, the zooplankton break down the aggregates and reduce the density of material, which is not compensated for by the increased size of diatoms that avoid the grazing (Moriceau et al., 2018). These two effects in diatom dominated communities can result in a net decrease in C export efficiency (Moriceau et al., 2018). Trace metal availability supporting bloom events and increased export flux (Boyd et al., 2007) is a complex relationship with the ecosystem structure (as demonstrated by Moriceau et al., 2018). This picture is further complicated by the concept that different trace metals, their speciation and even their source (biogenic or lithogenic; new or recycled) can drive different uptake paths with different efficiencies within the phytoplankton cells (Twining et al., 2015). For example, in subtropical waters east of New Zealand

a large diatom bloom was outcompeted by smaller microbes as they were more efficient at utilising the recycled Fe and thus had a negative effect on the BCP as the blooming diatoms fixed three-fold more C per unit Fe than resident non-blooming microbes (Boyd et al., 2012). Therefore, it is not just the availability of trace metals that effect ecosystem structure and hence the BCP strength and transfer efficiency but also their source (new from upwellings vs. recycled *in-situ*) which can be partially determined by the trace metals remineralisation length scale and subsequent resupply to the biota.

Iron has strong influences on the C cycle, from productivity, to the resulting sequestration of C into the ocean's interior, and consequent modulation of atmospheric CO_2 concentrations (Martin et al., 1990). However, there are still unknown interactions between Fe and the C cycle with more research needed, particularly in the understudied but important mesopelagic depth region (100 – 1000 m) also known as the twilight zone, where deeper POC remineralisation depths store more CO_2 in the deeper ocean and reduce atmospheric CO_2 (Kwon et al., 2009).

1.3 Research aims and objectives

The availability of Fe on phytoplankton and bacterial production and community composition is an important influence on Fe cycling and subsequent C cycling (Martin et al., 1990; Ducklow, 2000), The mesopelagic depth horizon is understudied but key for Fe and C remineralisation and determination of nutrient residence times (Ducklow et al., 2001; Boyd et al., 2010). Carbon-trace metal interactions within phytoplankton have been well studied in the ocean's surface (e.g. Boyd et al., 2010; Twining et al., 2014) but far less is known about these interactions in the oceans mesopelagic zone.

The overarching aim of this thesis is: What are the potentially reciprocal feedback processes which influence Fe cycling and consequently C cycling in the mesopelagic zone?

This was approached via two main objectives, each of which can be further sub-dived into more specific aims to tackle gaps in current knowledge:

1. Differentiating the biotic and abiotic factors influencing Fe cycling in the mesopelagic zone and the (de-) coupling of Fe and macronutrients at depth.
2. Investigating the potential for Fe and C (co-) limitation of mesopelagic bacteria with the hypothesis being; "upper mesopelagic bacteria are Fe and C limited, reducing their bacterial production and therefore decreasing the remineralisation rate of C in the mesopelagic zone".

To elucidate controls on upper ocean Fe cycling, as well as the potential for vertical transport and the cycling of Fe relative to C and Si in the upper mesopelagic (100-300 m), Chapter 3 details trace metal sampling and incubation experiments during the 2017 South Georgia diatom bloom (Sanders et al., COMICS SI). Depth profiles of Fe and other comparator trace metals (manganese (Mn), zinc (Zn), nickel (Ni), copper (Cu) and cobalt (Co)) provide a time series of initial conditions of Fe concentrations to compliment the experimental work. Experimental enrichment combined with observations of phytoplankton biomass and physiology were used to determine the surface phytoplankton response to Fe. Remineralisation experiments were performed to assess the uptake and relative movement of Fe, C and Si between particulate and dissolved phases when the live phytoplankton cells were resuspended in mesopelagic water. These remineralisation experiments aimed to aid in our understanding of the role biotic and abiotic mesopelagic processes play in the (re)cycling of major nutrients and trace metals.

Building on the work by Bidle and Azam (1999) and the remineralisation experiments detailed in Chapter 3, Chapter 4 compares the relative remineralisation rates of Si, C and Fe in two scenarios,

lysed diatoms and intact diatoms, in the upper mesopelagic. We hypothesised that the lysed diatoms would be unable to maintain their protective coating and be more susceptible to microbial activity (Patrick and Holding, 1985) and subsequent Si dissolution (Rageuneau et al., 2006) and C and Fe remineralisation than the intact diatoms. This would be observable by greater radio isotope activity in the dissolved pool for the experiments incubating lysed diatoms and will further enhance our knowledge of biotic and abiotic remineralisation processes and Fe, C and Si decoupling in the mesopelagic.

The influence of Fe and C availability on microbial activity for observation 2 is detailed in Chapter 5. Here we investigate the potential for (co-) limitation of bacterial production (via ^{3}H-leucine uptake) and cell abundance through measuring responses to sole Fe, sole Corg and combined Fe and Corg additions, focusing on the lesser studied depth horizon of the mesopelagic (70 to 500 m), at two contrasting Southern Ocean sites. Firstly, Fe limitation of heterotrophic bacteria in the surface and the upper mesopelagic was investigated in the naturally Fe fertilised region north west of South Georgia at the British Antarctic Survey site P3, and secondly, sole Fe, sole Corg and combined Fe and Corg limitation was investigated at multiple depths south of the Ocean Observatories Initiative (OOI) station in the Pacific sector of the Southern Ocean as an HNLC region. Chapter 6 synthesises all experiments and postulates the interaction between remineralisation rate of C and Fe and nutrient limitation of bacteria including how this may sit in the broader oceanographic picture.

Chapter 2 Material and Methods

The following chapter provides detail on existing methods that were frequently applied throughout this thesis to prevent repetition and will be referred to throughout the rest of the thesis. Chapters 3, 4 and 5 also contain information on the more specific or additional methods used solely for that chapter and the statistical analysis used on the data for each chapter.

Techniques presented in this chapter include:

- Trace metal water sampling during three research cruises;
- Trace metal extractions;
- Remineralisation experiments;
- Ancillary measurements.

Unless stated otherwise, all chemicals were either from Sigma Aldrich, UK, or Fisher Scientific, UK. All deionized water used was MilliQ water, with a resistivity of 18.2 MΩcm (Millipore, UK).

This chapter also presents the 3 cruises and study sites that were the basis of this research.

2.1 Research Cruises

All of the presented research has been based on fieldwork from three cruises on board the *RRS Discovery* (Figure 3). The majority of this research was part of the COMICS (Controls over Ocean Mesopelagic Interior Carbon Storage; Sanders et al., 2016) project which included 2 cruises (DY086 and DY090) to contrasting sites; a naturally Fe fertilised region around the British Antarctic Survey site P3 (52S, 40W), northwest of South Georgia, with gradients in ecosystem structure generated by the progression of a naturally Fe fertilised diatom bloom in the region, and the Benguela upwelling region of the South Atlantic (21.5S, 9.5E and 18S, 11E), sampled due to the strong gradients in dissolved oxygen concentrations within the upper mesopelagic. The COMICS project aimed to further understand the processes that contribute to mesopelagic remineralisation, to expand the knowledge on the C cycle as well as modelling to project how this will interact with global climate change in the future (Sanders et al., 2016). Outputs from the COMICS project are in the process of being written up and published within a special issue in Deep Sea Research II, contextual data for this thesis has referenced this special issue (which is still awaiting publication) by 'Author et al., COMICS SI'. The third cruise (DY111) was part of the CUSTARD (Carbon Uptake and Seasonal Traits in Antarctic Remineralisation Depth) project to the South Pacific sector of the Southern Ocean which aims to examine how seasonal changes in nutrient availability for

phytoplankton at a key junction of the global ocean circulation influences how long C is trapped in the ocean, rather than escaping back to the atmosphere as carbon dioxide. The CUSTARD cruise departed from Punta Arenas and performed multiple visits to 3 sites along 89 W between 54S and 59S (Figure 3).

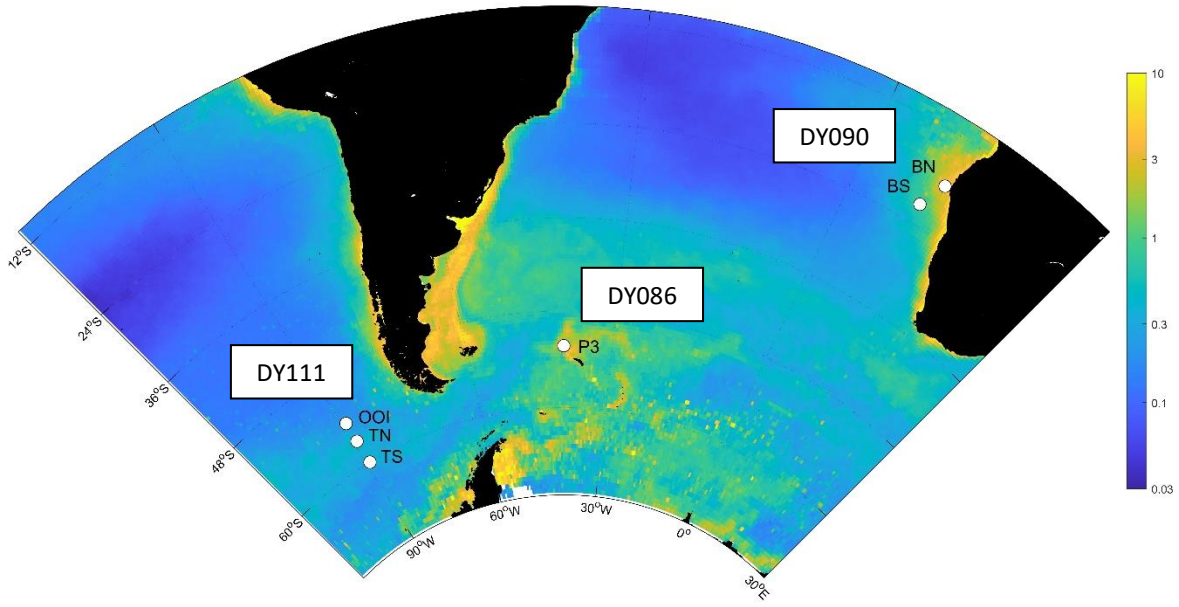

Figure 3: Location and maximum monthly average chlorophyll-*a* (mg m^{-3}) from SeaWIFS (Sea-Viewing Wide Field-of-View Sensor) for all 3 cruises. DY086 (12 Nov – 19 Dec '17) to P3, north west of South Georgia (52S, 40W). DY090 (23 May – 28 Jun '18) to the Benguela upwelling sites of Benguela North, BN (18S, 11E) and Benguela South, BS (21.5S, 9.5E) and DY111 (2 Dec '19 – 9 Jan '20) to the South Pacific sector of the Southern Ocean sites; Ocean Observatories Initiative, OOI (54S, 89W), Transect North, TN (57S.89W) and Transect South, TS (59S, 89W).

2.1.1 South Georgia

The South Georgia archipelago lies within the Antarctic Zone of the Antarctic Circumpolar Current, to the south of the Polar Front which is considerably further north in this region compared to much of the Southern Ocean (Orsi et al., 1995). The region to the north of South Georgia is characterised by high biomass and productivity of phytoplankton (Atkinson et al., 2001). The high productivity is widespread, occurring far downstream and possibly extending northwards to the Polar Front (Atkinson et al., 2001). High phytoplankton concentrations (>6 mg chlorophyll-*a* m^{-3}) within the central bloom may be linked to enhanced supply of Fe (Nielsdottir et al., 2012), though silicic acid concentrations may also be limiting in this region (Atkinson et al., 2001). The phytoplankton growth season is long, with blooms (>2 mg chlorophyll-*a* m^{-3}) persisting for 4 to 5 months (Atkinson et al.,

2001; Robinson et al., 2016). The blooms are fertilized by Fe from South Georgia sediments or from elsewhere within the basin (Antarctic peninsula or ice melt) (Nielsdottir et al., 2012; Robinson et al., 2016; Schlosser et al., 2018) and are dominated by large diatoms (Atkinson et al., 2001; Korb et al., 2008, 2010, 2012). Figure 4 and Table 4.

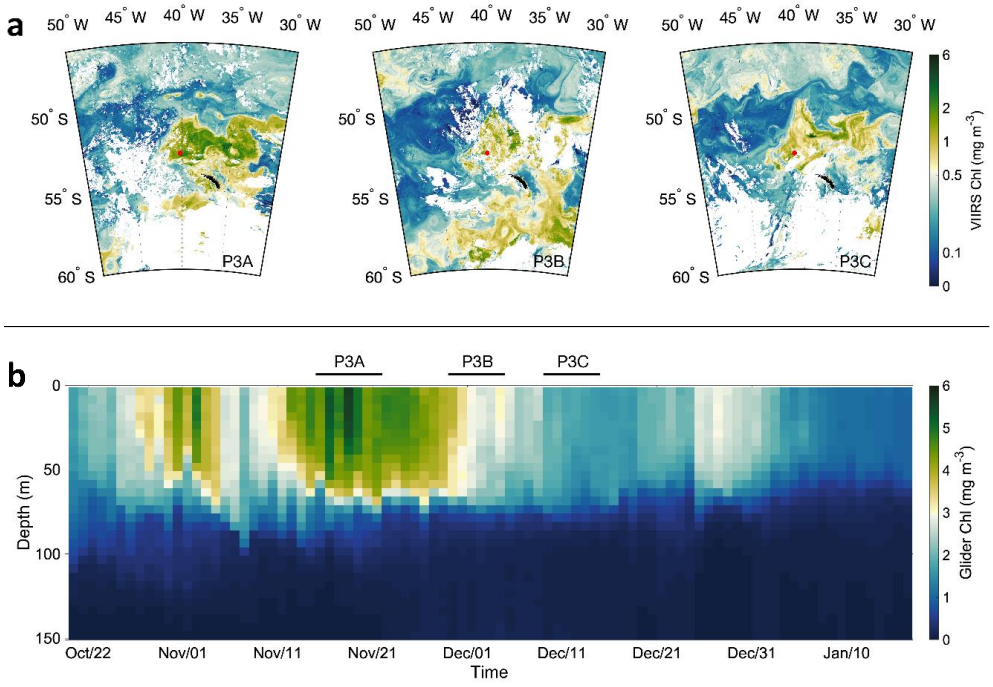

Figure 4: Sampling locations and chlorophyll-*a* concentrations (mg m^{-3}) around South Georgia. (a) Location of three sampling periods indicated by the red circles (P3A, P3B and P3C, respectively) relative to South Georgia (black landmass) and satellite-derived chlorophyll-*a* concentrations (week-long composites from VIIRS). (b) Depth distribution over time of calibrated chlorophyll-fluorescence from glider data (GOCART, Carvalho et al., COMICS SI), indicating the three temporal sampling periods. P3A was sampled between 15th and 22nd November 2017, P3B from 29th November to 5th December 2017 and P3C between 9th and 15th December 2017.

The P3 study site was within the naturally Fe fertilised HNLC region northwest of South Georgia (Figure 4). P3 was characterised by a relatively shallow seasonal mixed layer (<70 m; Carvalho et al., COMICS SI) with water temperatures increasing from the first time period sampled (P3A) of 2.29 ± 0.14 °C to 3.20 ± 0.28 °C during the final sampling period (P3C) (Table 4), with a band of colder winter water in the upper mesopelagic (100-200 m) of 0.98 ± 0.19 °C throughout the duration of the cruise. During all occupations, the phytoplankton community in terms of chlorophyll-*a* and net primary production was dominated by the >10 µm size fraction, consisting mainly of large diatoms such as *Fragilariopsis kerguelensis* and *Eucampia antarctica* (Poulton et al., COMICS SI). Over the course of the 3 occupations of the site, mixed layer chlorophyll-*a* concentrations decreased from

3.75 ± 1.87 mg m^{-3} during P3A to 1.3 ± 0.32 mg m^{-3} during P3C (Table 4). Mixed layer macronutrient concentrations declined between P3A and P3C; nitrate decreased slightly from 19.38 ± 1.24 µM to 17.61 ± 0.76 µM, while silicic acid declined from 5.03 ± 3.82 µM to 2.28 ± 2.12 µM. Water column variables corresponding to experimental sampling are presented in Table 12 and Figure 24 in Appendix A.

2.1.2 Benguela upwelling

The Benguela upwelling system off south-western Africa is highly productive and supports intense production of organic matter, the remineralisation of which contributes to the formation of oxygen minimum zones (Mohrholz et al., 2008). The Benguela region is delimited in the north by the Angola-Benguela Frontal Zone (ABFZ). North of this front the alongshore Angola Current (AC) transports oligotrophic equatorial warm, saline and low oxygen waters south, equatorial water intrusions across the ABFZ happen offshore via filaments of warm water and on the shelf via the poleward undercurrent (UC) (Hutchings et al., 2009). South of the ABFZ, the alongshore Benguela Current (BC) transports nutrient rich, cold, less saline and oxygenated waters north (Hutchings et al., 2009) (Figure 5a).

Two sites were sampled during DY090, a southerly site named BS (Benguela South) located at 21.5S, 9.5E and a more northerly site named BN (Benguela North) at 18S, 11E (Figure 5a, Table 5). DY090 completed 1 cycle of the super-station at BS and 3 cycles at BN (named BN.1, BN.2 and BN.3), it was decided to remain longer at the BN site and undertake a sequence of the 6 day station cycle to capture the temporal evolution of the mesopelagic oxygen minimum and hence study consequent influence on remineralisation depth.

BS was characterised by a deeper mixed layer than BN (60 ±5 m at BS, 24 ±8 to 36 ±10 m at BN) and low chlorophyll-*a* concentrations of between 0.06 and 0.14 mg m^{-3} (dominated by <10 µm cells). BN was located at the convergence of the BC and the UC (Figure 5a) and had higher chlorophyll-*a* concentrations than BS ranging from 0.03 to 0.31 mg m^{-3} (Figure 5b) with the first occupation BN.1 dominated by >10 µm cells and higher biogenic silica ($bSiO_2$) indicating diatom dominance and BN.2 dominated by smaller cells (Table 5). The surface dFe was similar between BS (with concentrations of 0.39 to 0.51 nM) and BN (0.28 to 0.5 nM), however BS surface nitrate was low at 0.08-0.40 µM compared to 3.09 to 17.24 µM at BN which may have contributed to the lower chlorophyll-*a* levels and smaller cell dominance at BS (Figure 5b, Table 5).

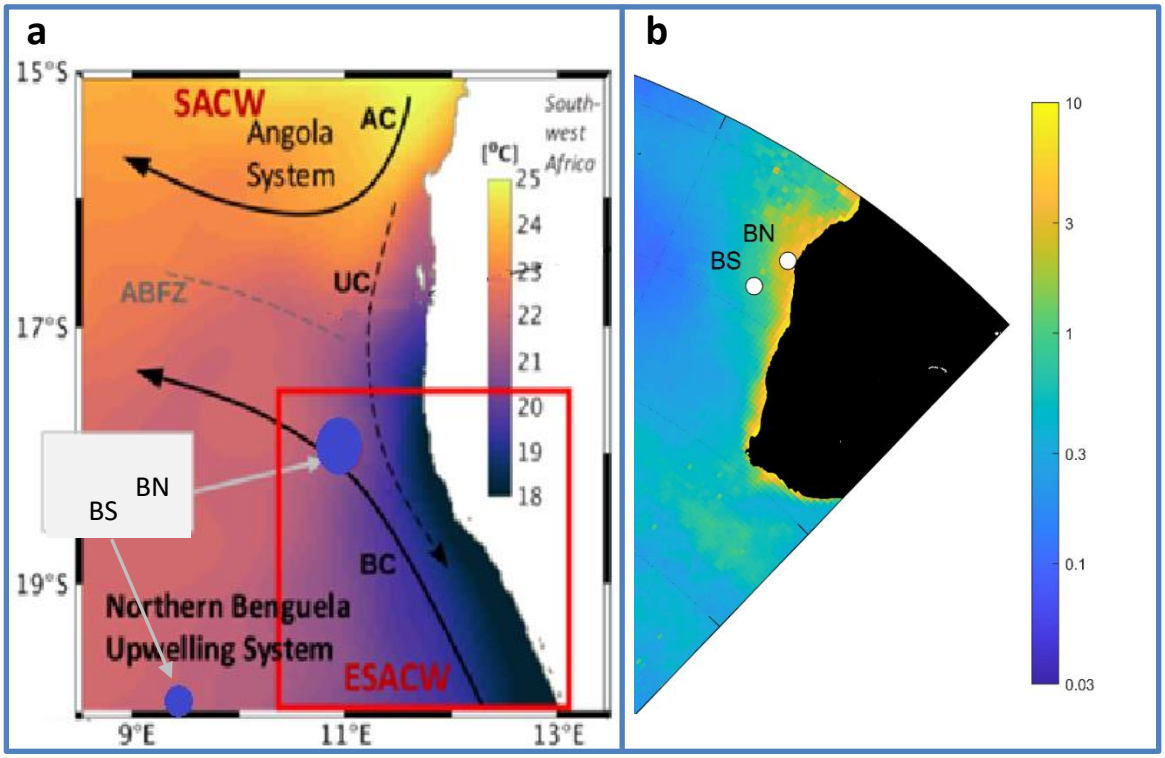

Figure 5: Benguela north (BN) at 18S, 11E and Benguela south (BS) at 21.5S, 9.5E site locations a) in/near the Benguela Upwelling System (red box), relative to the Angola Current (AC) and South Atlantic Central Water (SACW), the Benguela Current (BC) and Eastern South Atlantic Central Water (ESACW), the UnderCurrent (UC) and the Angola Benguela Frontal Zone (ABFZ) with sea surface temperature (SST) for June 2018 b) Maximum monthly average chlorophyll-*a* (mg m^{-3}) from SeaWIFS (Sea-Viewing Wide Field-of-View Sensor). BS was sampled once from 25th to 31st May 2018 and BN was sampled 3 times between 1st and 19th June 2018.

2.1.3 South Pacific sector of the Southern Ocean

This sampling region is at a key junction of the global ocean circulation and the CUSTARD project fieldwork contributed data to test the hypothesis that the seasonal interplay of upper limb surface biogeochemistry, circulation and remineralisation, controls which water mass remineralised C is stored within and hence how long the DIC resulting from the exported organic C is kept out of the atmosphere (Figure 6a,c). The cruise performed multiple transects along 89W from the US National Science Foundation (NSF) funded Southern Ocean Ocean Observatories Initiative (OOI) mooring site at 54S, south to two sites named transect north (TN) at 57S and transect south (TS) at 60S (Figure 6b, Table 6).

The OOI Southern Ocean mooring array, deployed in February 2015, provides the first high-quality time series of the surface fluxes and subsurface ocean properties in a key Sub Antarctic Mode Water (SAMW) formation region (Cerovečki et al., 2013; Holte et al., 2017). The array is located north of the Sub Antarctic Front (SAF) (Figure 6c) and contains the farthest south, long-term, open ocean

air-sea flux mooring ever deployed (Trowbridge et al., 2019). The Southern Ocean OOI site experiences episodic heat loss events in association with cold, dry air from the southwest (Ogle et al., 2018). These extreme heat losses lead to convective deepening of the mixed layer to >300 m (Ogle et al., 2018). This site is an HNLC region with high nutrient levels but low biological productivity due to Fe limitation (Morrissey and Bowler, 2012) (Figure 6b). Iron stressed diatoms could increase their sinking speed as the energy required to maintain their bouyancy was no longer available (Muggli et al., 1996) and Fe-limited conditions have led to the dominance of heavily-silicified diatoms (Assmy et al., 2013) also increasing sinking speed (Armstrong et al., 2002) , both of which could influence the remineralisation depth and therefore the water mass their C is stored and transported within.

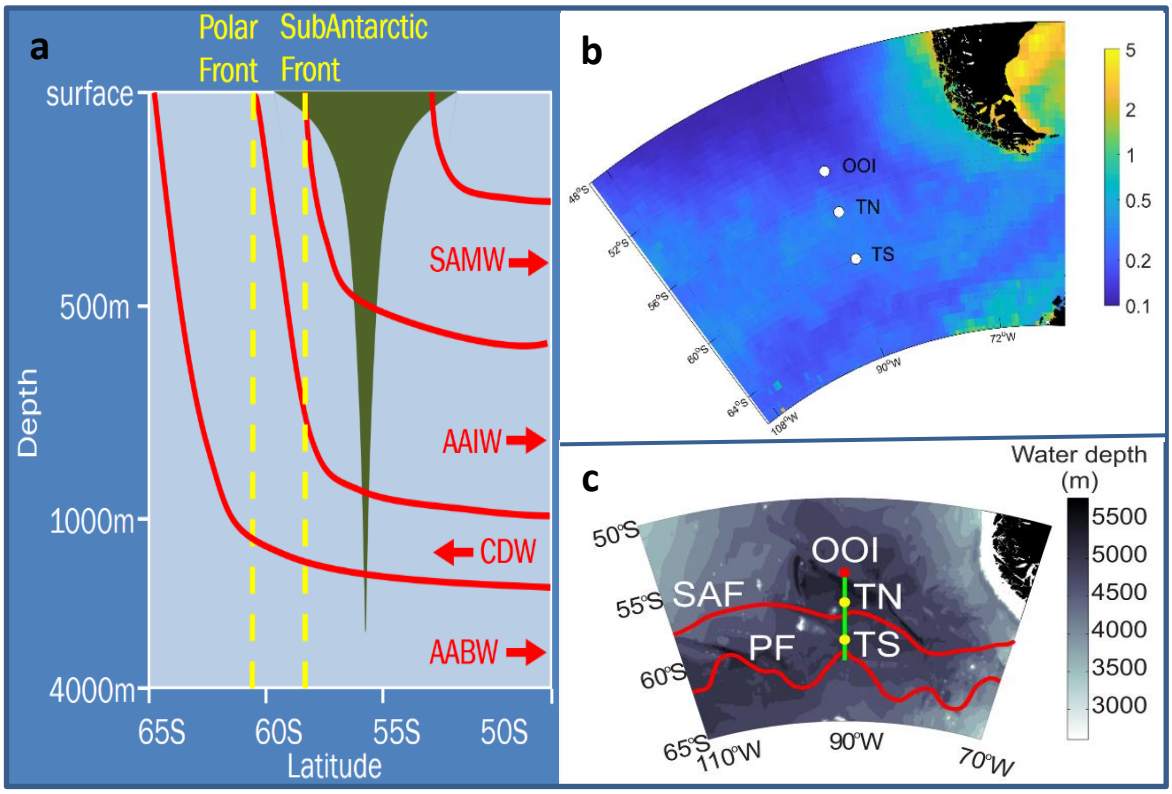

Figure 6: Water masses, water depth, chlorophyll-*a* concentrations and site locations of the CUSTARD cruise. a) Simplified schematic showing Circumpolar Deep Water (CDW) brought to the surface south of the Polar Front; some water heads south to form the lower limb feeding Antarctic Bottom Water (AABW); some moves north being subducted as Antarctic Intermediate Water (AAIW) or Sub Antarctic Mode Water (SAMW). The depth at which sinking organic material (green funnel) is remineralised is a major influence on which water mass it will reside in and how carbon leaves the Southern Ocean. b) Climatology mean chlorophyll-*a* (mg m^{-3}) for November - December at each of the CUSTARD sites; OOI at the Ocean Observatories Initiative, TN at transect north and TS at transect south. c) site location in relation to the polar front (PF) and Sub Antarctic Front (SAF) on water mass depth. OOI was sampled 3 times, 6th, 14/15th and 21/22nd December 2019, TN was sampled once on 29th December 2019 and TS sampled 3 times on the 9th, 17th and 27th December 2019.

Each station was visited four times, but only 3 occupations of OOI and TS and 1 occupation of TN were used for the experiments presented in this thesis. OOI had the warmest surface (top 20 m) water between 6.74 and 7.90 ^{o}C and the southerly TS station was the coolest at 4.34 to 5.74 ^{o}C (Table 6). Chlorophyll-*a* increased from 0.04 to 0.55 mg m^{-3} throughout the occupation of OOI and from 1.54 to 2.33 mg m^{-3} throughout the occupation of TS with corresponding increases in POC and biogenic silica and a decrease in silicic acid and nitrate (Table 6). The occupations were during the spring bloom but productivity still remained low due to dFe levels of generally <0.09 nM (Table 6), which resulted in Fe limitation of the surface phytoplankton communities (Wyatt et al., in prep)

2.2 Ancillary measurements

Samples for chlorophyll-*a* analysis (50 - 250 mL) were filtered onto 25 mm diameter Whatman™ glass fibre GF/F filters for total chlorophyll-*a* concentration or sequentially through 47 mm diameter polycarbonate 10 µm, 2 µm and 0.2 µm polycarbonate filters for size-fractionated chlorophyll-*a*. In all cases, chlorophyll-*a* was extracted in 6 mL of 90 % acetone over 18-20 hours at 4 °C in a fridge in the dark. Chlorophyll-*a* fluorescence was measured on a Turner Designs Trilogy™ fluorometer using a non-acidification module calibrated with solid and pure chlorophyll-*a* standards (Sigma-Aldrich, UK) (Welschmeyer, 1994).

Inorganic macronutrient concentration of nitrate (NO_3) and silicic acid ($Si(OH)_4$) were sampled in 15 mL centrifuge tubes rinsed three times with seawater from the same sampled Niskin bottle. Analysis was generally within 24 hours of the samples being taken. Analysis was performed by members of the team from the National Oceanographic Centre (NOC) and was on a QuAAtro 39 segmented flow autoanalyzer according to methods provided from *SEAL Analytical UK Ltd* (Kirkwood, 1989).

Biogenic Silica ($bSiO_2$) samples (500 mL) were filtered onto polycarbonate filters (0.8 µm pore size, Whatman™) and briefly rinsed with pH-adjusted MilliQ water (~pH 8.5) to remove any salt residue. Filters were placed into 15 mL corning tubes, dried overnight (40-50 °C) before being stored at room temperature until analysis. Analysis was performed by members of the NOC team and blanks were prepared by filtering 500 mL MilliQ and preparing the filter as described above. Filters were digested in 5 mL of 0.2 M sodium hydroxide solution, incubated at 85 °C for 2 h and subsequently allowed to cool to room temperature. The filters were then neutralised with 0.2 M hydrochloric acid solution. The solution was subsequently analysed using standard colourmetric techniques for silicate analysis using a QuAAtro 39 segmented flow autoanalyser, (Brown et al., 2003).

Particulate Organic Carbon (POC) samples of 1000 mL of seawater were filtered onto pre-ashed (400 °C, 12 h) Whatman™ GF/F filters (nominal pore-size 0.7 µm, 25 mm diameter). These were then placed in acid-clean Eppendorf tubes, and dried overnight (50 °C) for storage prior to analyses on shore. Analysis was performed by members of the NOC team and blanks were prepared by filtering 1000 mL MilliQ and preparing the filter as described above. On shore, the filters were fumed with 11 M hydrochloric acid for 24 hours to remove any inorganic carbon, dried (50 °C, >24 h) and pelleted in tin disks (Elemental microanalysis). The samples were analysed for POC using a *Thermo Fisher* Scientific FLASH 2000 Organic Elemental Analyser (Sanders et al., 2007).

Hydrographic variables (conductivity, temperature and hence salinity as a function of depth) were collected with a *SeaBird SBE 9 plus* CTD system by members of the NOC team.

2.3 Trace metal water column sampling

Iron is present in our daily lives as it's the fourth most abundant element in the earth's crust (Taylor, 1964). In the open ocean where our samples are sourced, Fe is found in extremely low concentrations and thus contamination of samples from equipment, handling and laboratory space needs to be avoided. Protocols have been developed to avoid contamination at all stages of the Fe sampling and analysis process (Cutter et al., 2017).

Trace metal clean techniques can avoid contamination but to truly measure uptake of iron, removal of extracellular iron is required. A number of methods have been developed to remove extracellular iron such as cation exchange, acid washes, isotopic exchange and the use of complexing agents such as ethylenediaminetetraacetic acid (EDTA) as compared in Hassler et al., 2004 and references therein, with EDTA washes most popular (Hassler et al., 2004). Hudson and Morel (1989) developed a Ti-citrate-EDTA buffer which was shown to remove ≥97 % of all extracellular iron via a reductive mechanism (Tang and Morel, 2006). The buffer results in minimal damage upon cells after washing (Hudson and Morel (1989); Tang and Morel, (2006)), although Sunda and Huntsman (1995) did note membrane damage upon use of this buffer. This Ti-citrate-EDTA buffer has been shown to leave iron contamination on the cell surface which could be reduced with further washes (Tang and Morel, 2006) and alternative oxalate washes can be made trace metal clean (Tovar-Sanchez, et al., 2003), however for our experiments we focus on radio labelled iron so non labelled iron contamination would not alter our results thus allowing the use of the Hudson and Morel (1989) Ti-citrate-EDTA buffer.

Water samples were collected through deployment of a Titanium CTD fitted with 24 x 10 L OTE bottles that have been modified for trace metal work with epoxy coated external springs, coating of stainless ferrules and fitting of PTFE taps. Trace metal clean protocols were employed in the deployment and subsequent sampling of the trace metal (TM) CTD (Cutter et al., 2010). Samples for trace metals and experiments were collected from the TM CTD whilst samples for chlorophyll-*a*, particulate organic carbon (POC) and biogenic silica ($bSiO_2$) were collected from stainless steel (SS) CTD deployments, macronutrients were collected from both the TM and SS CTDs.

2.3.1 Preparation of clean lab ware

For all shipboard and laboratory-based experiments, all plastic ware was acid washed prior to use. Low-Density Polyethylene (LPDE) bottles supplied by Nalgene® were used, all tubing was also acid

cleaned. This consisted of being soaked in 1 M hydrochloric acid for 24 hours and then rinsed 3 times with Milli-Q®. Plastic ware was then stored in sealed triple plastic bags until used.

For the trace metal extraction lab ware vials, the following cleaning protocol was used:

- Soak for 2 days in a 3 % DECON 90 solution;
- Rinse with De-Ionised tap water 3 times and then a final rinse with Milli-Q;
- Soak in a 20 % HCl bath for 5 days;
- Rinse with Milli-Q 3 times;
- Soak in 20 % HNO_3 bath for 5 days;
- Rinse with Milli-Q 4 times;
- Once rinsed leave on side under flow hood to dry.

2.4 Determination of water column trace metal concentrations

Seawater samples were collected from the Titanium rosette and the OTE bottles were transported into a class-1000 clean air laboratory. Subsamples for dissolved trace metals were gravity filtered (DY086 and DY090) or pressure filtered (DY111) through a 0.2 µm membrane cartridge filter (Sartobran-300, *Sartorius*) into 60 or 120 mL acid washed polycarbonate bottles. Separate unfiltered samples were collected for total dissolvable trace metals (TDTM). All samples were acidified with ultrapure (UPA) hydrochloric acid (HCl, Romil, UpA) under a class-100 laminar flow hood. For DY111, the dFe samples were acidified on board and were analysed using methods described in Obata et al. (1993) and Klunder et al. (2011) by members of the team from Plymouth University. For DY086 the concentration of trace metals (Fe, Zn, Mn, Ni, Co, Cu) in total dissolvable and dissolved (dTM) samples was determined using an offline semi-automated pre-concentration standard addition method that has been used previously for seawater samples (Milne et al., 2010) and analysed on a HR-ICP-MS (High Resolution – Inductively Coupled Plasma- mass Spectrometer) (Rapp et al., 2017). Apparent particulate Fe (PFe) can then be calculated as the difference between the total dissolvable and dissolved Fe.

Briefly, the trace metals in the acidified samples were extracted by loading 15 mL of the sample buffered to within the range of pH 6 to 6.4 with 2 M Ammonium Acetate onto a WAKO (Kagaya et al., 2009) chelate resin column (*Wako Pure Chemical Industries*, Japan), rinsing with 0.05 M Ammonium Acetate (Optima grade, Romil) for seawater matrix removal. The sample was then eluted by passing 1.5 mL distilled 1 M HNO_3 over the columns. The resin was then cleaned with the elution acid and preconditioned with 0.05 M Ammonium Acetate for the next sample. Method

blanks were determined by taking manifold blanks (contribution of trace metals leached by reagents from valves and pump tubing) and acidified de-ionised water blanks (contribution of trace metals from the UPA HCl used for sample acidification). The accuracy of the method was established by repeat quantification of trace metal concentrations of in-house reference seawater samples which have been checked for accuracy against inter-calibrated GEOTRACES SAFe reference samples and found to be within the quoted ranges (https://www.geotraces.org/standards-and-reference-materials/, see also Table 2). The elution acid containing metals extracted from samples were then run on the HR-ICP-MS (Element II, *Thermofisher*) alongside elution acid blanks and a known multi-element standard to monitor instrument drift. The percentage errors based on the repeat measurements of the in-house reference seawater against known values were: Fe, 28 % (n = 28); Zn, 21 % (n = 10); Mn, 4 % (n = 32); Ni, 10 % (n = 33); Co, 26 % (n = 32); Cu, 6 % (n = 33). Limits of detection for trace metals based on 3 x standard deviations of the blanks were: Fe, 0.26 nM; Zn, 0.41 nM; Mn, 0.02 nM; Ni, 0.30 nM; Co, 0.0001 nM; Cu, 0.25 nM. Any values beneath these limits could be inaccurate.

Table 2: SAFe references samples (May 2013) from www.geotraces.org/standards-and-reference-materials, nd indicates no data.

	SAFe reference samples (May 2013)	
Element	**D1 (nM)**	**D2 (nM)**
dFe	0.67 ± 0.04	0.933 ± 0.023
dZn	7.40 ± 0.35	7.43 ± 0.25
dMn	nd	0.35 ± 0.05
dNi	8.58 ± 0.26	8.63 ± 0.25
dCo	0.045 ± 0.0047	0.046 ± 0.0029
dCu	2.27 ± 0.11	2.28 ± 0.15

2.5 Remineralisation experiments

We adapted the protocols of Bidle and Azam (1999) and Boyd et al. (2010) in order to investigate the mesopelagic remineralisation potential of surface organic material. Experiments were performed to follow the partitioning between size fractionated particulate and dissolved phases during the incubation of surface material in mesopelagic water (see Table 3 for incubation times of each experiment). Briefly, the uptake rates of Fe, C and Si by the surface phytoplankton/microbial community were measured through separate radio-labelling (^{14}C, ^{55}Fe, ^{32}Si) of surface communities and parallel incubations. The large size fraction (see Table 3 for size fraction of each experiment) from these labelled microbial communities were then harvested via gravity filtration and particles re-suspended to determine the subsequent remineralisation potential of this material by the mesopelagic microbial community, through determination of the fractional (re-) distribution of each radio-isotope/element within dissolved and particulate phases (Boyd et al., 2010).

The size fractionation through filtering techniques defines the operational delineation between dissolved (<0.2 µm) and particulate (> 0.2 µm) fractions used in the subsequent experiments. The dissolved Fe fraction also contains colloidal Fe (0.02 to 0.2 µm - the size fraction equal to the difference between dissolved Fe and soluble Fe) (Raiswell and Canfield, 2012).

Stage 1: Near surface samples (see Table 3 for each experimental depth) were collected in TM OTE bottles and transferred into triplicate acid-washed 125 mL Nalgene polycarbonate bottles for each isotope (^{14}C, ^{32}Si and ^{55}Fe). To encourage the active uptake of isotopes through the generation of fresh labelled organic material, limiting nutrients were added to each sample (see Table 3 for nutrient concentrations). Samples were then spiked with the radio-isotopes; ^{55}Fe, 2 kBq in 10 % spa HCl (0.02 kBq/mL; 1.85 nM total addition); ^{14}C as sodium bicarbonate, ~74 kBq (7.4 kBq/mL); and ^{32}Si as orthosilicic acid, 3 kBq (0.05 kBq/mL). After spike addition, each bottle was placed in a dedicated *in-situ* temperature controlled refrigerated container laboratory (see Richier et al., 2014) for 48 hrs with temperature and light conditions as detailed in Table 3. Sub-samples of 10 mL were then harvested through filtration (<100 kPa) onto 0.2 µm and 5 µm or 2 µm polycarbonate filters in order to measure total community and size fractionated community uptake, respectively (see Table 3 for size fraction at each experiment). Additional 1 mL samples were taken to determine the total activities for the 3 isotopes added.

To differentiate between intracellular uptake and adsorption of ^{55}Fe onto external particulate surfaces, subsets of filtered particulates were washed at the end of the sample filtration with a buffered Ti-EDTA-citrate solution which scavenges adsorbed ^{55}Fe (Hudson and Morel, 1989). Once all subsamples had been removed, incubation bottles were rinsed clean with seawater and a further sample was taken to determine the ^{55}Fe stuck to the walls of the sample bottles by adding 5 mL of

10 % HCl, rinsing and then taking a 1 mL subsample of this HCl rinse. All filters, filtrates and acid rinses were placed in 6 mL Ultima Gold scintillation cocktail before being counted on a liquid scintillation counter (Perkin Elmer TriCarb 3180 TR/SL).

Stage 2: At the termination of stage 1, the remainder of the samples (~100 mL) not used for T0 measurements (see above) were harvested by gravity filtration through a 47 mm, 5 µm or 2 µm polycarbonate filter. Particulate material was then rinsed twice with filtered (0.2 µm) mesopelagic water from TM OTE bottles before being washed off and resuspended into a volume of trace metal clean water collected from OTE bottles in the mesopelagic (see Table 3 for mesopelagic depth) that represents 10 mL per time step. An even split of each resuspension per time point was further diluted into a total of 125 mL of whole (i.e., unfiltered, unamended) mesopelagic water (collected via TM OTE bottles from the same depth) for subsequent harvesting time steps for each isotope. This was repeated to create triplicates for each isotope at each time point (see Table 3 for number of time points).

All stage 2 samples were incubated in the dark at *in-situ* mesopelagic temperatures within a temperature controlled container (Richier et al., 2014) for a minimum of 24 hrs (to allow time for bacterial colonisation (Bidle and Azam, 1999) and processed at a number of time steps to determine the resultant activity partitioning in each phase of remineralisation. Quantification of activity within each phase (size fractionated particulate, adsorbed, dissolved and wall wash) used methods similar to the end-point measurements at the termination of stage 1. Additionally, determination of dissolved inorganic carbon ($DI^{14}C$) was undertaken through a modification of the Micro-Diffusion Technique (Paasche and Brutak, 1994; Balch et al., 2000) whereby 1 mL of filtrate subsamples were acidified (1 mL, 50 % HCl) in gas-tight containers with a CO_2 trap (Whatman™ filter soaked with 200 µL β-phenylethylamine, Sigma). The activity on the β-phenylethylamine soaked filters and filtrates was determined by liquid scintillation counting, and are assumed to correspond to the partitioning of the dissolved C pool into respired C (filters) and dissolved organic carbon (filtrates), respectively.

At the Benguela site, stage 2 experimental remineralisation potential was also investigated for dead cells, lysed through a freeze/thaw process as per below;

Stage 2: Similar to the live cell experiments, all the particulates (total uptake not required as stage 1 is the same as with the live cells) were harvested by gravity filtration through a 47 mm, 5 µm polycarbonate filter. Particulate material was then rinsed extensively with clean filtered (0.2 µm) mesopelagic water and the filter placed in a vial with 15 mL filtered (0.2 µm) mesopelagic water from TM OTE bottles, agitated to release the harvested particulates into the water and then the filter removed. The vials were placed in a plastic box in a -20 °C freezer for between 48 and 124 hrs. The samples were then thawed at room temperature (12 °C) for at least 15 hours until fully liquid.

The particulates (dead cells) were harvested by gravity filtration through a 47 mm, 5 µm polycarbonate filter. Particulate material was then rinsed twice with filtered (0.2 µm) mesopelagic water from TM OTE bottles before being resuspended in whole unfiltered mesopelagic water to create triplicate samples for 3 or 5 subsequent harvesting time steps for each isotope. All stage 2 samples were incubated in the dark at *in-situ* temperatures (see Table 3) within a refrigerated container and processed at 3 or 5 time steps (see Table 3) to determine the resultant activity in each phase of remineralisation using methods similar to the end-point measurements at the termination of experimental stage 1. See Figure 7 for a conceptual methods figure.

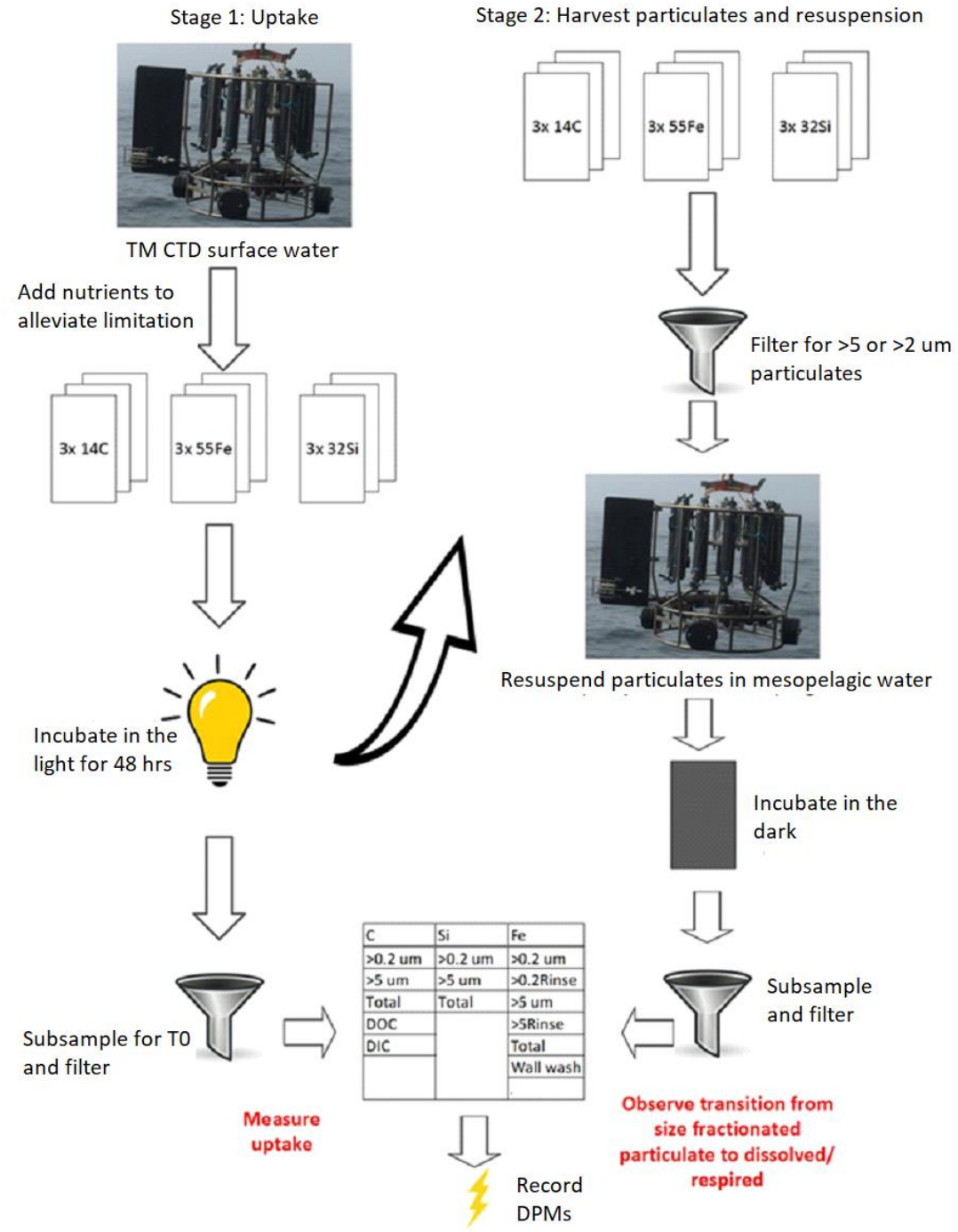

Figure 7: Conceptual figure for the remineralisation stage 1 and stage 2 methods.

Table 3: Remineralisation experiment details

Site	Depth (m)	Experimental stage	Size fraction	Incubation temp	Incubation light	Limiting nutrients added	Incubation days (post resuspension)
South Georgia							
P3A	30	Stage 1 surface material collection	>5 µm	2 ± 1 °C	16:8 hr light:dark cycle. Total daily irradiance dose of 21.2 mol quanta m^{-2} d^{-1} (~60 % daily surface irradiance).	2 nM of unlabelled Fe (50 µl of 10 µM $FeCl_3$ in 0.024 M spa HCl)	T1: 2 days T2: 4 days T3: 6 days
	110	Stage 2 mesopelagic resuspension – live cells		2 ± 1 °C	dark		
P3B	30	Stage 1 surface material collection		2 ± 1 °C	16:8 hr light:dark cycle. Total daily irradiance dose of 21.2 mol quanta m^{-2} d^{-1} (~60 % daily surface irradiance).		T1: 1 days T2: 4 days T3: 8 days
	110	Stage 2 mesopelagic resuspension – live cells		2 ± 1 °C	dark		
P3C	18	Stage 1 surface material collection		2 ± 1 °C	16:8 hr light:dark cycle. Total daily irradiance dose of 21.2 mol quanta m^{-2} d^{-1} (~60 % daily surface irradiance).		T1: 1 days T2: 3 days T3: 5 days
	110	Stage 2 mesopelagic resuspension – live cells		2 ± 1 °C	dark		

Site	Depth (m)	Experimental stage	Size fraction	Incubation temp	Incubation light	Limiting nutrients added	Incubation days (post resuspension)
Benguela							
BS	25	Stage 1 surface material collection	>2 µm	18 ± 2 °C	12:12 hr light:dark cycle. Total daily irradiance dose of 19.0 mol quanta m^{-2} d^{-1} (~60 % daily surface irradiance).	2nM unlabelled Fe (50 µL of 10 µM $FeCl_3$ in 0.024 M spa HCl), 5 µM nitrate, 5 µM silicate, 0.6 µM phosphate and 0.5 µM ammonia	T1: 2 days T2: 4 days T3: 6 days T4: 8 days T5: 10 days
	120	Stage 2 mesopelagic resuspension – live cells		12 ± 2 °C	dark		
BN.1	20	Stage 1 surface material collection	>5 µm	18 ± 2 °C	12:12 hr light:dark cycle. Total daily irradiance dose of 19.0 mol quanta m^{-2} d^{-1} (~60 % daily surface irradiance).		T1: 2 days T2: 4 days T3: 6 days T4: 8 days T5: 10 days
BN.1	120	Stage 2 mesopelagic resuspension – live cells		12 ± 2 °C	dark		
BN.1	20	Stage 1 surface material collection	>5 µm	18 ± 2 °C	12:12 hr light:dark cycle. Total daily irradiance dose of 19.0 mol quanta m^{-2} d^{-1} (~60 % daily surface irradiance).		T1: 3 days T2: 5 days T3: 7 days T4: 9 days T5: 11 days
BN.2	125	Stage 2 mesopelagic resuspension – dead cells		12 ± 2 °C	dark		
BN.2	22	Stage 1 surface	>5 µm	20 ± 2 °C	12:12 hr light:dark cycle.		T1: 2 days T2: 4 days

Site	Depth (m)	Experimental stage	Size fraction	Incubation temp	Incubation light	Limiting nutrients added	Incubation days (post resuspension)
		material collection			Total daily irradiance dose of 19.0 mol quanta m^{-2} d^{-1} (~60 % daily surface irradiance).		T3: 6 days
BN.3	125	Stage 2 mesopelagic resuspension – live cells		12 ± 2 °C	dark		
BN.2	22	Stage 1 surface material collection	>5 µm	20 ± 2 °C	12:12 hr light:dark cycle. Total daily irradiance dose of 19.0 mol quanta m^{-2} d^{-1} (~60 % daily surface irradiance).		T1: 2 days T2: 4 days T3: 6 days
BN.3	125	Stage 2 mesopelagic resuspension – dead cells		12 ± 2 °C	dark		

2.5.1 Remineralisation experiments data calculations and validation

Activity distributions were calculated from both the volumes and the measured activity in the total sample, >0.2 µm particulates, >0.2 µm rinsed (so the intra-cellular biologically retained particles), >5 µm particulates, and the >5 µm rinsed sample. The difference between the total in the sample and the total particulate (>0.2 µm extra and intra-cellular) was taken to calculate activity in the dissolved fraction. If the measured total failed validation checks (point 1 below) then the carried over total from stage 1 as the volumetric proportion of the activity associated with the resuspended particulates can be used as the total activity in each time step. The particulates were then size partitioned into the smaller size fraction of <5 µm (both intra and extra-cellular) from the difference between the >0.2 µm (i.e. all particles) and the >5 µm particles rinsed and non-rinsed samples. See Figure 8 for a graphical representation of the calculated values. The raw DPM (Disintegrations Per Minute) data (normalised to bottle volume) was validated using the following criteria before individual directly measured or calculated fractions were considered measurable and hence considered in further calculations or results interpretation.

1. The raw DPMs recorded by the scintillation counter should be above the instruments background level of 20 DPM (determined from running a clean filter in scintillation cocktail through the counter). Low raw DPM values could result from the sample volume being too small for the concentration of the isotope to be measurable.
2. The >0.2 µm particulates (i.e. all particles) should have the same or greater DPMs (within 1 standard deviation) than the >5 µm particulates (t-test, $p<0.05$).
3. The non-rinsed/washed particulate samples (^{55}Fe associated both intra and extra-cellular) should have the same or greater DPMs (within 1 standard deviation) as the rinsed/washed particulate samples (t-test, $p<0.05$).
4. The dissolved fraction calculated as the difference between the total DPM (measured or carried over) and the >0.2 µm particulates DPM was assumed measurable if significantly (t-test, $p<0.05$) greater than zero.
5. The <5 µm particulates fraction calculated as the difference between the >0.2 µm particulates DPM and the >5 µm particulates DPM was assumed measurable if significantly (t-test, $p<0.05$) greater than zero.

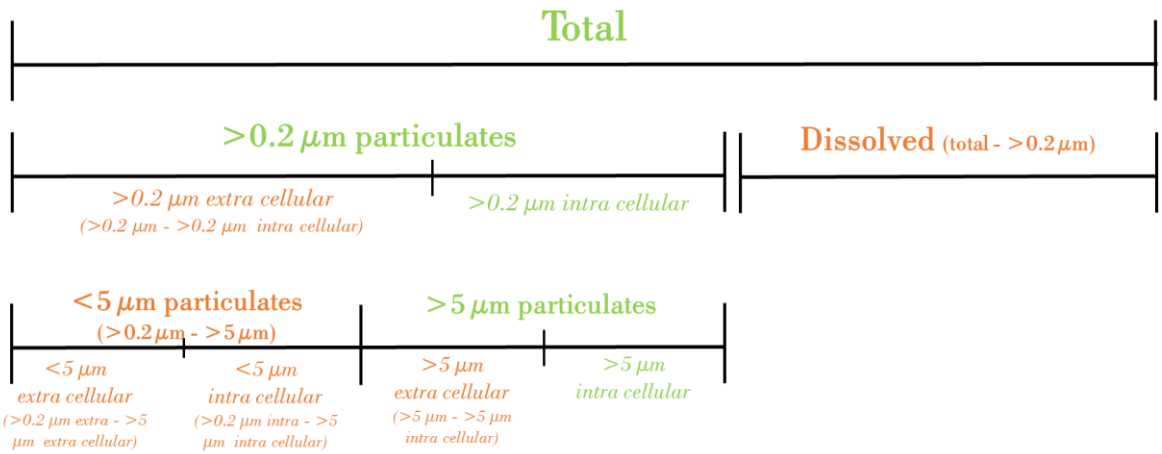

Figure 8: Measured fractions (green) and calculated fractions (orange) of radio isotope distributions with the equation for calculated fractions in brackets. Italic text for intra and extra cellular fractions are for Fe only.

2.6 Study sites oceanographic parameters

2.6.1 South Georgia

Table 4: South Georgia sampling station general oceanographic parameters and timescales. Data from calibrated CTD sensors and from CTD bottles. Diatom abundance (SEM cell counts) from Poulton et al., COMICS SI, bacterial abundance from Rayne et al., COMICS SI, seasonal mixed layer (Z_{ML}) depth from Carvalho et al. (COMICS SI). Surface data from the top 20 m, dFe sample was collected from between 20-40 m. Upper mesopelagic is taken as 100 – 300 m (Giering et al., COMICS SI). N/A not available.

Station	**P3A**	**P3B**	**P3C**
Date	15-22 Nov '17	29 Nov – 5 Dec '17	9 – 15 Dec '17
Latitude (S)		52	
Longitude (W)		40	
Z_{ML} (m)	70	70	60
Surface temperature, °C	2.31 - 2.48 (n=44)	2.89 - 3.38 (n=52)	3.24 - 3.62 (n=27)
Upper mesopelagic temperature, °C (110 m)	0.95 - 1.46 (n=10)	0.80 - 1.22 (n=12)	0.92 - 1.12 (n=6)
Surface dFe (nM)	0.03 (n=1)	0.17 (n=1)	0.15 (n=1)
Surface Nitrate, NO_3 (µM)	17.96 – 20.82 (n=14)	16.71 – 17.68 (n=10)	16.80 – 17.43 (n=6)
Surface biogenic silica, $bSiO_2$ (µM)	7.18 – 11.51 (n=3)	4.98 – 6.60 (n=3)	3.43 - 5.04 (n=4)
Surface silicic acid, $Si(OH)_4$ (µM)	1.51 – 8.34 (n=14)	0.81 – 0.77 (n=10)	0.63 – 1.02 (n=6)
Surface Particulate Organic Carbon (µM)	20.17 – 32.15 (n=5)	15.78 – 23.57 (n=3)	14.21 – 16.58 (n=4)
Surface chlorophyll-*a* (mg m^{-3})	1.14 – 5.01 (n=6)	1.59 – 4.30 (n=6)	1.18 - 1.59 (n=5)
Dominant chlorophyll-*a* fraction	>10 µm	>10 µm	>10 µm
Surface diatom cell abundance (cells mL^{-1})	1319 – 1855 (n=3)	502 – 1812 (n=3)	279 – 480 (n=2)
Surface bacterial abundance, ($x10^3$ cells mL^{-1})	424 – 512 (n=2)	391 – 639 (n=2)	639 (n=1)
Mesopelagic (110 m) bacterial abundance, ($x10^3$ cells mL^{-1})	N/A	319	N/A

2.6.2 Benguela upwelling

Table 5: Benguela sampling station general oceanographic parameters and timescales. Data from calibrated CTD sensors and from CTD bottles. Bacterial abundance from Rayne et al., COMICS SI, note the values are $x10^8$ rather than $x10^3$ as per the other locations. Mixed layer depth (Z_{ML}) based on a surface temperature difference of 0.5 °C (Hooker et al., 2000). Surface data from the top 30 m. N/A not available.

Station	**BS1**	**BN1**	**BN2**	**BN3**
Date	25–31 May ‘18	01–07 Jun ‘18	07–14 Jun ‘18	14-19 Jun’18
Latitude (S)	21.5		18	
Longitude (E)	9.5		11	
Z_{ML} (m)	55-67 (n=7)	25-45 (n=9)	11-33 (n=8)	17-45 (n=7)
Surface temperature, °C	20.35-20.75 (n=101)	16.45-20.41 (n=131)	16.24-19.33 (n=115)	16.56-19.63 (n=101)
Upper mesopelagic temperature, °C (120 m)	15.73-16.15 (n=14)	13.24-14.18 (n=18)	13.15-13.71 (n=14)	13.02-13.44 (n=14)
Surface dFe (nM)	0.39-0.51 (n=2)	0.28-0.57 (n=2)	N/A	N/A
Surface Nitrate, NO_3 (µM)	0.08-0.40 (n=25)	3.09-17.33 (n=38)	5.25-15.64 (n=27)	4.53-17.24 (n=25)
Surface biogenic silica, $bSiO_2$ (µM)	2.33-7.86 (n=4)	24.7-39.88 (n=7)	7.36-16.98 (n=9)	7.40-12.49 (n=5)
Surface silicic acid, $Si(OH)_4$ (µM)	0.50-0.74 (n=25)	0.75-2.89 (n=38)	0.99-3.33 (n=27)	0.58-3.31 (n=25)
Surface chlorophyll-*a* (mg m^{-3})	0.06-0.14 (n=4)	0.08-0.27 (n=7)	0.03-0.25 (n=5)	0.13-0.31 (n=7)
Dominant chlorophyll-*a* fraction	<10 µm	>10 µm	2-10 µm	2-10 µm
Surface bacterial abundance, ($x10^8$ cells mL^{-1})	N/A	342-760 (n=4)	343-732 (n=4)	458-928 (n=4)
Mesopelagic bacterial abundance, ($x10^8$ cells mL^{-1})	N/A	64-80 (n=2) (150 m)	N/A	131 (n=1) (100 m)

2.6.3 South Pacific sector of the Southern Ocean

Table 6: South Pacific sampling station general oceanographic parameters and timescales. Data from calibrated CTD sensors and from CTD bottles. Mixed layer depth (Z_{ML}) based on a surface temperature difference of 0.5 °C (Hooker et al., 2000). Surface data from the top 20 m. N/A not available.

Station	**OOI-1**	**OOI-2**	**OOI-3**	**TN-3**	**TS-1**	**TS-2**	**TS-3**
Date	06-Dec-19	14-15-Dec-19	21-22-Dec-19	29-Dec-19	09-Dec-19	17-Dec-19	27-Dec-19
Latitude (S)	54	54	54	57	59	59	59
Longitude (W)	89	89	89	89	89	89	89
Z_{ML} (m)	100	77	49	52	19	43	34
Surface temperature, °C	6.74-6.83 (n=5)	7.36-7.41 (n=4)	7.48-7.90 (n=9)	7.71 (n=4)	4.34-4.47 (n=5)	4.45-5.74 (n=4)	5.09-5.27 (n=4)
Upper mesopelagic temperature, °C (150 m)	5.64 (n=1)	5.61 (n=1)	5.71 (n=1)	4.94 (n=1)	3.55 (n=1)	2.59 (n=1)	2.66 (n=1)
Surface dFe (nM)	0.06 (n=1)	0.15 (n=1)	0.06 (n=1)	0.08 (n=1)	0.09 (n=1)	0.05 (n=1)	0.09 (n=1)
Surface Nitrate, NO_3+NO_2 (µM)	20.02-20.09 (n=5)	19.49-19.63 (n=4)	16.64-19.29 (n=9)	17.28-17.44 (n=4)	23.44-23.67 (n=5)	21.53-22.68 (n=4)	21.03-21.26 (n=4)
Surface biogenic silica, $bSiO_2$ (µM)	0.74 (n=1)	0.62 (n=1)	1.15 (n=1)	0.94 (n=1)	4.12 (n=1)	6.50 (n=1)	5.55 (n=1)
Surface silicic acid, $Si(OH)_4$ (µM)	4.68-4.77 (n=5)	4.34-4.38 (n=4)	0.23-3.62 (n=9)	0.12-0.16 (n=4)	5.72-6.64 (n=5)	0.41-0.99 (n=4)	0.22-0.24 (n=4)
Surface Particulate Organic Carbon (µM)	4.32 -8.08 (n=2)	5.51 (n=1)	9.07-14.59 (n=3)	11.73 (n=4)	11.34 (n=1)	16.46 (n=1)	18.27 (n=1)
Surface chlorophyll-*a* (mg m^{-3})	0.04-0.47 (n=9)	0.40-0.45 (n=4)	0.50-0.55 (n=4)	0.64-0.67 (n=4)	1.54-2.20 (n=5)	1.92-2.37 (n=4)	1.99-2.33 (n=4)
Dominant chlorophyll-*a* fraction	>10 µm	>10 µm	>10 µm	>10 µm	>10 µm	>10 µm	>10 µm
Surface bacterial abundance, (x10^3 cells mL^{-1})	477 (n=1)	NA	534 (n=1)	706 (n=1)	533 (n=1)	301 (n=1)	NA
Mesopelagic bacterial abundance, (x10^3 cells mL^{-1})	88 (n=1) (500 m)	NA	171 (n=1) (150 m)	257 (n=1) (150 m)	83 (n=1) (500 m)	134 (n=1) (150 m)	NA

Chapter 3 Iron cycling in the post peak South Georgia diatom bloom

Modified chapter in review at Deep Sea Research II as part of the COMICS Special Issue.

Ainsworth, J., Poulton, A. J., Lohan, M. C., Stinchcombe, M. C., Lough, A. J. M., Moore, C. M., 2022, 'Iron cycling during the decline of a South Georgia diatom bloom', *Deep Sea Research II*, In prep.

3.1 Introduction

The Southern Ocean forms an important component of the global biogeochemical cycles of carbon (C) and macronutrients of nitrogen, phosphorus and silica (N, P, Si), being the most extensive and biogeochemically significant of the so-called high nutrient low chlorophyll (HNLC) regions (Chisholm and Morel, 1991). Nutrient rich waters in the Southern Ocean could support large blooms of phytoplankton if limiting factors such as iron (Fe), low light availability and low temperatures were alleviated (Boyd, 2002), converting significant amounts of dissolved inorganic carbon (CO_2) into particulate organic carbon (POC) at the base of the marine food web. The high macronutrient levels of the Southern Ocean are due to strong upwelling of nutrient rich deep waters (Pollard et al., 2006) accompanied by low phytoplankton production due in part to Fe limitation (Martin, 1990). Enhanced primary production and drawdown of atmospheric CO_2 can thus occur in Fe enriched Southern Ocean waters (Martin, 1990; Blain et al., 2007; Pollard et al., 2009).

Phytoplankton need to access bioavailable Fe for key cellular processes, including nitrate and nitrite reduction, chlorophyll synthesis, and the electron transport chains of respiration and photosynthesis (Twining and Baines, 2013). The availability of Fe therefore influences the C and N cycles. However, Fe has low solubility in oxygenated waters, which limits concentrations and hence its bioavailability (Raiswell and Canfield, 2012). Iron is also particle reactive and rapidly scavenged from the water column onto particles (Goldberg, 1954), which can sink through the euphotic zone into mesopelagic waters (100-1000 m), with the possibility of being remineralised and recycled at all stages (Boyd et al., 2017). All of these factors make Fe a scarce resource for surface ocean biota in the modern oxic ocean, with surface waters bearing nanomolar dissolved concentrations and picomolar dissolved unchelated inorganic concentrations (Johnson et al., 1997), the most readily available form of Fe to phytoplankton (Morel et al., 2008). These low concentrations of bioavailable Fe exert significant controls on global phytoplankton productivity, species composition and therefore ecosystem structure and the C cycle (Chisholm and Morel, 1991; Boyd and Ellwood,

2010). The interactions between Fe and plankton are reciprocal: the plankton influence the distribution, chemical speciation, and cycling of Fe through cellular uptake and remineralisation processes (Sunda, 2012). Moreover, the depth of Fe remineralisation can exert a control on resupply to the surface phytoplankton (shallow recycling of Fe) or sequestration into deep mesopelagic waters, with subsequent upwelling following transit in the deep ocean and then potentially able to support further primary production elsewhere (Boyd et al., 2017, Tagliabue et al., 2017). Dissolved Fe (dFe: <0.2 µm) therefore displays nutrient like depth profiles due to its key biological role in the oceans; removal in surface waters by biological uptake and increased concentrations at depth from the breakdown of cells and remineralisation processes (Boyd and Ellwood, 2010).

Iron sources to the Southern Ocean can be in the form of new Fe (additions to the Fe inventory) or recycled Fe (turnover of the inventory) (Boyd and Ellwood, 2010). The majority of new Fe supply to the surface Southern Ocean comes in the form of upwelling of relatively Fe rich deep waters (Boyd and Ellwood, 2010; Tagliabue et al., 2014). Other sources of Fe can originate from coastal or shallow sediment resuspension, ice melt, dust deposition, hydrothermal activity, vertical diffusive flux and island wakes (Boyd and Ellwood, 2010). Within the Southern Ocean, natural exceptions to the low productivity HNLC regions are found downstream of continental shelves and islands such as the Kerguelen Plateau, Crozet Islands and South Georgia, where large phytoplankton blooms have been observed (Blain et al., 2007; Pollard et al., 2007; Korb et al., 2008; Nielsdottir et al., 2012), with South Georgia being one of the most intense (Robinson et al., 2016). It is generally accepted that enhanced Fe supply to surface waters predominately occurs from sediments through internal waves and turbulence in these systems (Blain et al., 2007; Schlosser et al., 2018). Iron not immediately used to produce new biomass can be transported downstream via lateral advection, alleviating the limitation of phytoplankton further afield (Boyd et al., 2007: Korb et al., 2008; Nielsdottir et al., 2012; Schlosser et al., 2018).

The South Georgia region lies within the Antarctic Zone of the Antarctic Circumpolar Current, to the south of the Polar Front (Orsi et al., 1995) and is characterised by high biomass and productivity of phytoplankton (Atkinson et al., 2001). The high productivity is widespread, occurring far downstream and possibly extending northwards to the Polar Front (Atkinson et al., 2001). High phytoplankton concentrations (>6 mg chlorophyll-*a* m^{-3}) within the central bloom may be linked to enhanced supply of Fe, though silicic acid concentrations may also be limiting in this region (Atkinson et al., 2001). The phytoplankton growth season is long, with blooms (>2 mg chlorophyll-*a* m^{-3}) persisting for 4 to 5 months (Atkinson et al., 2001; Robinson et al., 2016). The blooms are fertilized by Fe from South Georgia sediments or from elsewhere within the basin (Antarctic

peninsula or ice melt) (Nielsdottir et al., 2012; Robinson et al., 2016; Schlosser et al., 2018) and are dominated by large (<50 µm) diatoms (Atkinson et al., 2001; Korb et al., 2008, 2010, 2012).

Iron cycling can exert significant control on primary production and ultimately the strength or overall efficiency of the BCP, especially in naturally Fe fertilised regions of the Southern Ocean such as downstream of South Georgia (De Baar et al., 1995) or the Crozet Islands (Pollard et al., 2009). Surface ocean interactions between trace metal and C cycles have received significant attention, however, less work has been performed on the (de-) coupling of these cycles within the mesopelagic zone (the so-called 'twilight zone' at ~100-1000 m) (Boyd et al., 2017; Tagliabue et al., 2019). Iron is remineralised differently to both C and the macronutrients such as N and Si. Differential cycling in the twilight zone could ultimately influence atmospheric CO_2 through multiple feedback mechanisms, including influences on the depth of C, Si and Fe remineralisation and the corresponding potential for different nutrients to become limiting to surface production (especially Fe and Si in the Southern Ocean) either locally or through interactions with the large-scale oceanic circulation, remotely and/or globally (Lamborg et al., 2008).

Previous work has investigated the cycling of radio-isotope labelled surface ocean particulate material in the surface mixed layer with one (Fe) (Boyd et al., 2010) or two (C and Si) (Bidle and Azam, 1999) elements being investigated for their relative remineralisation rates, presumably mediated by bacteria. In the case of Boyd et al. (2010), rapid algal Fe mobilisation by bacteria collected in the mixed layer was observed over a 72-hour incubation period, however in these experiments it was not possible to discriminate between the pools of intra- (sequestered) and extra- (adsorbed) cellular algal Fe.

To elucidate controls on upper ocean Fe cycling, as well as the potential for vertical transport and the cycling of Fe relative to C and Si in the upper mesopelagic (100-300 m), we performed trace metal sampling and incubation experiments during the 2017 South Georgia diatom bloom (Sanders et al., COMICS SI). Depth profiles of Fe and other comparator trace metals (manganese (Mn), zinc (Zn), nickel (Ni), copper (Cu) and cobalt (Co)) provide a time series of initial conditions of Fe concentrations to compliment the experimental work. Experimental enrichment combined with observations of phytoplankton biomass and physiology were used to determine the surface phytoplankton response to Fe. Remineralisation experiments were performed to assess the uptake and relative movement of Fe, C and Si between particulate and dissolved phases when the live phytoplankton cells were resuspended in mesopelagic water. These remineralisation experiments aimed to aid in our understanding of the role mesopelagic processes play in the (re)cycling of major nutrients and trace metals.

3.2 Material and Methods

The experiments performed for this chapter were the remineralisation experiments of live cells (section 2.5) and surface community iron limitation experiments (detailed below in section 3.2.1) performed at P3 in the region of South Georgia. See Table 4 for oceanographic parameters of this region and sections 1.1, 2.3 and 2.4 for appropriate general methods.

3.2.1 Surface community iron limitation

To determine whether the surface phytoplankton communities were Fe limited, four (once during P3A, twice during P3B and once during P3C) surface community Fe limitation experiments were performed using protocols similar to those employed by Moore et al. (2007a&b) and Nielsdottir et al. (2012). Water was collected from a trace metal clean Titanium CTD rosette, with OTE bottles transferred into a class-1000 clean air laboratory for sampling. For each experiment, 6 sub-samples were collected from OTE bottles fired in the upper mixed layer (20-30 m nominal depth) into acid-washed 250 mL polycarbonate bottles. Of these, 3 bottles were left as un-amended controls and 3 were amended with 2 nM Fe additions (50 µL of 10 µM $FeCl_3$ in 0.024 M HCl). Unamended controls and Fe amended bottles were incubated for up to 5 days in a dedicated temperature controlled refrigerated container laboratory (see Richier et al., 2014) maintained close to *in-situ* temperatures at 2 ± 1 ^{o}C under a daily light cycle (16:8 hr light:dark) with a total daily irradiance dose of 21.2 mol quanta m^{-2} d^{-1} (i.e. ~60 % daily surface irradiance). Bottles were removed to a clean laboratory where subsamples (100 mL) were collected for active chlorophyll fluorescence measurements and determination of chlorophyll-*a* (50 mL; see section 1.1) at 2 days and 4-5 days within each incubation. Active chlorophyll fluorescence measurements on the incubated samples were performed with a prototype 'single turnover fluorescence of enclosed samples (STAFES)' instrument (designed by Chelsea Technologies (UK) Ltd.) and were analysed to recover the apparent photochemical quantum efficiency (Fv/Fm) using protocols similar to those used previously (Moore et al., 2007a; Nielsdottir et al., 2012). The experiment metadata is provided in Table 12 in Appendix A.

3.2.2 Statistical analysis

A one-way analysis of variance (ANOVA) and a post hoc Bonferroni multi comparison test were performed on each time point between the control and Fe amended treatments (chlorophyll-*a* and Fv/Fm measurements). Differences were considered statistically significant at $p < 0.05$.

Data validation detailed in section 2.5.1 were performed on the remineralisation DPMs.

3.3 Results

3.3.1 Trace metal profiles

Dissolved Fe (dFe) concentrations indicated 'nutrient like' profiles (Bruland and Lohan, 2003), with lower surface concentrations at all station occupations (Figure 9a). Surface samples typically had dFe concentrations less than 0.17 nM. Dissolved Fe peaks (between 150 and 250 m) were observed within the colder winter water of the upper mesopelagic, which has presumably accumulated dFe, with higher concentrations (> 0.27 nM) below 250 m (Figure 9a). Apparent particulate Fe (PFe) (calculated as the difference between the total dissolvable and dissolved Fe) followed similar 'nutrient like' profiles as dFe. Apparent particulate Fe peaked around 160 m depth at P3A and P3B with lower concentrations below this (Figure 9b). The PFe peaks coincided with the colder water band between 100-200 m in the mesopelagic.

Consistent with the dFe profiles, the other measured trace metals which frequently show surface depletion due to biological uptake displayed 'nutrient-like' (Cu, Zn, Ni) or 'hybrid' (Co, Mn) profiles (Figure 25 in Appendix A). Dissolved concentrations were substantially depleted in the surface layer for all these elements, with values increasing beneath the mixed layer, with peaks at depths > 400 m for Cu and Zn, while concentrations decreased below ~150-200 m for the scavenged elements Co and Mn. Generally, concentrations of the dissolved trace metals showed little temporal variability, although dFe showed some increases over the three sampling periods, particularly below the mixed layer (Figure 9a).

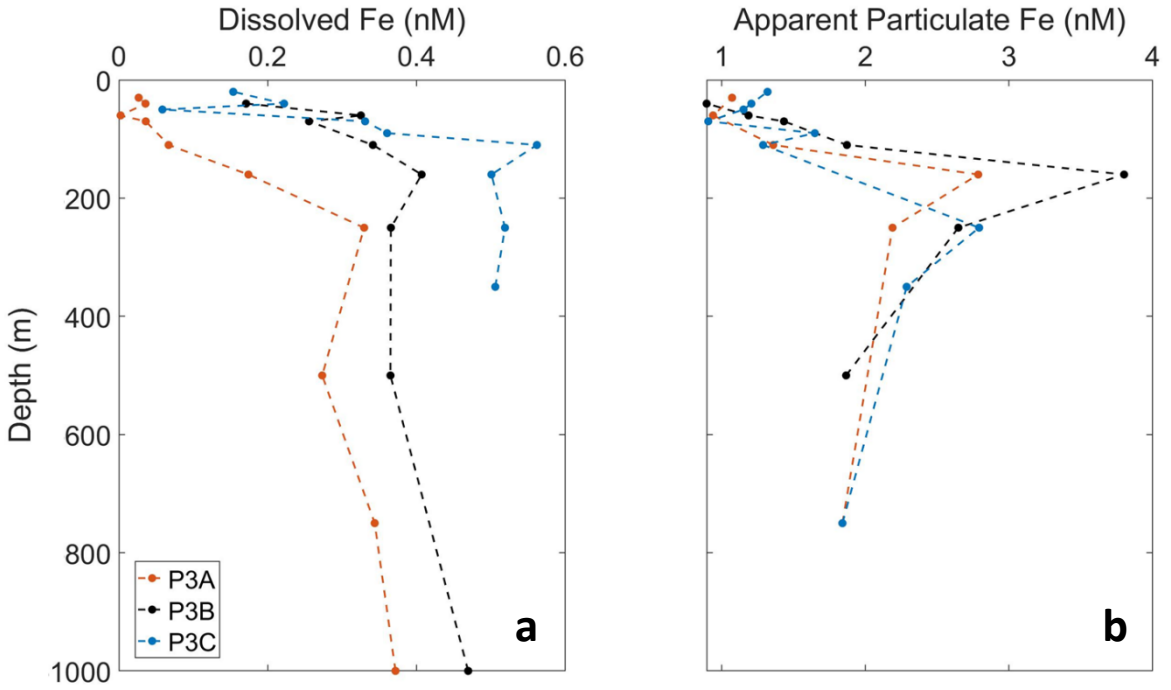

Figure 9: Iron depth profiles over the P3 occupation: (a) Dissolved Fe, and (b) Apparent particulate Fe (calculated from total dissolvable Fe minus dissolved Fe). Station occupations separated by colour: P3A orange line, P3B black line and P3C blue line.

3.3.2 Phytoplankton iron limitation

Measurements of the apparent quantum yield of photochemistry (Fv/Fm) using active chlorophyll fluorescence indicated low values (<0.3) within the bloom (Figure 10a), which are likely indicative of Fe stress (Kolber et al., 1998; Greene et al., 1992; Moore et al., 2005; Nielsdottir et al., 2012). Moreover, measured values of Fv/Fm within Fe-addition experiments indicated significant differences ($p<0.05$) between the control and Fe amended samples at every time point measured across all four Fe limitation experiments Figure 10a). Over the duration of the occupation of the P3 site, both the control and Fe amended samples displayed increasing values of Fv/Fm, potentially indicating a reduction in the extent of *in-situ* community Fe stress over time (Figure 10a).

Chlorophyll-*a* concentrations measured in all Fe limitation experiments were also significantly different ($p<0.05$) between the control and Fe amended samples by the end points of all incubations, with a general decrease in the percentage difference of chlorophyll-*a* between the control and Fe amended samples over the occupations from P3A to P3C (Figure 10b). For experiments at P3B and P3C a significant increase in chlorophyll-*a* was also detected in the Fe amended samples after just 2 days of incubation while none of the control samples at 2/3 and 4/5 days showed any significant change (Figure 10b).

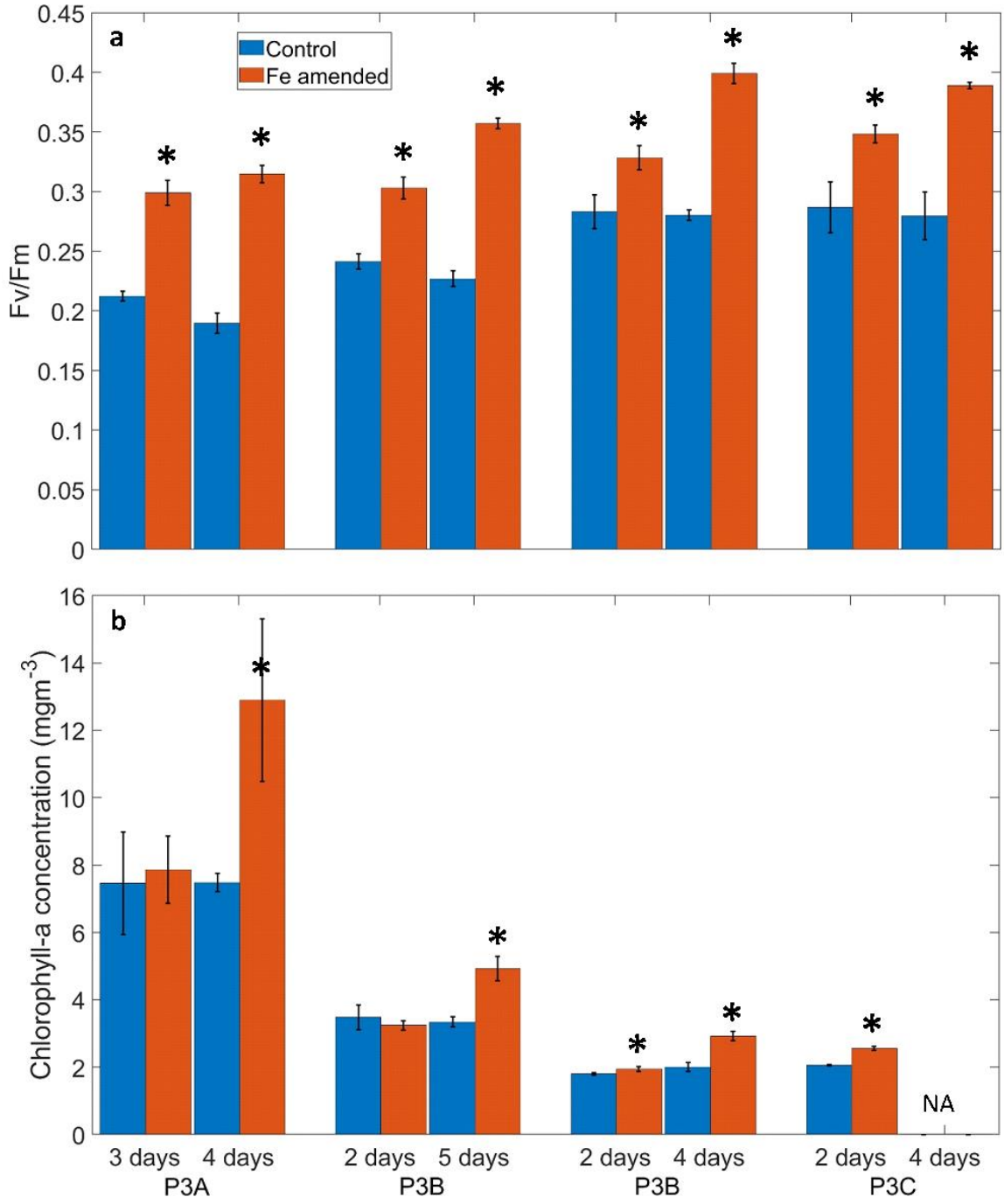

Figure 10: Phytoplankton Fe limitation responses. (a) Responses of algal physiology to Fe addition; (b) Responses of chlorophyll-*a* concentrations to Fe addition. In (a) and (b) a significant difference ($p<0.05$) is indicated by * in the Fe amended samples (red) compared with the control samples (blue). Error bars are shown as 1 standard deviation from triplicate samples. NA indicates not available.

3.3.3 Phytoplankton uptake of Fe, C and Si

Total uptake rates of ^{55}Fe, ^{14}C and ^{32}Si by surface phytoplankton were calculated after 48 hr incubations approximating *in-situ* light and temperature conditions (Table 4). Corresponding with the overall decline in upper ocean biomass over the 3 sampling periods, the total ^{14}C uptake decreased over the occupation of P3, from 21.00 µmol C L^{-1} d^{-1} at P3A to 4.75 µmol C L^{-1} d^{-1} at P3C (Table 7). Silica total uptake similarly indicated a decrease in uptake by the surface phytoplankton over time, from 0.58 µmol Si L^{-1} d^{-} 1 at P3A to 0.08 µmol Si L^{-1} d^{-1} at P3C (Table 7). The total uptake of ^{55}Fe decreased the least out of the 3 isotopes, from 0.20 nmol Fe L^{-1} d^{-1} at P3A to 0.14 nmol Fe L^{-1} d^{-1} at P3C (Table 7).

Total Si:C uptake ratios ranged from 0.028 mol mol^{-1} during P3A to 0.017 mol mol^{-1} during P3C (Table 7). These Si:C uptake ratios are slightly lower than independently made mixed layer uptake rates on non-nutrient enriched communities (Poulton et al., COMICS SI). Ratios of Fe:C uptake ranged from 9.5 µmol mol^{-1} during P3A to 29.5 µmol mol^{-1} during P3C, while ratios of Fe:Si uptake ranged from 0.35 µmol mol^{-1} during P3A to 1.75 µmol mol^{-1} during P3C. For Si:C uptake ratios, P3B had noticeably lower ratios than during the other sampling time points, whereas the other ratios were more similar over time. In general, stoichiometric uptake ratios for the >5 µm particles were similar to total >0.2 µm particulates for all elements (Table 7).

Table 7: Average (and Standard Deviation) elemental uptake rates for carbon (C), silica (Si) and iron (Fe), and average stoichiometric ratios at P3. NA indicates not determined.

	P3A		P3B		P3C	
	Total	>5 µm	Total	>5 µm	Total	>5 µm
Uptake rates						
Carbon (C, µmol C L^{-1} d^{-1})	21.00 (5.80)	12.76 (0.71)	8.01 (1.12)	6.70 (1.25)	4.75 (2.06)	3.56 (0.46)
Silica (Si, µmol Si L^{-1} d^{-1})	0.58 (0.15)	0.47 (0.05)	0.03 (0.004)	0.04 (0.01)	0.08 (0.01)	0.07 (0.02)
Iron (Fe, nmol Fe L^{-1} d^{-1})	0.20 (0.04)	NA	0.18 (0.03)	0.12 (0.03)	0.14 (0.01)	0.14 (0.04)
Stoichiometry						
Si:C (mol:mol)	0.028	0.037	0.004	0.006	0.017	0.019
Fe:C (µmol:mol)	9.50	NA	22.50	17.90	29.50	39.30
Fe:Si (µmol:mol)	0.35	NA	6.00	3.00	1.75	2.00

3.3.4 Remineralisation experiments

The remineralisation experiments were performed three times, once during each sampling period (P3A, P3B and P3C). Each experiment consisted of 3 time points after the stage 2 resuspension, each of these time points were a separate standalone bottle and so represents a pseudo time series.

Following stage 1 resuspension of the >5 µm particulates, the activity associated with these particulates becomes the carried over total activity for stage 2. The retention or redistribution of the carried over total activity into size fractionated particulates or the dissolved fraction were then assessed. Comparison of the activity within the carried over total from stage 1 to the retention of activity in the measured particulate (all particulates, >0.2 µm) within stage 2 for ^{14}C were statistically ($p<0.05$) indistinguishable for all but a single time point. As such, the majority of activity remained in the particulate fraction for 5-6 days when the community was kept in the dark. For ^{32}Si and ^{55}Fe the carried over total and particulates were statistically different ($p<0.05$) in 30 and 60 % of the time points respectively, indicating a measurable dissolved fraction (

Figure 11). In keeping with decreasing biomass (Figure 4) and decreasing uptake of each isotope from P3A to P3C (Table 7), the particulate activity for ^{14}C and ^{32}Si also decreased whilst ^{55}Fe showed less variability (

Figure 11). The ^{55}Fe data was offset the furthest beneath the 1:1 line indicating greatest measurable dissolved activity (

Figure 11).

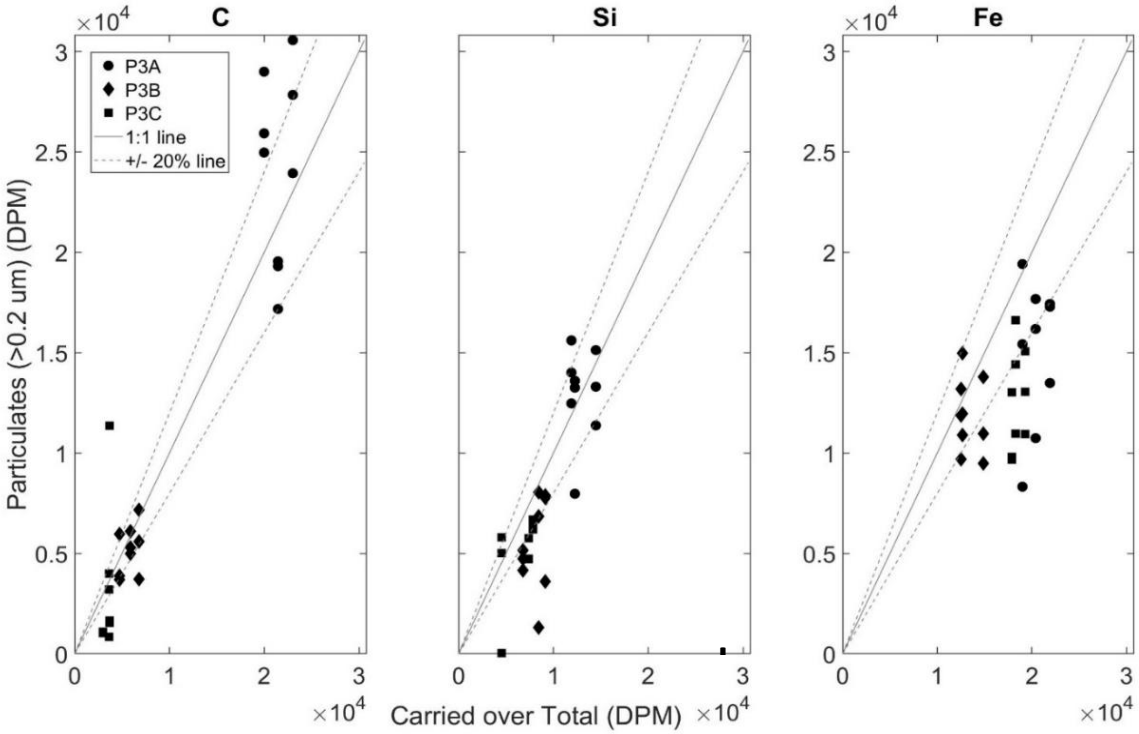

Figure 11: Carried over total to particulate activity relationship in disintegrations per minute (DPM) for ^{14}C, ^{32}Si and ^{55}Fe in panels a, b and c respectively. Each panel plots all triplicates from each experiment, P3A (circles), P3B (diamonds) and P3C (squares) alongside a 1:1 line (solid grey line) with ±20 % offset lines (dashed grey lines). Data points beneath the line represent less activity in the particulate fraction than the carried over total fraction and indicate a loss of particulate activity into the dissolved fraction.

3.3.4.1 Carbon and silica cycling

In the majority of time points (80 %), the ^{14}C particulate activity remained within the >5 µm particles, with only a single time point each during the P3A and P3B experiments showing a significant (*p<0.05*) measurement of ^{14}C in the <5 µm particles. This coupled with only 10 % of time points having measurable activity in the dissolved fraction indicates very limited remineralisation of ^{14}C. Acid labile dissolved ^{14}C, assumed to be DIC, was however detected in all time points of all experiments, presumably indicating continuous respiration of the fixed ^{14}C.

For ^{32}Si, there was also little evidence of remineralisation or dissolution (i.e., movement of ^{32}Si into the smaller particles and/or into the dissolved phase) with 90 % of time points showing particulate activity retained within the >5 µm particles and only a single time point at P3A resulting in a significant measurement (*p<0.05*) of ^{32}Si in the small particle fraction (<5 µm). Measurable activity in the dissolved fraction was only detected in 30 % of time points.

3.3.4.2 Iron cycling

Out of the 3 isotopes, ^{55}Fe showed the greatest transfer of activity from the particulates into the dissolved fraction (

Figure 11). Carryover of the ^{55}Fe from resuspension could only come from the particulate material carried across, and so this is the only possible source of ^{55}Fe in the dissolved phase during the subsequent time points.

Following the resuspension of the >5 µm sized particulates, where all of the ^{55}Fe activity was associated with particles (both intra and extra-cellular) at day 0 (or T0), the subsequent transfer of the ^{55}Fe into smaller particles (potentially due to phytoplankton cell fragmentation and/or remineralisation, microzooplankton or bacterial cell uptake or adsorption) or into the seawater (dissolved and stuck to the bottle walls) of the sample was assessed. We classify the partitioning of the isotope as being either 'Particle Associated' (PA; ^{55}Fe activity associated either intra and/or extra-cellularly) or 'Seawater' (SW; ^{55}Fe activity either in the dissolved fraction or stuck to the bottle walls). Given the extant community was dominated by diatoms throughout our sampling at P3 (Poulton et al., COMICS SI), we assume that the >5 µm fraction (grown from nutrient addition to the surface water community), and resuspended into stage 2 of the remineralisation experiments, was also diatom dominated.

From the first experiment at P3A, the >5 µm resuspended particulates dominated the total (>0.2 µm) particulate pool throughout the experiment (Figure 12) in that there was no measurable evidence of activity within the <5 µm size fraction particulates at any time point (Figure 12). Throughout the P3A experiment, the largest proportion of the total activity remained associated with the particles rather than in the seawater (Figure 12), although 30-40% of the activity was transferred from the PA fraction into the SW fraction.

During P3B, the particulate size fraction was again dominated by the >5 µm particles as with P3A, however after 1 day and 4 days incubation there was significant ($p<0.05$) measurable <5 µm particulate activity (Figure 12). This transfer of ^{55}Fe from the re-suspended large particles to small particles could be as a consequence of cell fragmentation and/or the uptake of isotope by small phytoplankton, heterotrophic flagellates or bacterial cells found in the mesopelagic water used for re-suspension. However, all of the small size fraction associated ^{55}Fe was extra-cellular, so was adsorbed onto cell surfaces rather than taken up intracellularly. Further, ~20 % of total activity was in the seawater fraction after 1 day and 4 days (Figure 12), again indicating movement of activity off (or out) of the particles.

Consistent with the other experiments, the P3C activity in the >5 µm particles remained dominant at all time points. For P3C, only the first time point (at day 1 post resuspension) showed significant (*p<0.05*) activity measurable in the <5 µm particulates. This single time point indicated the strongest evidence of remineralisation (i.e., a transfer of elements from particle associated to the seawater phase and/or uptake by small particulates) as the measurable activity associated with the <5 µm particles contained non-adsorbed (i.e., potentially intra-cellular) ^{55}Fe contributing to 60 % of the <5 µm particle associated ^{55}Fe (Figure 12). From our results, it is unclear if the small particles were fragments from breakdown of the re-suspended phytoplankton cells or bacterial cells within the resuspension seawater. However, the persistence of both ^{32}Si and ^{14}C within the >5 µm fraction indicates cell fragmentation was likely limited. Within the P3C experiment, there was detectable (~32 % of the total activity) transfer of particulate associated ^{55}Fe into the 'seawater' of which 24 % was in the dissolved fraction and 8 % stuck to the walls after 1 day (Figure 12). While the dissolved proportion decreased (with no measurable dissolved fraction after 5 days), increased ^{55}Fe was scavenged onto the incubation bottle walls (Figure 12).

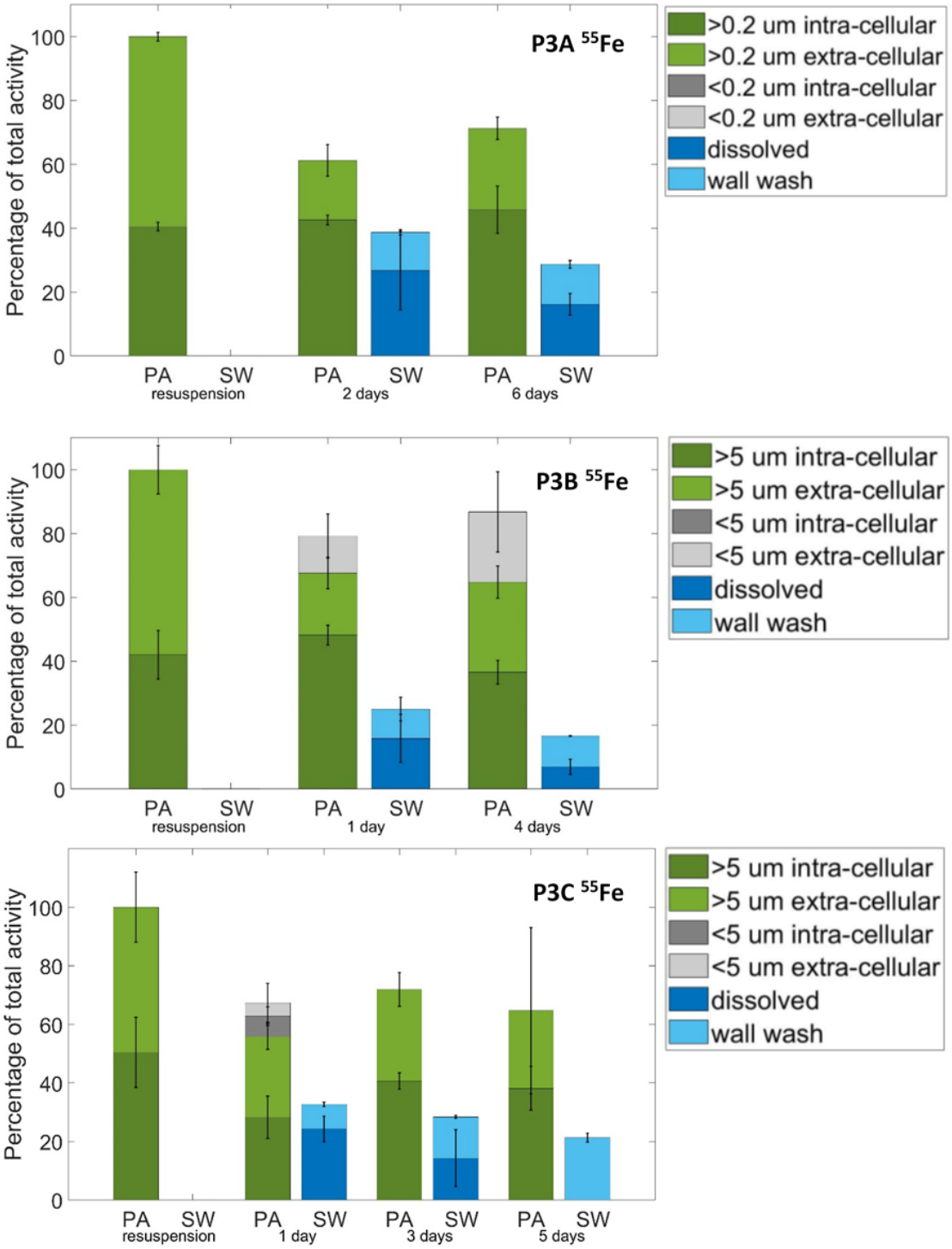

Figure 12: Relative contribution of each ^{55}Fe fraction to the total activity per time step in each experiment highlighting the presence or absence of ^{55}Fe in the small particulate size fraction and the dissolved phase. For P3B and P3C, PA is particulate associated ^{55}Fe, either >5 µm intra-cellular (dark green) or >5 µm extra-cellular (light green), or <5 µm intra-cellular (dark grey) or <5 µm extra-cellular (light grey) – P3A the size fractions are >0.2 and <0.2. SW is seawater associated ^{55}Fe, dark blue is the dissolved fraction and light blue is the wall wash fraction. Absence of a coloured fraction means that fraction was not significantly measurable at that time point. Error bars are shown as 1 standard deviation from triplicate samples.

3.3.4.3 Synthesis of remineralisation experiments

Dissolved inorganic ^{14}C was measurable at all time points of all experiments and indicated that respiratory loss from the particulate organic pool was likely the main process transferring ^{14}C from the particulate to dissolved fractions. Dissolved ^{32}Si had measurable activity in only 30 % of the time points indicating limited loss of Si from the particles. In support of such evidence of limited remineralisation of the particles into the dissolved phase, both ^{14}C and ^{32}Si similarly showed only a single time point each of activity in the <5 µm particulate fraction, however it is unknown in this case if the smaller particulates were fragments from the re-suspended phytoplankton or bacterial cells within the whole seawater used for resuspension.

In contrast to both ^{14}C and ^{32}Si, the presence of ^{55}Fe in the 'seawater' fraction was measurable in all experiments at all time points, right from the first sample point post resuspension from the T0 time point, where there would be by definition no dissolved or wall associated activity. In all experiments, the dissolved activity increased to between 7 % and 26 % of the total activity in the bottle, while the wall wash activity increased by between 8 % and 22 % (Figure 13). Moreover, the extra-cellular adsorbed ^{55}Fe on particles simultaneously decreased from the start of all experiments and time points (apart from time point 2 in P3B where the change was insignificant), dropping from 58 to 63 % of the total activity at T0 to 19 to 50 % of the resuspended total activity in subsequent time points (Figure 13). Given that the non-adsorbed (internal) particle associated ^{55}Fe did not display large changes from resuspension (Figure 13), the loss of adsorbed ^{55}Fe is the only likely source for the increases observed in ^{55}Fe in the dissolved pool and adhered to the bottle walls. Only a single time point measured intra-cellular ^{55}Fe in the small particle fraction (Figure 12). Presumably, all of the dissolved ^{55}Fe was at least transiently available for uptake by the organisms present, potentially indicating (re)cycling of ^{55}Fe between extra-cellular adsorbed to dissolved phase followed by uptake to become intra-cellular, or direct uptake of adsorbed extra-cellular ^{55}Fe. Following the initial significant transfer of adsorbed particle associated ^{55}Fe into both seawater associated phases (dissolved or stuck to bottle walls), there was no further significant measurable transfer of ^{55}Fe across subsequent time points. This implies that the processes responsible for the transfers observed had broadly reached equilibrium by the time of the first sampling point in all experiments (i.e., after 1-2 days).

Turnover rates for each isotope were calculated by the loss in particulates from resuspension to the last time point. The average turnover rate of ^{14}C was 0.03 d^{-1} (turnover only measurable for a single experiment) and similarly ^{32}Si average turnover rate of 0.03 ± 0.01 d^{-1}, whilst ^{55}Fe turned over at an average rate of 0.06 ± 0.03 d^{-1}.

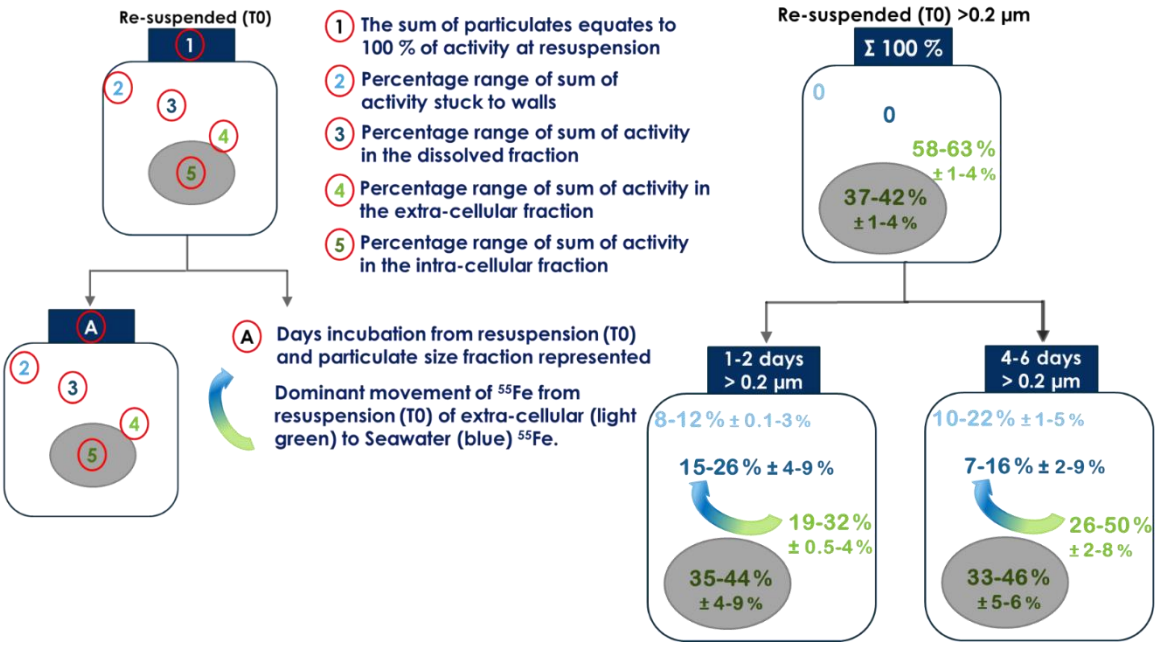

Figure 13: Summary plot of all 3 experiments showing ^{55}Fe fractions change from re-suspension into subsequent time points for all particulates (>0.2 µm fraction), showing movement of extracellular ^{55}Fe into the seawater. The top bottle represents the distribution at resuspension (T0) and the bottom bottles represents the distribution of ^{55}Fe at the stated incubation time. Each percentage distribution represents the range from all 3 experiments. All error ranges are 1 standard deviation from triplicate samples.

3.4 Discussion

3.4.1 Iron limitation

We sampled the marked annual naturally Fe fertilised phytoplankton bloom north of South Georgia during a strong change in bloom characteristics (Poulton et al., COMICS SI) around and shortly after the peak chlorophyll concentration (Figure 4). Phytoplankton populations within the bloom at P3 were Fe limited during our sampling, as indicated by low (<0.3) absolute values of Fv/Fm (Kolber et al., 1998; Greene et al., 1992; Moore et al., 2005; Nielsdottir et al., 2012) and, importantly, significantly increased values rapidly followed Fe amendment (Figure 10a). Development of Fe limitation during the bloom is consistent with previous observations around South Georgia (Nielsdottir et al., 2012; Hinz et al., 2012) and other sub-Antarctic island systems (Moore et al., 2007a&b; Blain et al., 2007). However, Fe stress appears to be less severe later in summer and in autumn within the bloom region (Holeton et al., 2005; Nielsdottir et al., 2012; Hinz et al., 2012).

Surface dFe concentrations concurrent to the Fe limitation experiments ranged from 0.03 to 0.17 nM (Figure 9, Table 4), indicative of conditions of low Fe bioavailability (<0.5 nM; Johnson et al., 1997). Despite overall low concentrations of Fe (Figure 9), alongside other bioactive trace metals such as Co, Cu, Ni, Mn and Zn (Figure 25 in Appendix A), within surface waters, there was some evidence of increasing near surface concentrations of Fe over the occupations of P3, potentially indicating remineralisation of Fe within and below the diatom bloom. During P3A there was a loss of surface biomass so potentially less Fe demand as the surface community shifted to a recycling regime (Poulton et al., COMICS SI). However, mixing (Blain et al., 2007) could also have contributed to the increased surface concentrations of Fe. This slightly increasing dissolved Fe pool may reduce Fe stress, as indicated by increasing Fv/Fm from P3B to P3C of 0.35 to 0.40 (Figure 10a).

The observed Fe stress, combined with low (<2 µM) upper ocean Si concentrations (Poulton et al., COMICS SI, Table 4) may both have been contributing to the decline in bloom intensity following the P3A sampling period (Figure 4, Table 4). As with other island systems (Planquette et al., 2007), enhanced Fe is likely to accumulate proximal to the islands and shallow sediments around South Georgia in the low light conditions of autumn and winter (Holeton et al., 2005; Nielsdottir et al., 2012). Onset of the bloom in spring would be expected to rapidly deplete Fe and other trace metals (Figure 9; Figure 25 in Appendix A), resulting in the development of significant Fe stress within an extant population dominated by large celled diatoms (Korb et al., 2010). Diatoms, which dominated the bloom, are lost through a combination of grazing (Cook et al., COMICS SI) and export (Henson et al., COMICS SI). These loss mechanisms, potentially combined with termination of the increasing phase of the bloom in part due to Fe limitation (Figure 10) and Si stress (Poulton et al., COMICS SI) will thus contribute to the export of multiple elements, including Fe, from the mixed layer (Boyd et al., 2017).

3.4.2 Uptake and particulate stoichiometry

The observed Si:C uptake ratios (<0.04 mol mol^{-1}) are low compared to average values for diatoms (0.13 mol mol^{-1}; Brzezinski, 1985). These low values in our experiments are similar to those measured for the *in-situ* community at P3 for Si:C uptake (0.04-0.07 mol mol^{-1}) and lightly silicified diatom species such as *Chaetoceros sp*. and *Pseudonitzscia sp*. (Brzezinski, 1985), whereas the Si:C ratios for the upper ocean standing stocks indicated heavily silicified cells (0.30-0.57 mol mol^{-1}; Poulton et al., COMICS SI). This discrepancy between low Si:C ratios for uptake relative to high Si:C ratios for the standing stock likely relates to decreasing Si availability and hence a shift towards lower silicification rates and potentially more lightly silicified diatom species accompanied by export of the more heavily silicified community from the earlier bloom phase (Poulton et al., COMICS SI).

In contrast to C and Si uptake, which can be considered indicative of the ambient conditions due to the tracer concentrations of ^{14}C and ^{32}Si added, measured Fe uptake should be considered potential upper bounds as significant increases (+2 nM unlabelled Fe and 1.85 nM ^{55}Fe) above the ambient Fe concentrations (0.03 - 0.17 nM (Figure 9, Table 4) are associated with the additions made to the surface community. Correspondingly, the calculated Fe:C ratios (9.5 – 29.5 µmol mol^{-1}) thus unsurprisingly fall towards the upper end of observed culture ranges (0.7 to 70; Strzepek et al., 2012), while also increasing from P3A (Fe:C = 9.5 µmol mol^{-1}) to P3C (Fe:C = 29.5 µmol mol^{-1}) indicating an increase in Fe uptake potential. Although the low dFe concentrations observed during the sampling period (Figure 9) suggest that these high Fe:C uptake values may not have been reached *in-situ*, they do indicate significant potential for rapid biotic Fe accumulation (Schlosser et al., 2018).

Comparing surface PFe concentrations of around 1 nM (Figure 9) with POC concentrations of around 14-32 µM (Table 4), surface PFe:POC (Fe:C) were around 31 to 70 µmol mol^{-1} during the sampled stages of the bloom. These ratios were comparable with, although slightly higher than, our calculated potential uptake ratios, suggesting a proportion of the PFe pool may be lithogenic (Schlosser et al., 2018). Irrespectively, the observed export of particulate material from the surface during the bloom, combined with shallow C remineralisation (Giering et al., COMICS SI) were both likely to have been significant factors contributing to the observed surface dFe and PFe minima and mesopelagic PFe maxima at depths of ~160 m (Figure 9), alongside that of other trace metals (Figure 25 in Appendix A).

3.4.3 Remineralisation

The fate of both major (C, Si) and minor (Fe) elements within any exported material will depend on a number of biotic and abiotic processes (Boyd et al., 2017). We thus investigated the potential importance and magnitude of different processes within a series of controlled remineralisation experiments. The fresh radio-labelled surface particulates generated within stage 1 of these experiments would have been dominated by diatoms, as with the surface *in-situ* community (Poulton et al., COMICS SI). Resuspension of this material in mesopelagic water resulted in relatively restricted movements of isotopes between different phases (Figure 12, Figure 13). Particles labelled with ^{14}C and ^{32}Si showed little evidence of isotope transfer from particulate into the dissolved phase. In contrast, particles labelled with ^{55}Fe indicated a consistent transfer from the particulate-associated pool into the 'seawater' pool, with this transfer occurring relatively rapidly (<24 – 48 hrs) before the first sampling time point (Figure 12, Figure 13).

Some limited accumulation of ^{14}C in the dissolved pool was detected at all time points in the dissolved acid-labile fraction (i.e. ^{14}C labelled dissolved inorganic carbon). It is unlikely that any significant proportion of the ^{14}C labelled dissolved inorganic C pool resulted from carryover of the initially added ^{14}C bicarbonate from stage 1, as particulates were rinsed twice with ~50 mL of unlabelled, 0.2 µm filtered mesopelagic seawater prior to re-suspension. Consequently, this pool most likely resulted from respiration of (photosynthetically fixed) ^{14}C labelled particulate organic C. To determine if the respiration was from the re-suspended diatom dominated surface particulates or from bacteria that may have taken up dissolved organic ^{14}C released from the diatoms and subsequently respired it as $DI^{14}C$, a parallel experiment was performed at P3B that pre-filtered (0.2 µm) out bacteria from the resuspension water collected from the mesopelagic. The dissolved inorganic ^{14}C results of the filtered (surface >5 µm particulates only) relative to 'whole' (surface particulates and mesopelagic community) samples were not significantly different ($p<0.05$). This strongly supports the suggestion that the respiration of fixed C to aqueous CO_2 ($PO^{14}C$ to $DI^{14}C$) is from the >5 µm particulates carried over from the first phase of the experiments rather than uptake by mesopelagic bacteria followed by respiration. Evidence of respiration within stage 2 of the experiments indicates that the diatom cells remained metabolically active after being incubated in the dark, and that bacteria mediated remineralisation did not contribute to the respiration signal. Further evidence for the lack of bacterial remineralisation is provided by almost no subsequent appearance of ^{14}C activity in the small particle fraction. Within the parallel ^{32}Si experiments, the small particulate fraction (<5 µm) only had measurable activity for a single time point in one of the three experiments, supporting the evidence of a lack of remineralisation and dissolution of the diatoms. Dissolution of $bSiO_2$ requires bacterial activity to remove the organic matrix before

chemical dissolution can act on the $bSiO_2$ (e.g., Bidle and Azam, 1999), which presumably did not occur within our experiments.

Consistent with the results for the major elements C and Si, there was little evidence for bacterial mediated remineralisation for Fe (indicated by isotope activity in small particles), with only a third of all the ^{55}Fe labelled experimental time points having statistically measurable activity in the <5 µm particulates and only one of these time points indicating intra-cellular rather than adsorbed ^{55}Fe. Bacteria might be expected to remineralise small particles faster than large particles (Cavan et al., 2017b), so the experiment timeframes with large (often >50 µm; Poulton et al., COMICS SI) live diatoms may not have been long enough for the bacteria to break down the particles (cells), despite being more than double the duration of a previous equivalent series of remineralisation experiments (Boyd et al., 2010).

The mesopelagic water for re-suspension from 110 m contained a bacterial abundance of 319 $x10^3$ cells mL^{-1} (Rayne et al., COMICS SI; Table 4), whereas a similar experiment that focused on Fe remineralisation by surface bacteria recorded an abundance of 410 to 560 $x10^3$ cells mL^{-1} and observed rapid (within 72 hours) remineralisation of about 40 % of the Fe (Boyd et al., 2010). In these previous experiments, the activity in the small size fraction suggested rapid colonization of the phytoplankton cells by heterotrophic bacteria (Boyd et al., 2010). The slightly higher bacterial abundance in surface waters compared to our mesopelagic abundance could be a contributing factor as to why we observed less transfer of the labelled isotopes into the smaller particulate size fraction. Bidle and Azam (1999) concluded that colonisation intensity rather than overall bacterial abundance had the greatest effect on remineralisation rates. Boyd et al. (2010) and Bidle and Azam (1999) are the only semi-comparable experiments to those we performed. Both showed stronger evidence of remineralisation, though resuspended different phytoplankton populations in warmer surface waters (16 to 18 ^oC, Bidle and Azam, 1999). Boyd et al. (2010) samples were dominated by haptophytes, which are likely more susceptible to remineralisation than the Southern Ocean diatoms in our experiments. Conversely, while Bidle and Azam (1999) used various species of diatoms, one heavily and one lightly silicified, their experiments used already lysed diatoms to represent diatom detritus rather than a living diatom community (see also Chapter 4).

Lack of significant remineralisation in our experiments thus likely resulted from the relatively short (5-8 day) incubation duration in cold waters, the dominance of the freshly produced particulates by large, live diatoms and potentially low bacterial abundance in the upper mesopelagic. Bacteria have been shown to act on live diatoms (e.g., Passow et al., 2003) in an experiment with a plankton wheel simulating sinking. However, our experimental results are more consistent with *in-situ* observations which conclude that large diatoms can sink intact, biologically retaining the micro-nutrients (and

the C) and increasing the remineralisation length scale of various elements (Twining et al., 2014). Indeed, although relatively short, the 5 to 8 day duration of our experiments would be comparable to transit times out of the 70 m mixed layer (Carvalho et al., COMICS SI) and through the upper mesopelagic (100-300 m) given even modest sinking rates of 18 to 60 m d^{-1} for large diatoms (see Villa-Alfageme et al., COMICS SI).

The particulates generated within stage 1 of our experiments were likely dominated by diatoms which were significantly enriched in Fe relative to the Fe limited *in-situ* surface community (Figure 10). Consequently, these organisms might be expected to have an enhanced potential to persist in our simulated dark mesopelagic conditions relative to the *in-situ* community. However, measured values of quantum efficiency (Fv/Fm) of photosynthetic cells of sinking material collected in PELAGRA sediment traps (see Manno et al., COMICS SI) were frequently comparable to surface values for collection depths shallower than 250 m, and on one occasion for a collection depth of 500 m, strongly suggesting that live diatoms were an important export vector *in-situ* during our sampling of P3. Consequently, apparent shallow C remineralisation *in-situ* within the sampled declining bloom (Giering et al., COMICS SI) must be coupled with processes not captured in our experiments, likely due to a different export vector and/or other processes acting on sinking diatoms within the mesopelagic such as grazing or viral lysis.

3.4.4 Abiotic release and implications for iron cycling

The most significant transfer of ^{55}Fe we observed was via the (re-)mobilisation of the adsorbed (extra cellular) pool into the dissolved phase (Figure 12 and Figure 13). This pool comprised over 58 % of the total activity carried over from stage 1 in all experiments, but reduced rapidly to less than 50 % of the total in the majority of time points and contributed to a significant measurable increase in the seawater (dissolved and stuck to incubation bottle walls) fraction (Figure 12). Boyd et al. (2010) concluded that rapid colonisation of the phytoplankton cells by heterotrophic bacteria facilitated Fe transfer in their experiments, however they did not distinguish been intra-and extra-cellular associated ^{55}Fe. The mobilisation of adsorbed ^{55}Fe into the non-particle associated phases was key in determining the cycling of Fe in our experiments, as well as our tracking of the ^{55}Fe activity stuck to the bottle walls and its consideration as part of the total activity. Adsorbed ^{55}Fe (from the total particulates) present at the point of resuspension was transferred into the dissolved and wall wash fractions by the first time-point in all experiments. Relating our experiments to *in situ* Fe cycling is complicated by a range of factors. Given the extensive production of organic matter within the bloom, it is likely that biogenic material dominated overall particulate matter both in the

surface and subsurface. However, *in situ* acid labile Fe:POC ratios suggested that the total PFe pool may have been comprised of a proportion of lithogenic Fe, which may be more prone to scavenging than regeneration (Bressac et al., 2019). Such lithogenic Fe could be a contributing factor to the transfer of mesopelagic Fe from the adsorbed extra cellular pool into the dissolved phase rather than being available for uptake or biological remineralisation. However, it is likely that the majority of the acid (HCl) labile Fe was biogenic.

The (re-)mobilisation of adsorbed Fe we observed in our experiments would be expected to depend on a range of factors, including the concentration and affinity of ligand binding sites of the total particulate pool and in the seawater. The design of our experiments resulted in a ~1:4 dilution of the particulate density between the 1st and 2nd stage. Consequently, depending on ligand concentrations and binding strengths in surface and mesopelagic waters, it is highly likely that the ligand binding equilibrium was significantly altered between the two experimental stages. Moreover, the 2 nM addition of unlabelled Fe and 1.85 nM ^{55}Fe would mean that dFe concentrations during stage 1 of our experiments would have been significantly higher than those during stage 2, which, in the absence of other changes, would have favoured re-mobilisation of adsorbed Fe. Further, as the particulate (both intracellular and adsorbed) pools of ^{55}Fe dominate the initial condition within stage 2 of our experiments, the ability to resolve abiotic exchange will be biased towards any initial de-adsorbtion, while any subsequent re-adsorption would be difficult to observe, let alone quantify.

Consequently, due to the likely complex kinetic and equilibrium processes involved in (re-)adsorption processes, it is difficult to quantitatively relate the mechanisms we observed in our experiments to those which may be occurring *in-situ*. However, given the magnitude of abiotic release, which was on the order of 10-40 % of the particulate pool (Figure 13) such a process could be significant *in situ*. For example, if a similar fraction of the particulate Fe concentrations of up to 4 nM in the upper mesopelagic (Figure 9b), were involved in such a process, this could have a significant impact on the 0.2-0.6 nM dFe pool *in situ* (Figure 9a). Thus the enhanced observed particulate and dissolved Fe concentrations (and other trace-metals) within the upper mesopelagic (Figure 9) suggest that such abiotic processes need to be considered in the context of Fe cycling (Boyd et al., 2017). Specifically, though caution needs to be applied in inferences from repeat observations at a fixed station due to potential advective effects, it is at least conceivable that abiotic release from sinking material, which presumably constitutes at least some of the PFe (Figure 9b), could be responsible for a substantial fraction of the apparent increase in sub-surface dFe as the bloom declined and significant organic material was exported from the surface. Similarly, abiotic release from biogenic particles may be significant for other elements (Janssen et al.,2021) and may thus influence sub-surface profiles of other biologically active elements (Figure 25). If such

a process were indeed significant *in situ*, such rapid (in our case at least <2 days) abiotic release of adsorbed Fe could act to retain this limiting micro-nutrient within the upper mesopelagic, potentially resupplying the surface biota and maintaining the bloom through any subsequent mixing into the euphotic zone (Blain et al., 2007; Boyd et al., 2015). Although the reversibility of the (de/re-adsorption) process would again need consideration. Enhanced dFe concentrations at depth (Figure 9a) and/or a potentially available adsorbed Fe pool also has potential consequences for the fate of exported material. Any exported live diatoms are likely to be deficient in Fe, as indicated by the low surface concentrations (Figure 9) and clear evidence of surface mixed layer Fe limitation (Figure 10). Access to a sub-surface pool could thus prolong the viability of phytoplankton that have sunk out of the euphotic zone, through replenishing cellular Fe. Hence this could be speculated to increase resistance to remineralisation, increasing C and Si remineralisation length scales, and potentially increasing the chance of these deep diatom populations being to be mixed back into the upper ocean. Overall, albeit within our experimental context, the (re-)mobilisation of adsorbed Fe resulted in significant decoupling of C, Si and Fe cycling, with calculated particulate losses corresponding to average turnover rates of 0.06 (± 0.03) d^{-1} for ^{55}Fe, which were twice those of both ^{14}C and ^{32}Si.

3.5 Conclusions

We sampled during the peak and post-peak phase of the South Georgia spring bloom, which had reduced surface Fe concentrations and Fe limited phytoplankton. Recycling and mixing of Fe potentially increased the upper ocean dissolved Fe pool, reducing the Fe stress (as indicated by Fv/Fm) of the phytoplankton community. The bloom was diatom dominated, and these organisms can act as recognised vectors of Fe export to the deep-sea (Hutchins and Bruland, 1998; Twining et al., 2015). Iron associated with the exterior of the cells (adsorbed extracellularly) may be released rapidly as these cells are transferred to depth. Ultimately, the kinetics and equilibrium conditions of such exchange will be influenced by ligand binding site density on cell surfaces of phytoplankton, bacteria, and other particulates, as well as in the dissolved ligand pool. However, the magnitude of any such de-absorption at least has the potential to drive substantial differences in the sub-surface dFe concentrations. Given the apparent resistance to degradation intracellular pools of Fe (along with C and Si) would be expected to be exported to deeper depths with a slower turnover rate if processes such as grazing or cell lysis do not act to break cells up and speed up remineralisation. Our experiments indicate that mesopelagic microbial communities are not the main agents of remineralisation acting directly on sinking healthy, diatom cells. Such a lack of microbe-mediated respiration, dissolution and cell breakdown would tend to increase the remineralisation length scale of the intra-cellular Fe as well as the C and Si, suggesting that other processes (e.g. zooplankton grazing, viral lysis) are important in driving any shallow remineralisation.

Chapter 4 Dead or Alive? Influence on Fe, C and Si remineralisation pathways

4.1 Introduction

The remineralisation experiments from South Georgia at P3 (detailed in Chapter 3) concluded that mesopelagic microbial communities are likely not the main primary remineralisation process acting on sinking, large, healthy, diatom cells with little Si dissolution.

Due to their high sinking rates (Armstrong et al., 2002, Assmy et al., 2013) diatoms have the capacity to transfer organic C and biogenic silica ($bSiO_2$) from the productive surface layer to the deep ocean (Smetacek, 1985; Smetacek et al., 2012) with the possibility of remineralisation of the macro and micronutrients at all depths (Twining et al., 2014). As a result, diatoms are widely identified as the most relevant phytoplankton group for understanding organic C cycling (Smetacek et al., 2012; Krause and Lomas, 2020). The viability of diatoms allows them to maintain the organic membrane surrounding their silica (Si) frustule, this protective membrane is very effective in obstructing dissolution, even in the presence of an active microbial community (Moriceau et al., 2007; Nelson et al., 1976; this thesis Chapter 3). The removal of the protective membrane once diatoms are unable to maintain it is regulated by microbial activity (Patrick and Holding, 1985), microbial composition, and the environmental conditions affecting the microbial community (Bidle and Azam, 1999, 2001; Bidle et al., 2002). Dissolution of the exposed frustules then occurs that depends on the silicic acid concentration, temperature, pH, salinity and pressure of the seawater (Cappellen and Qui, 1997; Hecky et al., 1973; Kamatani et al., 1988; Loucaides et al., 2008) and the characteristics of the diatom frustules themselves (composition, thickness, reactive surface area) (Passow et al., 2011). Aggregation of diatom cells or package within fecal pellets can also influence dissolution rates compared to dispersed cells with dispersed cells showing faster dissolution (Passow et al., 2003).

Live particulate organic carbon (POC) of viable phytoplankton cells can release dissolved material that the bacteria can directly consume (Sondergaard and Schierup, 1982; Chróst, 1991; Nakano, 1996) whereas dead cells need more effort by the bacteria to break down via

hydrolytic enzymes for subsequent uptake and remineralisation of the POC (Davis and Mahaffey, 2017). In the specific case of the diatom communities that can represent a significant fraction of export flux, particularly in the Southern Ocean, the frustule and any organic coating of the frustule can play a significant role. For example, experiments by Bidle and Azam (1999) show that surface bacterial colonisation of lysed diatoms hastens the dissolution of the Si frustules by degrading the organic matrix which protects the Si from dissolution. The microbial destruction of the protective membrane and the subsequent dissolution have been studied in detail (see review by Ragueneau et al., 2006), whereas the relative remineralisation of iron (Fe) and C post Si dissolution has not been investigated once the diatom viability has been compromised.

Diatoms that avoid grazing can sink through the water column into the mesopelagic zone and undergo cell lysis in response to physiological stress such as light limitation (Berges and Falkowski, 1998) as well as sinking intact (Martin et al., 2011; this thesis, chapter 3). It has been observed that the $bSiO_2$ dissolution rate increases with depth (Bidle et al., 2003), not as a consequence of increased bacterial colonisation but by the progressive removal of the organic matter from frustules during sinking (Bidle et al., 2003).

Building on the work by Bidle and Azam (1999) and the results from upper mesopelagic remineralisation experiments detailed in Chapter 3, we compared the relative remineralisation rates of Si, C and Fe in two scenarios, lysed diatoms and intact diatoms, in the upper mesopelagic. We hypothesised that the lysed diatoms would be unable to maintain their protective coating and be more susceptible to microbial activity (Patrick and Holding, 1985) and subsequent Si dissolution (Rageuneau et al., 2006) and C and Fe remineralisation than the intact diatoms. This would be observable by greater radio isotope activity in the dissolved pool for the experiments incubating lysed diatoms.

The original remineralisation experiments from P3 were repeated at a different site in the Benguela upwelling system off south-western Africa, with methodological differences aimed at investigating, the use of diatom detritus generated using a free/thaw process, instead of live cells, to assess the remineralisation potential of dead cells in the upper mesopelagic. The comparison of whole vs detrital cells remineralisation potential was the main objective of participating in the DY090 Benguela cruise.

4.2 Material and Methods

The remineralisation experiments followed the method detailed in section 2.5 for the whole and detrital cell resuspensions

4.2.1 Statistical analysis

A one-way analysis of variance (ANOVA) and a post hoc Bonferroni multi comparison test were performed on each time point for each fraction (>5 µm particulates, <5 µm particulates, dissolved and DIC) between the whole and detrital incubations, and South Georgia vs Benguela comparison (see section 6.2.1). Differences were considered statistically significant at $p<0.05$ and indicated in the plots as different letters.

Data validation detailed in section 2.5.1 were performed on the remineralisation DPMs. The measured total samples were deemed invalid as the raw DPMs were below the background threshold level of the scintillation counter. The carried over total between stage 1 and stage 2 resuspension were used instead of the measured total at stage 2. Also the non-rinsed/washed particulate samples (^{55}Fe associated both intra and extra-cellular) did not consistently have the same or greater DPMs (within 1 standard deviation) as the rinsed/washed particulate samples indicating that the Ti-EDTA wash did not work, therefore the division between intra- and extra-cellular Fe could not be made.

4.3 Results

4.3.1 Phytoplankton uptake of Fe, C and Si at Benguela

Total uptake rates and ratios of ^{55}Fe, ^{14}C and ^{32}Si by surface phytoplankton were calculated after 48 hr incubations approximating *in-situ* light and temperature conditions (Table 8). Corresponding with the low surface chlorophyll-*a* (0.06 - 0.14 mg m^{-3}) dominated by picoplankton (0.2-2 µm), low surface nitrate (0.08 – 0.40 µM) and low $bSiO_2$ (2.33 – 7.86 µM), the uptake of C and Si isotopes were the lowest at the Benguela South (BS) site, with total C uptake of 0.85 µmol C L^{-1} d^{-1} and total Si uptake of 0.003 µmol Si L^{-1} d^{-1} (Table 8). At the Benguela North (BN) site total C and Si uptake rates were higher but more variable between occupations, with BN.1 experiencing higher total uptake rates compared to BN.2 (Table 8). The first occupation of BN had a total C uptake rate of 11.88 µmol C L^{-1} d^{-1} which reduced to 9.11 µmol C L^{-1} d^{-1} at BN.2 (Table 8). Total Si uptake rates declined further between occupations from 0.16 to 0.02 µmol Si L^{-1} d^{-1} (Table 8). BN was thus considerably more productive than BS, with ~>10-fold higher C and Si uptake rates, while BN.1 was also more productive than BN.2, with higher chlorophyll-*a* and a community dominated by large phytoplankton and subsequently lower nitrate and higher $bSiO_2$ concentrations (see Table 5 for comparison) . Total Fe uptake was more consistent between BS and BN with Fe uptake rates of 2.92 nmol Fe L^{-1} d^{-1} at BS and 3.10 and 2.64 nmol Fe L^{-1} d^{-1} at BN.1 and BN.2, respectively (Table 8).

All total Si:C uptake ratios were low, ranging from 0.002 to 0.01 mol mol^{-1} (Table 8) and indicative of either a significant fraction of community production by non-diatoms and/or lightly silicified diatoms with BN.2 5-fold lower than BN.1. Ratios of Fe:C uptake ranged from 0.26 and 0.29 µmol mol^{-1} at BN to 3.4 µmol mol^{-1} at BS, while ratios of Fe:Si uptake ranged from 19 µmol mol^{-1} at BN.1 to 973 µmol mol^{-1} at BS (Table 8). Iron uptake rates were generally high, with low Si uptake resulting in large Fe:Si stoichiometric ratios. Stoichiometric uptake ratios for the >2 µm particles at BS were similar to total >0.2 µm particulates for Si:C and about half of the total particulates for Fe:C and Fe:Si as Fe uptake was comparatively low in the >2 µm fraction (Table 8). At BN.1, the Fe:Si stoichiometry was similar between the total and >5 µm fraction as the majority (~80 %) of both Si and Fe were taken up in the >5 µm fraction whereas only ~ 65 % of the total C uptake was in the >5 µm fraction (Table 8). At BN.2, ~25 % and 50 % of Fe and C respectively were taken up in the >5 µm fraction whereas 100 % of the Si was taken up in this fraction (Table 8).

Table 8: Average (and Standard Deviation) elemental uptake rates for carbon (C), silica (Si) and iron (Fe), and average stoichiometric ratios at Benguela. Note the Fe intra vs extracellular results from using the Ti-EDTA wash at T0 passed the validation checks so were used to calculate the uptake rates.

	BS		BN.1		BN.2	
	Total	>2 µm	Total	>5 µm	Total	>5 µm
Uptake rates						
Carbon (C, µmol C L^{-1} d^{-1})	0.85 (0.03)	0.27 (0.08)	11.88 (2.06)	7.72 (0.75)	9.11 (0.48)	4.42 (0.35)
Silica (Si, µmol Si L^{-1} d^{-1})	0.003 (0.0001)	0.001 (0.0001)	0.16 (0.01)	0.13 (0.05)	0.02 (0.002)	0.02 (0.002)
Iron (Fe, nmol Fe L^{-1} d^{-1})	2.92 (0.60)	0.43 (0.15)	3.10 (0.65)	2.58 (0.54)	2.64 (0.99)	0.68 (0.19)
Stoichiometry						
Si:C (mol:mol)	0.004	0.004	0.01	0.02	0.002	0.005
Fe:C (µmol:mol)	3.40	1.59	0.26	0.33	0.29	0.15
Fe:Si (µmol:mol)	973	430	19	20	132	34

4.3.2 Whole and detrital cell resuspension

A key conclusion of the experiments performed north of South Georgia was that the resuspended cells were likely live and healthy and that this was the likely cause for the relatively high resistance to remineralisation indicated by the results. To further explore this within the Benguela system, parallel detrital cell resuspensions were performed. It was hypothesised that detrital cells would be more susceptible to remineralisation than whole live cells, as bacteria would more readily colonise the dead detrital material and hence hasten silica dissolution by degrading the organic matrix which protects diatom frustules from dissolution (Bidle and Azam, 1999). It would thus be expected that in the detrital resuspended cells a greater proportion of radio isotope would be measured in the dissolved fraction (and possibly the smaller size fraction if microbes take up the dissolved isotopes) than the whole live cells. As previously, in the case of ^{55}Fe, the activity associated with the wall wash has been considered a part of the dissolved fraction. These paired experiments were performed twice at the northern site, BN, named BN.1 and BN.2, as these were the sites for the stage 1 harvesting of surface material (Table 3).

Following stage 1 resuspension of the >5 µm whole and detrital particulates, the activity associated with these particulates becomes the carried over total activity for stage 2. The retention or redistribution of the carried over total activity into size fractionated particulates or the dissolved fraction were then assessed and compared between whole and detrital cell resuspension.

In the majority of time points from both experiments the ^{14}C and ^{32}Si particulate activity remained within the >5 µm particles, with only a single time point from both experiments showing a significant ($p<0.05$) measurement of ^{14}C and ^{32}Si in the <5 µm particles. Both these time points with ^{14}C and ^{32}Si activity in the <5 µm particulate fraction were in the whole live cell resuspension (BN.1 for ^{32}Si and BN.2 for ^{14}C, both after 4 days incubation), with no <5 µm particulate fraction evident in the detrital resuspensions (Figure 14 and Appendix B).

Despite minimal evidence of ^{14}C and ^{32}Si transfer from the resuspended >5 µm particulates into the smaller particulate fraction there was greater consistent activity in the dissolved fraction. In the first experiment (BN.1), a proportion of the ^{14}C had transferred to the dissolved fraction in 80 % of the time points in the whole cell resuspensions and 100 % of the time points in the detrital samples (Figure 14). In the 2nd experiment (BN.2), all of the time points in both the whole and detrital cell resuspensions had significant ($p<0.05$) presence of ^{14}C in

the dissolved fraction (Appendix B). Dissolved inorganic ^{14}C (DIC) was measurable at all time points in both the whole and detrital resuspensions at BN.1 (Figure 14) and 66 % of time points at BN.2 (Appendix B). Similarly, ^{32}Si transferred into the dissolved fraction in both experiments. In the first experiment (BN.1), 100 % of the detrital cell resuspension time points resulted in significant ($p<0.05$) ^{32}Si activity in the dissolved fraction whilst only 20 % of time points in the whole cell resuspensions had significant ($p<0.05$) dissolved ^{32}Si activity (Figure 14). In the 2nd experiment (BN.2), the dissolved results were somewhat reversed between dead and potentially live material, with the whole cell resuspensions resulting in significant ($p<0.05$) dissolved ^{32}Si activity in 100 % of time points whereas in the detrital cell resuspensions 60 % of time points resulted in significant ($p<0.05$) dissolved ^{32}Si activity (Appendix B).

The detrital cell resuspension dissolved activity was significantly ($p<0.05$) greater than the whole cell resuspension dissolved activity in 40 % of the ^{14}C measurements at BN.1 (Figure 14). However, despite some qualitative indication of more ^{32}Si release, relatively large errors meant that none of the ^{32}Si time points for experiment BN.1 showed statistically significant differences between whole cell and detrital material (Figure 14). However, the qualitative differences for the ^{32}Si dissolved data were partially backed up through whole cell resuspensions not having any time points for which there was a significant dissolved fraction (i.e. where the measurement of the dissolved fraction was statistically distinguishable from zero, t-test $p<0.05$), whereas the detrital resuspensions indicated a significant presence of the dissolved fraction at all time points (Figure 14). Thus, there was some evidence of increased movement of ^{32}Si into the dissolved phase for the detrital versus whole cell experiments, but, due to the variability in the whole resuspension dissolved results, the results from the experiments were not significantly different between each other using the ANOVA / Bonferroni test performed. For experiment BN.2, there was no significant difference between the whole and detrital resuspensions dissolved activity apart from after 2 days of incubation where the whole cell resuspension was greater than the detrital cell resuspension in the ^{14}C samples (Appendix B).

In contrast, ^{55}Fe showed more evidence of transfer out of the resuspended particulate phase across both experiments and both whole and detrital cell resuspensions, as 69 % of all time points resulted in significant ($p<0.05$) transfer of activity from the resuspended >5 µm to <5 µm particulates (Figure 14, Appendix B), potentially due to phytoplankton cell fragmentation and/or remineralisation, microzooplankton or bacterial cell uptake or adsorbtion. This, coupled with all of the time points in both experiments for both whole and detrital cell

resuspension indicating transfer of particle associated ^{55}Fe to dissolved ^{55}Fe indicates release of ^{55}Fe, as was observed in the South Georgia experiments presented in Chapter 3. There was however no significant ($p<0.05$) difference of either the dissolved fraction or the <5 µm particulate fraction as a percentage of the total activity between whole and detrital cell resuspension (Figure 14, Appendix B) which indicates that abiotic processes rather than biotic processes may be dominating the transfer of ^{55}Fe.

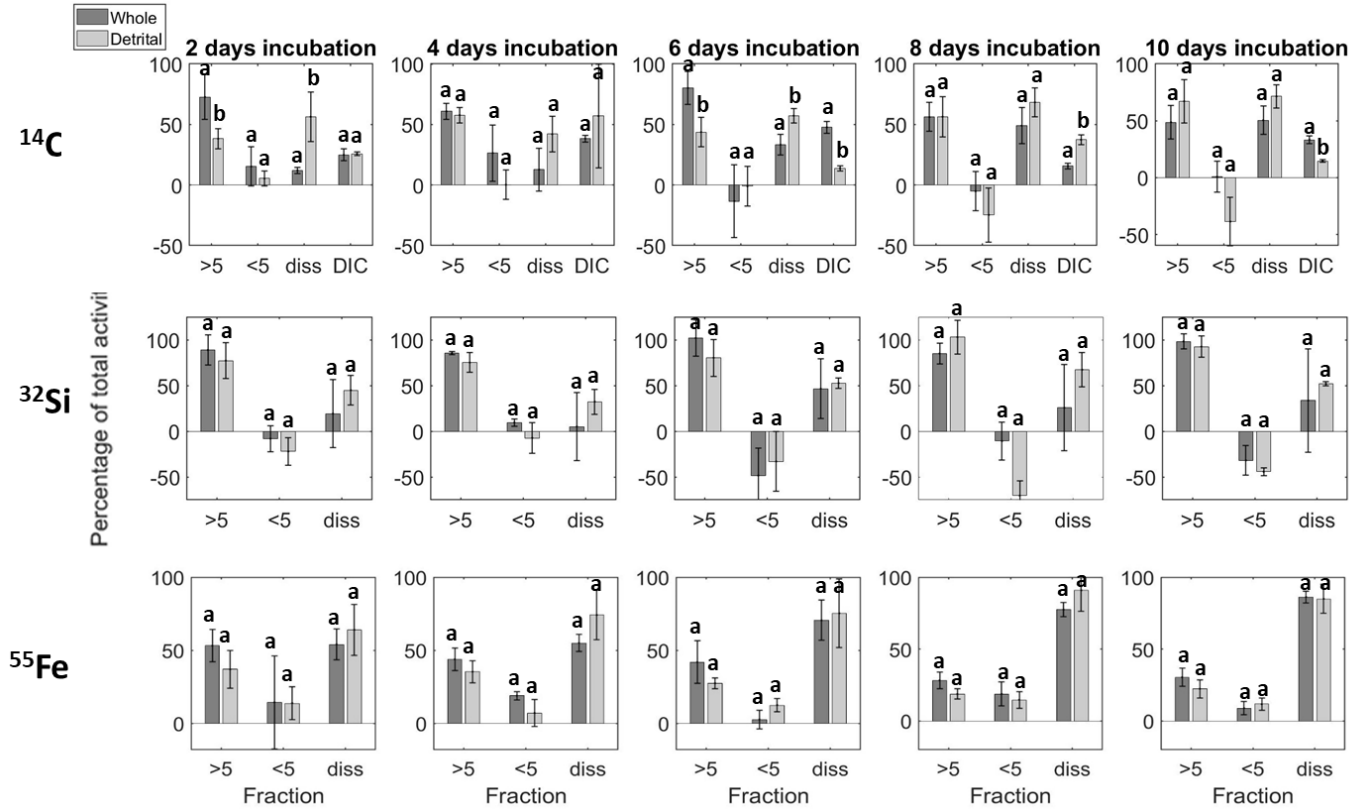

Figure 14: Distribution of >5 µm particulates, <5 µm particulates, dissolved (+ wall wash for Fe) and DI^{14}C radio isotope activity as a percentage of total activity in whole live (dark grey) and detrital (light grey) remineralisation experiments. ^{14}C (top), ^{32}Si (middle) and ^{55}Fe (bottom) panels for expt. 1 at BN.1 with 5 time points from 2 to 10 days incubation from resuspension. Error bars are standard deviation from triplicate samples, results of ANOVA with Bonferroni multi comparison test (*p<0.05*) shown as lowercase letters: levels not connected by the same letter are significantly different between whole and detrital incubations per fraction

4.4 Discussion

4.4.1 Whole and detrital cells Fe, C and Si remineralisation de-coupling

The movement of ^{55}Fe from the resuspended >5 µm particulates to the smaller <5 µm particulates and into the dissolved fraction was strongly evident in both whole and detrital experiments at BN indicating remineralisation of the Fe. The Ti-EDTA wash did not work to distinguish between intra- and extracellular Fe at BN (as the washed cells of the >5 µm fraction had significantly ($p<0.05$) greater activity than the unwashed cells at a number of time points, see section 2.5.1). However, the lack of consistent <5 µm particulates associated with ^{14}C and ^{32}Si suggests that the smaller particles with isotope activity observed were not fragmented resuspended larger particles, nor did they likely result from uptake of the radio isotopes by smaller celled microbes. Rather it was likely that abiotic movement of the particle reactive Fe was occurring, with the ^{55}Fe becoming adsorbed onto smaller particles from the whole water used for resuspension, in a similar manner to that found around South Georgia (Chapter 3). The abiotic movement of ^{55}Fe was similar between the whole and detrital resuspended cells (Figure 14), indicating that neither particulate types were highly susceptible to microbe mediated remineralisation in the upper mesopelagic water. As concluded from the South Georgia experiments, the (re-)mobilisation of adsorbed Fe likely depended on a range of factors, including the concentration and affinity of ligand binding sites of the total particulate pool and in the seawater, noting seawater characteristics would be consistent across both experiment types that used consistent bottle volumes and dilutions between the stage 1 and stage 2 resuspension.

Despite no significant ($p<0.05$) difference in the dissolved ^{32}Si fraction between whole and detrital cell resuspension at BN.1, there was some indication of greater dissolved activity in the detrital cell resuspensions, as these were only statistically distinguishable from zero for the detrital experiments. This would corroborate with the conclusion of Bidle and Azam (1999), that lysed diatoms have enhanced silica dissolution, however in our experiments it is unknown whether this is microbe mediated or due to abiotic processes. The lack of evidence of ^{32}Si activity in smaller particulates would indicate that the freeze thaw process itself did not break down the cells or remove the organic coating to allow for Si dissolution, which could help enforce the argument that the removal of the organic coating was microbe mediated to allow dissolution of the Si from diatom frustules. Greater silicification was occurring at BN.1 as indicated by the greater uptake of ^{32}Si than at BN.2 (Figure 26), thus allowing for a stronger signal of Si dissolution

at BN.1 than at BN.2. Detrital diatom frustules can dissolve rapidly under the right conditions (Passow et al., 2011) so the time frame of our experiments (6-10 days) would have allowed for the dissolution process to occur.

It is unlikely that any significant proportion of the ^{14}C labelled dissolved inorganic carbon pool resulted from carryover of the initially added ^{14}C bicarbonate from stage 1, as particulates were rinsed twice with ~50 mL of unlabelled, 0.2 µm filtered mesopelagic seawater prior to re-suspension. Consequently, this pool likely resulted from respiration of (photosynthetically fixed) ^{14}C labelled particulate organic carbon from any live and isotopically labelled components of the community (as per P3 at South Georgia, see section 3.4.3). However additional bacterial respiration of the $DI^{14}C$ may have occurred. The lack of smaller particulate associated ^{14}C indicates no significant cell break down or ^{14}C uptake and conversion into biomass by microbes, but the parallel detrital cell resuspensions also resulted in consistent measurable amounts of $DI^{14}C$. A measurement of the apparent quantum yield of photochemistry (Fv/Fm) using active chlorophyll fluorescence before and after the freeze thaw process indicated that the live whole cells were not stressed (0.51) but the detrital cells were not active (0.014) (Kolber et al., 1998; Greene et al., 1992; Moore et al., 2005; Nielsdottir et al., 2012), so the presence of $DI^{14}C$ in the detrital cell resuspensions could not have been from active phytoplankton cell respiration. The $DI^{14}C$ pool in the detrital subset of experiments could have originated from the breakdown of the diatom organic coating (which supported Si dissolution as possibly seen at BN.1) which could have incorporated the labelled C in the polysaccharides of the outer diatom layer. Although it is likely that this organic coating would only make a very small contribution to the overall organic C pool and hence would have limited potential to generate a substantial $DI^{14}C$ pool. It is thus more likely that the lysed cells were leaking $DO^{14}C$ (as can be seen by the presence of dissolved C, Figure 14), which was subsequently taken up by the bacteria. With a theoretical bacterial growth efficiency[1] of 30 %, as previously determined in other upwelling systems (Lønborg et al., 2011) a large proportion of any $DO^{14}C$ taken up would be expected to be respired as $DI^{14}C$ rather than converted to bacterial biomass, potentially explaining why <5 µm particulate ^{14}C was not detectable.

[1] Bacterial growth efficiency (BGE) is the amount of new bacterial biomass produced per unit of organic C substrate assimilated and is a way to relate Bacterial Production (BP) and Bacterial Respiration (BR): BGE = (BP)/(BP + BR) (Ducklow and Carlson, 1992). If the BGE is < 50 % then more carbon is respired than converted to biomass (BP).

The detrital cell ^{14}C and ^{32}Si remineralisation pathways don't significantly ($p<0.05$) differ from the whole cells but the mechanisms driving the transfer of particulate to dissolved ^{14}C and ^{32}Si may differ. The lysed detrital cells organic outer coating removal and subsequent Si dissolution and $DO^{14}C$ conversion to bacterial $DI^{14}C$ fuelled the dissolved ^{14}C and ^{32}Si pools without the presence of cell breakdown to <5 µm particulates. The particle reactive nature of ^{55}Fe is likely the main transfer mechanism of particulate ^{55}Fe to dissolved ^{55}Fe in both whole and detrital cell resuspensions.

Diatoms are known vectors of Fe export to the deep-sea (Hutchins and Bruland, 1998; Twining et al., 2015) and these results suggest that both lysed detrital and intact diatoms intracellular Fe could be transported into deeper waters if other processes such as grazing don't act to break the cells up. The remineralisation of extracellular Fe is de-coupled from Si and C. Silica dissolution and C remineralisation have been well studied (see review by Ragueneau et al., 2006) with hydrolysis of diatoms protective membrane by bacteria accelerating the remineralisation of the POC of the membrane and Si dissolution (Bidle and Azam et al., 1999; Patrick and Holding, 1985). This study gives an additional bacterial mediated process in the remineralisation of C from detrital diatoms via the bacterial uptake and subsequent respiration of lysed diatom leaked $DO^{14}C$. The detrital diatoms will therefore relatively shallow the remineralisation of Si and C compared to the whole live diatoms with the movement of extracellular Fe consistent between both detrital and whole diatoms. The shallower remineralisation of the detrital Si, C and extracellular Fe may support the recycling and surface resupply of nutrients available for uptake by the phytoplankton community (Boyd et al., 2015) whereas the whole live diatoms transport intracellular Fe, Si and C to depth for potential longer term storage (Martin et al., 2011; Kwon et al., 2009).

4.5 Conclusion

The remineralisation rates of ^{55}Fe, ^{14}C and ^{32}Si are de-coupled due to abiotic and biotic processes acting to transfer the radioisotopes from the particulate fraction to the dissolved fraction. Abiotic movement of extracellular ^{55}Fe is the likely transfer mechanism from PFe to dFe which is independent of whole or detrital cells used for resuspension, whilst removal of the diatoms organic coating by microbes allowed dissolution of the ^{32}Si from diatom frustules of the lysed diatoms. Respiration of the ^{14}C labelled particulate organic carbon from both the whole diatoms and the bacterial community (via diatom detrital derived $DO^{14}C$) contributed to the dissolved C pool. Cell lysis did not appear to significantly act to speed up remineralisation of any of the 3 isotopes compared to whole cells, however the lysed cells did provide additional/alternative pathways of radioisotope transfer from particulate fractions to the dissolved pool for ^{32}Si and ^{14}C which could result in shallower remineralisation than whole diatoms but not for ^{55}Fe which showed a consistent transfer mechanism between lysed and whole diatoms.

Chapter 5 Iron and carbon (co-) limitation of mesopelagic bacterial production in the Southern Ocean

5.1 Introduction

Liebig's law of the minimum states that growth is dictated not by the total resources available, but by the scarcest resource (limiting factor) (see review by De Baar, 1994). Although this concept has been a key principle in developing an understanding of oceanic nutrient limitation, it is now recognised that multiple factors can contribute to (co-) limitation of microbial cell growth in marine systems, with potentially important consequences for ocean biogeochemistry (Arrigo, 2005; Saito et al., 2008; Harpole et al., 2011).

The term (co-) limitation can be interpreted in many ways, but for the purposes of this study we refer to two types of resource (co-) limitation. Firstly, when two or more nutrients are present at concentrations too low to support microbial requirements and secondly, the enhanced concentrations of one limiting nutrient may facilitate the uptake of another (Saito et al., 2008). *In-situ* bulk concentrations of the limiting nutrients, such as dissolved iron (dFe) and dissolved organic carbon (DOC), cannot identify the bioavailable fraction so *in-situ* data cannot be used to determine limiting concentrations. For this study, a population is described as nutrient limited from an operational viewpoint on an experimental basis. Nutrient limitation is thus diagnosed if addition of a given nutrient or nutrients stimulates a positive biological response (e.g., an increase in cell abundance or metabolic activity when compared to a control sample), (Browning et al., 2017).

In oceanic systems, extensive studies have investigated the role of iron (Fe) as a limiting nutrient for upper ocean autotrophic communities in so-called High Nutrient-Low Chlorophyll (HNLC) regions which have excess nutrients that aren't fully utilised by the phytoplankton due to the lack of Fe (see review by Boyd et al., 2007) and in naturally Fe fertilised regions (Blain et al., 2007; Pollard et al., 2009), with positive responses of phytoplankton productivity and growth to Fe amendment indicating that Fe controls primary productivity and CO_2 drawdown in large areas of the ocean.

Heterotrophic bacteria exert a control on oceanic C cycling via remineralisation of phytoplankton derived particulate and dissolved organic matter (POM and DOM respectively) and subsequent respiration (Ducklow, 2000). Heterotrophic bacteria thus form an important part of the ocean Biological Carbon Pump (BCP). Heterotrophic bacteria remineralise labile POM and DOM at all depths, including within surface waters and within the mesopelagic zone (100-1 km) where much of the downward particle flux is attenuated via zooplankton and bacterial respiration (Ducklow et al., 2001) replenishing dissolved nutrients and trace metals back into the water column.

Heterotrophic bacteria perform two major functions in the transformation of phytoplankton derived organic matter: they produce new bacterial biomass (bacterial secondary production [BP]), and they respire organic C to inorganic C (bacterial respiration [BR]). Bacterial growth efficiency (BGE) can thus be defined as the amount of new bacterial biomass produced per unit of organic C substrate assimilated and is a way to relate BP and BR: BGE = (BP)/(BP + BR) (Ducklow and Carlson, 1992).

The depth at which remineralisation of sinking organic carbon occurs is important, as the deeper the remineralisation depth of C the increased likelihood of long-term storage in the deep water and sediment rather than being released back into the atmosphere (Kwon et al., 2009). Heterotrophic bacteria can thus play a key role in controlling the transfer efficiency of the BCP, both through respiration of organic material (both DOC and POC) both in the surface prior to export and at depth. Any nutrient limitation of bacterial production and growth could influence the rate of remineralisation of organic carbon (POC or DOC) and thus the export depth and long-term sequestration of biologically stored C in the oceans.

Heterotrophic bacterial production and growth can be limited by Fe (Obernosterer et al., 2015 and references therein) as considerable Fe is required within the cellular respiratory chain, which can represent more than 90 % of the intracellular Fe pool in bacteria (Tortell et al., 1999; Andrews et al., 2003). In oligotrophic regions where macronutrients are scarce, bacteria can also be limited by Nitrogen (N), which is used for building proteins and nucleic acids (Mills et al., 2008). Church et al. (2000) investigated (co-) limitation of Fe and N and found that bacterial growth efficiency and N utilization may be partly constrained by Fe availability in the HNLC Southern Ocean.

Heterotrophic bacteria are highly efficient competitors for Fe, in part due to siderophore production coupled with subsequent uptake of siderophore bound Fe (Braun and Killmann,

1999; Armstrong et al., 2004). Phytoplankton are not known to produce or release their own siderophores (Fourquez et al., 2020) but phytoplankton may be able to take up bacterial-produced siderophores to aid in Fe acquisition (Hogle et al., 2016; Kazamia et al., 2018; McQuaid et al., 2018). However, in addition to evidence for Fe limitation, heterotrophic bacteria may also be organic C limited in surface waters (Obernosterer et al., 2015) with the release of labile DOC derived from primary production increasing the Fe demand in heterotrophic bacteria (Fourquez et al., 2015), which can be already Fe limited in some systems (Obernosterer et al., 2015). A modelling study by Ratnarajah et al. (2021) found that bacteria can outcompete phytoplankton for Fe leading to a decrease in phytoplankton biomass if sufficient labile DOC is available. The increase in DOC supplied via phytoplankton exudation leads to an increase in bacterial growth rate but is insufficient to stimulate bacterial biomass to an extent that bacteria outcompete phytoplankton (Ratnarajah et al., 2021). Southern Ocean surface waters are characterized by relatively low concentrations of DOC (about 50 µM, Hansell (2013)), of rather refractory nature, potentially due to Fe-limited phytoplankton primary production (Boyd et al., 2000; Blain et al., 2007) in combination with permanent upwelling of DOC depleted deep water around Antarctica. Landa et al. (2018) observed higher DOC bioavailability (but identical DOC concentrations) in diatom derived DOM compared to Southern Ocean winter water, resulting in increased bacterial abundance and DOC consumption, revealing that differences in origin and chemical composition of the organic matter sources can also be a driver of the observed patterns in bacterial community composition.

The chemical composition, bioavailability and concentration of DOM, as the main substrate for heterotrophic bacteria, can influence the structure of bacterial communities, with taxa adapted based on resource exploitation strategies (Lauro et al., 2009) either associated with particles or free-living in the water column while feeding on the released DOM (Duret et al., 2019). Prokaryotic communities associated with particles generally show higher concentrations, growth rates, enzymatic activities and metabolic diversity than their free-living counterparts (Grossart et al., 2007; Ganesh et al., 2014; Satinsky et al., 2014; Dang and Lovell, 2016). Taxa can also be characterised by their ecological behaviour with *K*-strategist (specialist) prokaryotes thriving on suspended particles and *r*-strategists (generalists) being observed in high proportions on sinking particles (Duret et al., 2019). Carbon loss rates and associated microbial species richness can be different between suspended and fast sinking particle fractions (Baumas et al., 2021), with the potential for prokaryotes detaching from fast-sinking particles constantly enriching non-sinking communities in the mesopelagic zone (Baumas et al., 2021).

A number of experiments have investigated Fe, Corg (organic carbon) and combined Fe and Corg limitation in natural heterotrophic bacterial communities, but mainly in upper (~40 m) surface mixed layer waters (Table 9). Several experiments looking at Fe limitation used incubations performed in illuminated conditions which could have indirectly enhanced DOM availability through production by ambient phytoplankton following their release from Fe limitation, making it difficult to conclude whether sole Fe additions increased bacterial abundance and production or it was a combination of Fe and inadvertent DOC addition (Obernosterer et al., 2015). A small number of experiments have looked at Fe and Corg as limiting factors in heterotrophic bacterial abundance and production in dark incubations of surface waters with variable results in sole Fe additions, whereas more consistent results have been observed in sole Corg and combined Fe and Corg additions (Table 9). Only a single experiment to date (Baltar et al., 2018) has investigated Fe limitation of heterotrophic bacteria abundance and production in mesopelagic waters, in which an increase in bacterial production, but not cell abundance, was observed following addition of Fe alone (in waters collected from a depth of 500 m from the South Pacific edge of the East Auckland Current (Table 9)). In some regions, such as the Southern Ocean, the ferricline depth is often found below the maximum winter mixed-layer depth (Tagliabue et al., 2014), implying some regions are permanently Fe-limited despite strong and deep winter mixing. Deep ferriclines could set the conditions for Fe limitation of bacteria at depth.

Table 9: Summary of results from Fe and C enrichment dark incubation experiments in the Southern Ocean. A positive (Y) or negative (N) response to the treatments in bacterial production (BP) (using either ^{3}H leucine or ^{3}H thymidine as tracers) and bacterial cell abundance from surface mixed layer and mesopelagic waters are presented. Final concentrations of added Fe (as $FeCl_3$) and C (as trace metal clean glucose) are given with the fraction of seawater used for incubation. Nd = not determined.

Southern Ocean region	Dark incubation experiment description	Treatment and evidence of limitation in BP			Treatment and evidence of limitation in cell abundance			Study
		+Fe	+C	+Fe+C	+Fe	+C	+Fe+C	
Surface mixed layer (top 40 m)								
Naturally Fe fertilised region off Kerguelen Islands	Whole seawater, 1 nM Fe, 10 µM glucose	Y	Y	Y	Y	Y	Y	Obernosterer et al. (2015)
Polar front	Whole seawater 10 nM Fe	N	nd	nd	N	nd	nd	Jain et al. (2015)
Ross Sea	<0.65 µm size fraction, 1 nM Fe	Y	nd	nd	Y	nd	nd	Bertrand et al. (2011)
Subtropical front	Whole seawater, 2.5 nM Fe, 1-10uM glucose	N	Y	Y	N	Y	Y	Church et al. (2000)
Subantarctic zone		N	Y	Y	N	Y	Y	
Subantarctic front		N	Y	Y	N	Y	Y	
Antarctic Polar front		N	N	N	N	N	N	
Gerlache strait	<0.8 µm size fraction, 3.8 nM Fe	Y	nd	nd	Y	nd	nd	Pakulski et al. (1996)
SOTS site HNLC (47S, 142E) SAZ Indian sector	whole seawater, 1 nM Fe, 10 µM glucose	N	Y	Y	N	Y	Y	Fourquez et al. (2020)
	<20um seawater, 1 nM Fe, 10 µM glucose - note 12:12 light dark	N	nd	Y	nd	nd	nd	
	<1um seawater, 1 nM Fe, 10 µM glucose - note 12:12 light dark	N	nd	Y	nd	nd	nd	
Mesopelagic (500 m)								
South Pacific edge of East Auckland Current	Whole seawater, 12 nM Fe	Y	nd	nd	N	nd	nd	Baltar et al. (2018)

Here we investigated the potential for (co-) limitation of bacterial production (via ^{3}H-leucine uptake) and cell abundance through measuring responses to sole Fe, sole Corg and combined Fe and Corg additions, focusing on the lesser studied depth horizon of the mesopelagic (70 to 500 m), at two contrasting Southern Ocean sites. Firstly, Fe limitation of heterotrophic bacteria in the surface and the upper mesopelagic was investigated in the naturally Fe fertilised region north west of South Georgia at the British Antarctic Survey site P3 (see section 2.1.1), and secondly, sole Fe, sole Corg and combined Fe and Corg limitation was investigated at multiple depths at and south of the Ocean Observatories Initiative (OOI) station in the Pacific sector of the Southern Ocean as an HNLC region (see section 2.1.3).

Bacterial community can be categorised by cell size and nucleic acid content and for the context of these experiments the following bacterial groups are defined as very large high nucleic acid (vLHNA), large high nucleic acid (LHNA), and small low nucleic acid (SLNA) bacteria.

5.2 Material and Methods

5.2.1 Experimental design

The effects of iron (Fe) and organic carbon (Corg) additions on bacterial production and abundance were investigated in two contrasting Southern Ocean regions, P3 to the northwest of South Georgia (SG), a naturally Fe fertilised region and three HNLC sites (OOI, TN and TS) in the Pacific sector of the (sub-) Antarctic Southern Ocean (Figure 15). The first cruise to SG only investigated the effects of Fe, mainly at the upper mesopelagic depth horizon (70-110 m), with a single experiment in the surface mixed layer (20 m) for comparison. The second cruise to the HNLC sites extended the experiments to additionally investigate Corg addition effects on bacterial production and abundance at multiple depths (20 to 500 m).

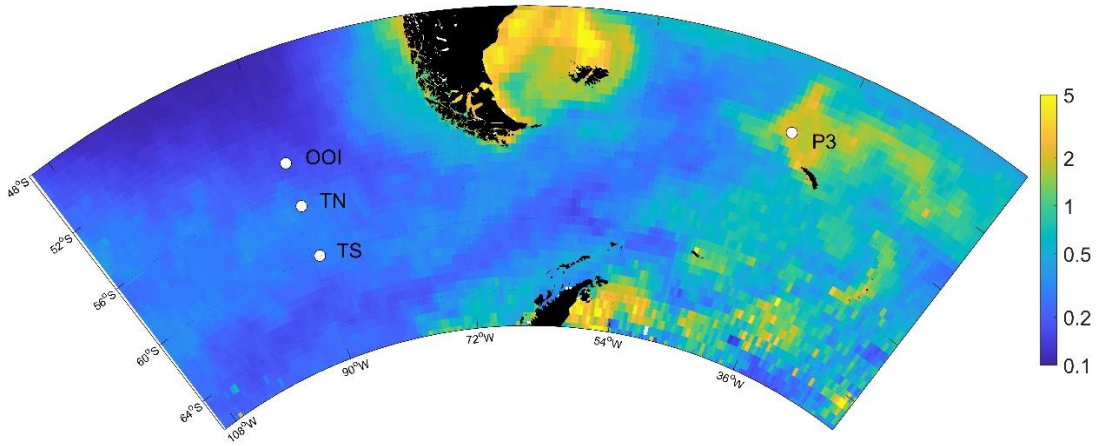

Figure 15: Mean chlorophyll-*a* (mg m^{-3}) from SeaWIFS (Sea-Viewing Wide Field-of-View Sensor) climatology November - December around P3 and the three HNLC sites of OOI (Ocean Observatories Initiative), TN (Transect North) and TS (Transect South).

Water from within the surface mixed layer and the mesopelagic were taken from the trace metal clean CTD (see section 2.3) and subsampled into 500 mL acid washed polycarbonate bottles. The samples were transferred into another trace metal clean laboratory where the following treatments were prepared in triplicate: whole seawater +Fe, whole seawater plus organic carbon (+C, excluding P3) and whole seawater +Fe+C (excluding P3), as well as an unamended control of just whole seawater. The Fe was added as $FeCl_3$ in 0.024 M HCl to a final concentration of 2 nM, the Corg used was trace metal cleaned glucose to a final concentration of 10 µM. The glucose had been passed over a Chelex ion exchange resin to remove any trace metal contamination. Samples were then incubated in the dark to minimise the influence of

phytoplankton derived C production, at *in-situ* temperatures (Table 4, Table 6), with bacterial production and cell abundance subsequently measured at 2 time points. At each time point the incubation bottles were taken to the trace metal clean laboratory for subsampling into 30 mL acid washed polycarbonate bottles and the following processing.

5.2.1.1 Heterotrophic bacterial production

For each treatment triplicate at each depth, 3 x 1.8 mL subsamples were placed in each of the 3 vials. Sixteen µL of a 3.7 kBq/µl ^{3}H Leucine stock solution (10 nM final concentration) (Perkin Elmer L-[4,5-3H(N)] 60 Ci/mmol) was added to result in 59.2 kBq total activity added to each sample. One sub-sample was amended with paraformaldehyde (PFA) or formaldehyde to a final concentration of 1 % as a killed control and the remaining 2 sub-samples were taken as duplicate live samples. The spiked samples were then incubated in the dark for 4 hours to allow for Leucine uptake. After 4 hours, PFA or formaldehyde to a final concentration of 1 % was added to the live samples to terminate the incubation and all samples were filtered onto 0.2 µm polycarbonate filters and placed in 6 mL of scintillation cocktail for determination of total incorporated activities within a liquid scintillation counter (Perkin Elmer TriCarb 3180 TR/SL) onboard. The Leucine uptake (nM d^{-1}) is calculated from the percentage uptake of the total activity added, multiplied by the concentration of Leucine added (10 nM) and the incubation time (Kirchman et al., 1985). The leucine uptake will be used as a proxy for the relative measure of bacterial production, relative comparisons will only be made between controls and treatments rather than as absolute indicators of bacterial production.

5.2.1.2 Bacterial cell abundance

For each treatment (including the control) at each depth, 1.8 mL subsamples were fixed with either PFA or formaldehyde to a final concentration of 1 %. The samples were transferred to a -80 ^{o}C freezer for return to shore and subsequent analysis by flow cytometry.

Flow cytometry is a technique that allows the enumeration and characterisation of cell cultures by passing a steady stream of cell suspension across a laser. Each particle that crosses the laser will scatter the light, forward light scatter (refraction) allows assessment of cell size and side scatter (SSC) provides an additional indication of cell size further influenced by cell surface characteristics (Olson et al, 1993). Cells that do not naturally fluoresce can have their DNA

stained with SYBR® Green to produce a detectable fluorescence of which the specific wavelengths are detected via filters and can be plotted against SSC to help determine cell populations (e.g., Marie et al., 1997). Only heterotrophic bacteria were of interest in this study so the results for filter (FL1) of 530 ± 15 nm that detects green fluorescence after SYBR® Green was added were recorded. This study used a FACS Calibur flow cytometer from Becton Dickinson with polypropylene sample tubes with a length of 75 mm and diameter of 12 mm to create an air-tight seal around the flow cytometer samples extraction needle. All samples were run at a low flow rate of 21 µL min^{-1} for 60 – 120 seconds.

After defrosting the samples at room temperature, between 80 – 240 µL of filtered (0.2 µm sterile filter, Sartorius) 0.3 M tri-potassium citrate and between 8 – 24 µL of SYBR® Green I were added to 800 – 1600 µL of sample (depending on dilution with filtered seawater). For samples with high cell counts that could have led to inaccurate readings due to overlapping sample events, 800 µL of filtered (0.2 µm sterile filter, Sartorius) seawater were added to the sample, all proportions of tri-potassium citrate, SYBR® Green I and sample plus filtered seawater were consistent. Alongside the samples, blanks were included that used MilliQ in place of the cell suspension sample. Samples and blanks were incubated at room temperature in the dark for 60 minutes to allow for staining of the DNA. After incubation, 10 – 120 µL (depending on overall volume of sample) of a calibrated (Zubkov et al., 2001) bead stock with a fluorescent microbeads (Polysciences) concentration of 11,433 $µL^{-1}$ was added to the sample which was then placed into the flow cytometer.

Data were collected and analysed using the Becton Dickinson supplied Cell Quest Pro Software using the FL1 vs SSC plots, an example of which can been seen in Figure 16. Each data point (or event) is a particle passing across the laser so represents a bacterial cell. Clusters of events having similar characteristics can be grouped (or gated) into regions for analysis. The regions of interest selected for the current study are highlighted in Figure 16 and delineate the beads and bacterial cells with different green fluorescence and hence nucleic acid content. The mean bacterial cell fluorescence in each flow cytometer gated region can be multiplied by the cell counts to obtain a proxy for the total nucleic acid concentration contributed by each of the differentiated groups and hence a relative measure of the overall contribution of that group to the total bacterial community.

The groups were categorised as very large high nucleic acid (vLHNA), large high nucleic acid (LHNA), and small low nucleic acid (SLNA) bacteria (Figure 16). To obtain the final sample concentration, the number of events in the beads region were compared to the known

concentration of microbeads in the sample to provide the volume of sample analysed via Equation 1. The concentration of cells in the sample tube can then be determined by dividing the cell count in the gated region of interest by the volume analysed (Equation 2) which can then be converted into the final sample concentration (cells/µL) by multiplying the cell concentration in the sample tube by the total volume in the sample tube and dividing by the original sample volume (Equation 3). Flow cytometer analysis was performed on samples from South Pacific HNLC sites of OOI-1, OOI-3, TS-1, TS-2, TN-3 and P3 from South Georgia.

Equation 1:

$$Volume\ analysed\ (\mu L) = \frac{Number\ of\ microbead\ events}{Concentration\ of\ beads\ in\ sample\ (beads/\mu L)}$$

Equation 2:

$$Cell\ concentration\ in\ tube\ (cells/\mu L) = \frac{cell\ count}{volume\ analysed\ (\mu L)}$$

Equation 3:

$$Sample\ conc.\ (cells/\mu L) = \frac{cell\ conc.\ in\ tube\ (cells/\mu L) \times total\ vol.\ in\ tube\ (\mu L)}{original\ sample\ volume\ (\mu L)}$$

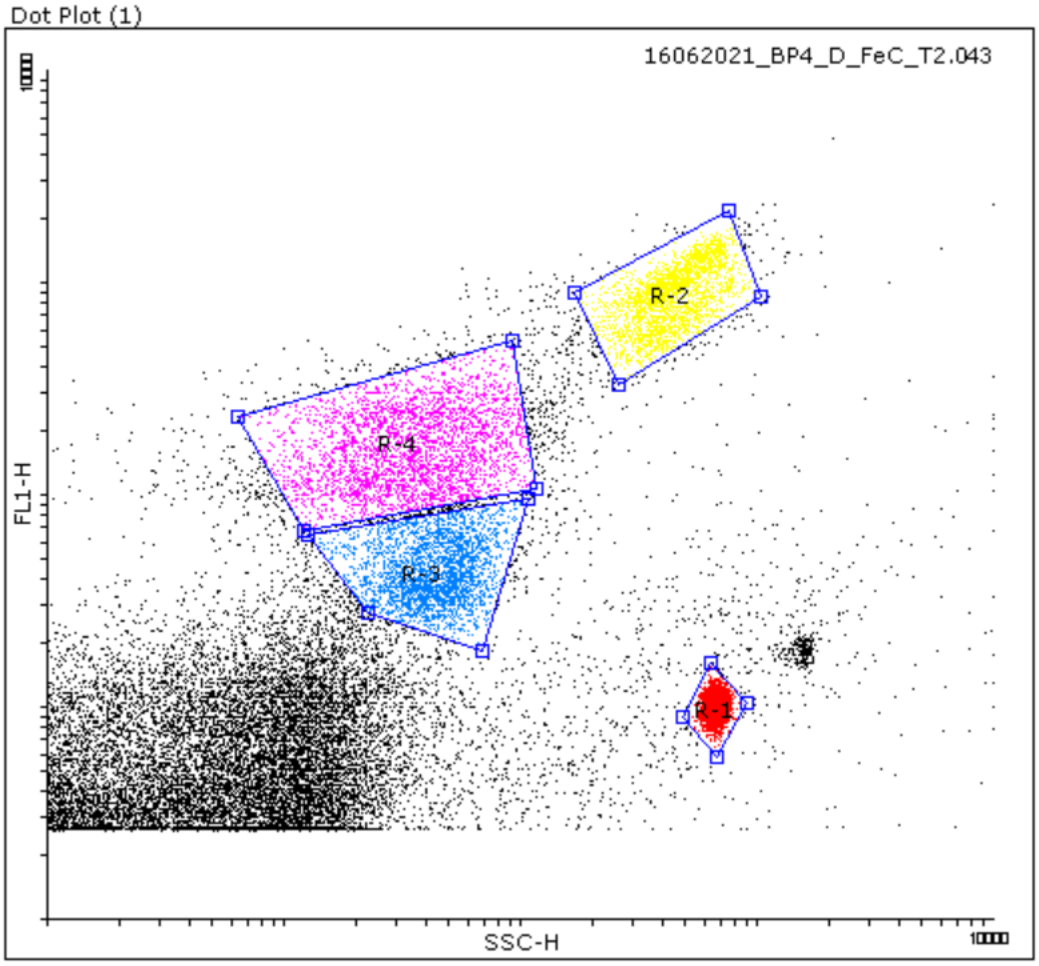

Figure 16: Example flow cytometer FL1 vs SSC plot. Gated regions of interest are red R-1, the calibration beads. Yellow R-2 are the very large high nucleic acid (vLHNA) cells, blue R-3 are the small low nucleic acid (SLNA) cells and the purple region R-4 is the large high nucleic acid (LHNA) cells. Each dot is a cell, the cells with low FL1 and low SSC are viruses and are not part of this analysis. Figure generated from Flowing Software 2.5.1.

5.2.2 Statistical analysis

A one-way analysis of variance (ANOVA) and a post hoc Bonferroni multi comparison test were performed on each time point for each experimental depth between the control and treatment measurements of bacterial production. Differences were considered statistically significant at $p<0.05$ and indicated in the plots by different letters.

5.3 Results

5.3.1 Oceanographic setting

The naturally Fe fertilised South Georgia site (P3) is the most productive out of the experimental locations with relatively high surface chlorophyll-*a* concentrations (4.31 mg m^{-3}), POC standing stocks (17.85 µM) and dFe (0.36 nM). The HNLC sites increased productivity from north (OOI; chlorophyll-*a* of 0.61 mg m^{-3}) to south (TS; chlorophyll-*a* of 2.3 mg m^{-3}) with all locations having low surface dFe (<0.17 nM).

In more detail, the two oceanographic regions where these experiments were performed show contrasting profiles of chlorophyll-*a*, POC, dFe and AOU (Apparent Oxygen Utilisation; the difference between observed dissolved oxygen concentration and its saturation concentration). The naturally Fe fertilised region of P3 at South Georgia (SG) had the deepest mixed layer (60-70 m), with chlorophyll-*a* concentrations of between 1.37 and 4.31 mg m^{-3} and standing stocks of POC of between 8.98 and 17.85 µM (Figure 17 a, b), which would in part be due to the relatively high dFe concentrations in the mixed layer (between 0.17 and 0.36 nM) and at depth (0.56 nM at 110 m) (Figure 17 c). The mixed layer AOU is negative at P3 (Figure 17 d) indicating over saturation as significant disequilibrium of oxygen can be observed in high latitude surface oceans (Ito et al., 2004) potentially due to the strong bloom increasing surface O_2 levels which have yet to outgas. Beneath the mixed layer at P3 the AOU rapidly increases to the highest values (146 µM) of all the sites, indicating strong remineralisation, which correlates with the increasing dFe profiles as well as large surface standing stocks of POC available for remineralisation (Figure 17 b, c, d).

In the Pacific sector of the Southern Ocean consisting of the three sampled HNLC sites, the most northern site of OOI had mixed layer depths which shallowed over the 3 occupations from 100 to 49 m and was the least productive with low mixed layer chlorophyll-*a* (between 0.31 and 0.61 mg m^{-3}) and low (between 3.25 and 14.59 µM) mixed layer POC (Figure 17 a, b), likely driven by low (0.04 to 0.17 nM) mixed layer and subsurface dFe concentrations (Figure 17 c). The OOI AOU concentration (Figure 17 d) shows minimal variation with depth down to 500 m but does show an increase in the depth region at ~100 m where the dFe profile also shows a small peak (Figure 17 c), potentially indicating some small replenishment of dFe from remineralisation. The southernmost HNLC site of TS was the most productive of the HNLC sites with shallow mixed layers (19 to 53 m), chlorophyll-*a* levels of between 1.3 and 2.3 mg m^{-3} and relatively high mixed layer POC ranging from 10.06 to 18.96 µM (Figure 17 a, b) despite the mixed layer dFe

concentrations remaining low (0.05 to 0.09 nM) (Figure 17 c). Similarly to OOI, the TS AOU profile suggests some minor sub surface (~100 m) remineralisation, resulting in a small increase of dFe (Figure 17 c, d). The most southerly TS site had the shallowest ferricline (for this study defined as the depth at which the change in dFe with depth is the greatest (Tagliabue et al., 2014)) of the HNLC sites, between 300 – 400 m (Figure 17 c) with the increase in dFe in parallel with an increase in AOU concentration (Figure 17 d). The ferricline deepened at the more northerly HNLC sites (from 400-600 m at TN to 600-800 m at OOI) to beneath our maximum sampling depths (150 m at TN and 500 m at OOI) for the experiments (Appendix C).

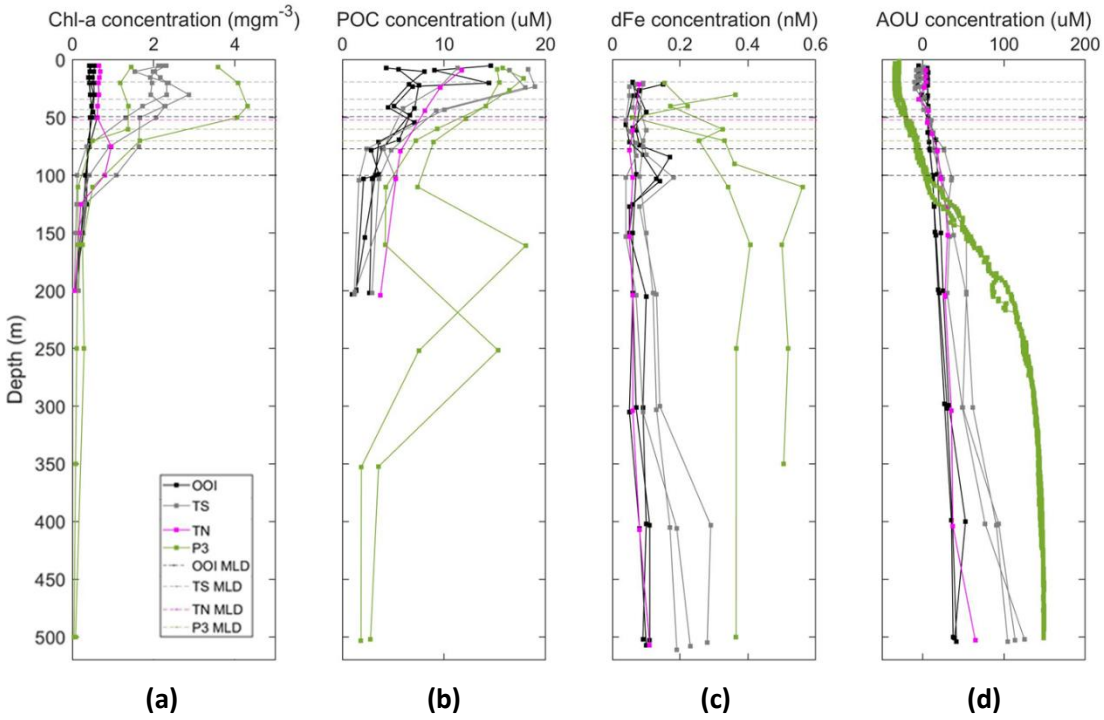

Figure 17: Oceanographic parameter depth profiles of a) Chlorophyll-*a* (mg m^{-3}), b) POC (µM), c) dFe (nM) and d) AOU (µM) for all sites. Naturally Fe fertilised region of P3 in green with 2 CTD profiles. HNLC site most northern occupation at OOI in black with 3 CTD profiles, HNLC most southern occupation at TS in grey with 3 CTD profiles and the HNLC middle occupation of TN in purple with 1 CTD profile. Mixed layer depths from Table 4 and Table 6 are drawn as horizontal dashed lines in the same colour as the depth profiles for each site.

5.3.2 Bacterial productivity and cell abundance

The bloom to the north of South Georgia at P3 had the highest phytoplankton biomass and bacterial production rates of all sites. A trend of increasing phytoplankton biomass and bacterial production from north to south in the sampling region of the Pacific (sub-)Antarctic was observed. Total bacterial cell abundance was also the highest at South Georgia but the southerly HNLC site (TS) in the Pacific (sub-)Antarctic had the lowest bacterial cell count despite having one of the greatest bacterial production rates. The bacterial community was dominated by the Large High Nucleic Acid (LHNA) group both at South Georgia and Pacific (sub-)Antarctic.

Leucine uptake rates, as a relative measure of bacterial production, in the initial unamended control samples at 20 m from the HNLC Pacific sites were greatest at TS ranging, from 0.57 ± 0.12 to 0.72 ± 0.10 nM d^{-1}. The OOI site was characterised by the lowest leucine uptake in the initial 20 m control samples, ranging from only 0.03 ± 0.01 to 0.29 ± 0.19 nMd^{-1}. The single surface water (20 m) control sample from TN resulted in leucine uptake of 0.50 ± 0.03 nM d^{-1}, which sits between OOI and TS in relative leucine uptake rates. These observations coincided with similar trends in Chl-*a* concentrations from the upper ocean at 20 m (Table 6, Figure 17 a) indicating an overall increase in both phytoplankton biomass and bacterial production from north to south in the sampling region of the Pacific (sub-)Antarctic. Within the bloom to the north of South Georgia at P3, the leucine uptake rates from the 20 m initial control samples were the highest of all sites at 0.80 ± 0.46 nM d^{-1}. Leucine uptake rates were lower at depth for all sites, ranging from 0.03 ± 0.01 nM d^{-1} at OOI to 0.08 ± 0.006 nM d^{-1} at P3, with differences between all sites generally reflecting the trends observed for surface bacterial production.

The total cell abundance in the initial unamended control samples (sum of the 3 gated flow cytometer regions, SLNA, LHNA and vLHNA) at 20 m were lowest at the TS site, with an average of 417 $x10^3$ ± 209 $x10^3$ cells mL^{-1}, and highest at South Georgia (1042 $x10^3$ cells mL^{-1}), with OOI averaging 505 ± 202 $x10^3$ cells mL^{-1} and TN having the highest of the HNLC sites (706 $x10^3$ cells mL^{-1}). Bacterial cell abundances within the upper mesopelagic at ~150 m (110 m for South Georgia) followed the same trend as for the surface samples, with P3 having the highest total cell count and TS the lowest (275 and 134 $x10^3$ cells mL^{-1} respectively). However, at 500 m (OOI and TS only) the total cell counts were similar at 88 and 83 $x10^3$ cells mL^{-1}, respectively.

The relative nucleic acid abundance of the initial unamended control samples was dominated by the LHNA fraction at all HNLC sites and all depths, representing between 61 and 78 % of the total bacterial nucleic acid (i.e the nucleic acid content of the LHNA fraction of cells as a

proportion of the nucleic acid content of the sum of all 3 fractions). The smaller SLNA bacteria had a lesser presence at all HNLC sites and depths of between 15 and 31 % of the total bacterial nucleic acid. The vLHNA bacteria were more variable in relative abundance across the HNLC sites and depths, with the smallest presence of between 0.5 to 12 % of the total bacterial nucleic acid. At the South Georgia P3 site the LHNA bacteria dominated at 20 and 70 m with 76 and 61 % of total bacterial nucleic acid, respectively, whereas at 110 m the SLNA bacteria dominated with 53 %. At all depths, the vLHNA had the smaller presence with between 0.6 and 2 % relative abundance.

5.3.3 Response of heterotrophic bacterial production to sole iron or carbon additions

The bacteria were Fe limited (from sole +Fe additions) only in the surface experiments at P3, OOI and TN. Conversely the bacteria were C limited (from sole +C additions) in the surface experiments at OOI and at 500 m at TS, which demonstrated the largest difference in bacterial production from the control sample.

In the sole Fe (+Fe) additions, bacterial production (measured by leucine uptake) only increased significantly ($p<0.05$) in assemblages collected from 20 m depth within the surface mixed layer. Responses to Fe alone were observed in a subset of the near surface experiments at all sites, apart from TS (Figure 18). Single experiments towards the late bloom stages at OOI (OOI-3), TN (TN-3) and P3 near SG all resulted in an increased leucine uptake in the Fe addition samples at 20 m. All other depths and repeated experiments at these sites showed no significant difference between the control and sole Fe additions (Figure 18). When significant increases in leucine uptake were detected, the Fe addition samples only increased from the control by 1.4-fold at OOI-3, 1.5-fold at TN-3 and 1.7-fold at SG. The bacterial production increases due to Fe additions were significant after 2 days of incubation at OOI and TN and 4 days of incubation at SG, with further time points at OOI and TN not retaining the significant difference between control and Fe addition samples.

Sole Corg (+C) additions (only performed at the HNLC Pacific sites) resulted in significant ($p<0.05$) increases in leucine uptake at 20 m at OOI after 2 days of incubation (twice (OOI-1 and OOI-3)) and 500 m at TS after 6 days incubation (Figure 18). At 500 m, the leucine uptake increased 69-fold, whereas the shallower depths increased only by 1.5-fold from the control sample.

5.3.4 Response of heterotrophic bacterial production to combined iron and carbon additions

Sole additions of +Fe and +C did not repeatedly result in a significant increase in bacterial production (leucine uptake) at the HNLC sites of OOI, TS and TN across a range of depths. Conversely, combined Fe and Corg additions (+Fe+C) resulted in a significant increase ($p<0.05$) in leucine uptake in 53 % of experiments at all HNLC sites and at all sampled depths, with 65% of those significant results observed after 6 days of incubation and the remainder after 2 days (Figure 18).

At the OOI site, the +Fe+C additions increased leucine uptake once at 20 m (1.4-fold increase from the control after 2 days incubation), once at 60 m at both time points (1.3- and 2.3-fold increase from the control) and twice at 150 m (48- and 91-fold increase from the control, both after 6 days incubation) (Figure 18). At 20 m, the +Fe+C addition did result in a large 20.5-fold increase from the control after 6 days incubation, but this was not statistically significant (Figure 18). At the more southerly TS site, experiments at all depths resulted in a significant increase in leucine uptake in the +Fe+C additions with the greatest difference from the control sample at depth and after 6 days of incubation (same as OOI). Samples from 150 m resulted in a 74-fold increase in leucine uptake and an 81-fold increase at 500 m (Figure 18). At TN, both depths and both time points showed a significant increase ($p<0.05$) with the greatest increases of 8.4-fold from control at 20 m and again a greater 19-fold increase at 150 m in the +Fe+C additions after 6 days of incubation (Figure 18).

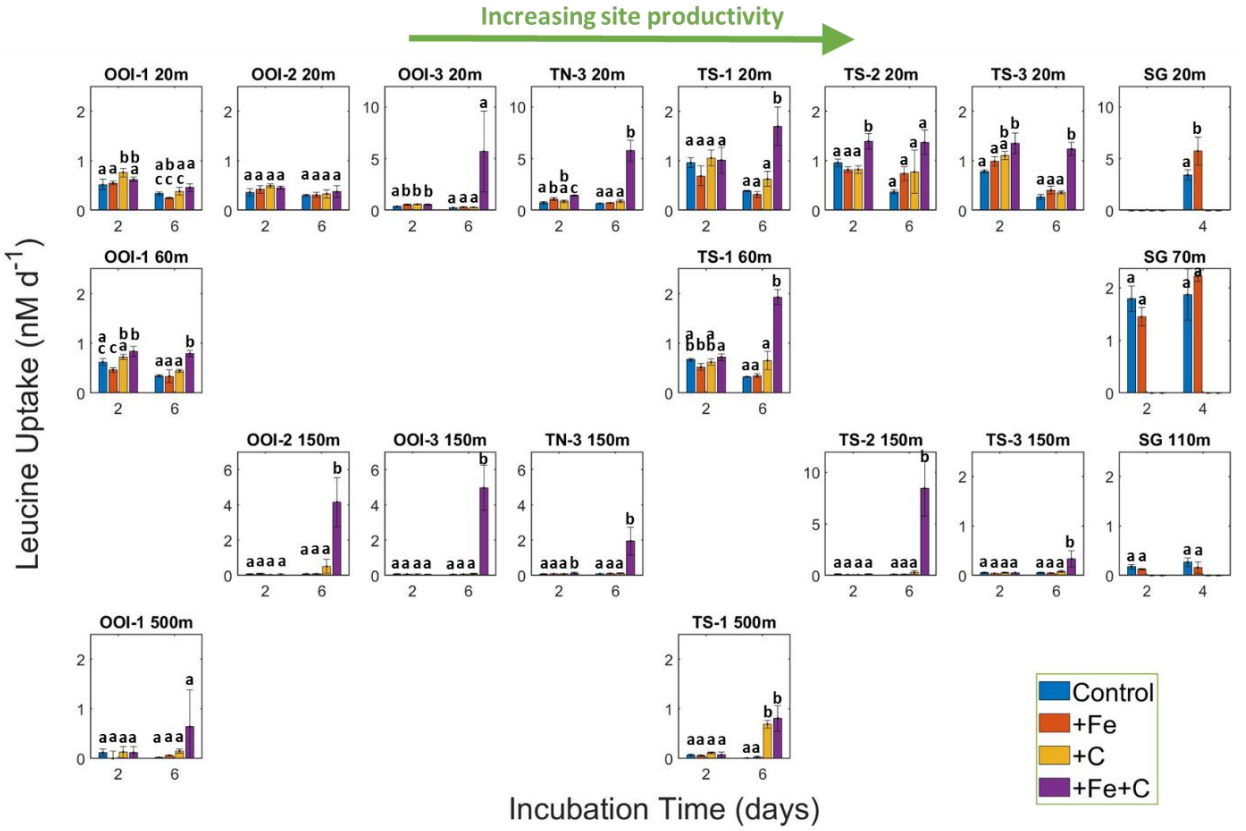

Figure 18: Average leucine uptake (nMd^{-1}) response in control (blue), sole +Fe (red), sole +C (yellow) and combined +Fe+C (purple) amended treatments at all sites at both time points (note the P3 South Georgia (SG) experiments were only performed with control and sole +Fe additions). The subplot layout is ordered by increasing depth down the page and sites by increasing productivity across the page. Error bars are standard deviation from triplicate samples, results of ANOVA with Bonferroni multi comparison test ($p<0.05$) shown as lowercase letters: treatments which are statistically indistinguishable ($p<0.05$) are labelled with the same letter.

5.3.5 Bacteria community composition change in response to the different treatments

The large fold increases in the leucine uptake of the +Fe+C samples (predominately after 6 days incubation in the upper-mesopelagic) (Figure 18) were not reflected by similar magnitude increases in cell concentrations of the initially dominant LHNA and SLNA bacteria fractions, which did not increase by more than 2.5-fold from the control in any experiment. In contrast, the vLHNA bacteria, despite having the overall lowest cell concentrations, consistently increased in cell abundance in the experiments that resulted in the greatest increases in leucine uptake (bacterial production). The parallel increases between leucine uptake and vLHNA cell abundance is particularly prevalent at upper mesopelagic depths in the +Fe+C additions (and the single +C addition at TS_1 at 500m). At all the sites that resulted in a significant leucine uptake at 150 or 500 m depth (Figure 18), the vLHNA cell concentration increased between 10- and 187-fold from the control sample.

Despite the vLHNA bacterial fraction having relatively low cell concentrations, even after increasing in cell abundance from the +Fe+C additions, the relative contribution of the vLHNA to overall bacterial nucleic acid showed large increases over the smaller bacterial fractions for the experiments which resulted in increased leucine uptake. The nucleic acid relative abundance of the vLHNA bacteria from OOI_3 at 150 m increased by 33 % between the unamended control sample and the +Fe+C addition (Figure 19). For the TS_1 experiment sampled from 500 m, both the sole +C and the combined +Fe+C exhibited increases (from the unamended control) in the relative abundance of nucleic acid of the vLHNA bacteria by 17 and 10 %, respectively (Figure 19). The TS_2 +Fe+C addition treatment at 150 m showed the greatest increase in relative nucleic acid abundance of the vLHNA bacteria with a 74 % difference from the unamended control, while TN_3 +Fe+C addition at 150 m showed the smallest increase of 8 % of the relative abundance of nucleic acid vLHNA bacteria from the control samples, but was enough to increase the leucine uptake significantly (Figure 19).

The sole +C addition at TS_1 from 500 m significantly ($p<0.05$) increased 69-fold from the control in leucine uptake (Figure 18), and this was accompanied by a 12-fold increase from the control in vLHNA bacteria cell abundance and an increase by 17 % of the relative abundance of the vLHNA nucleic acid content when compared to the control (Figure 19). Further parallel increases between leucine uptake and vLHNA relative nucleic acid content can be seen at the OOI_1 500 m +Fe+C experiment, which had too large a variability across the biological triplicates to be significantly greater than the control (Figure 18), but still resulted in an

increase in relative dominance of the vLHNA bacteria from 7 % of estimated bacterial nucleic acid in the unamended sample to 53 % in the +Fe+C sample (Figure 19). In contrast, experiments at South Georgia (SG) only resulted in small (1.7-fold) increases in bacterial production in the sole +Fe addition at 20 m, while there was no shift in community composition (Figure 19).

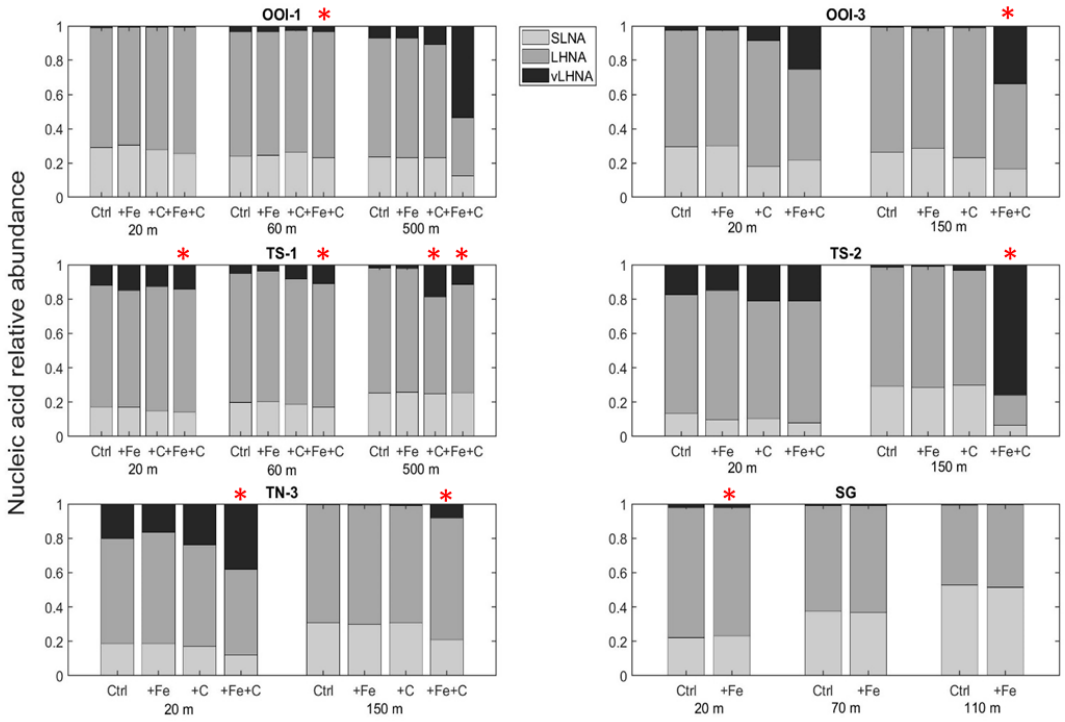

Figure 19: Relative abundance of different bacterial groups as indicated by estimated nucleic acid contribution by small low nucleic acid bacteria (SLNA), large high nucleic acid bacteria (LHNA) and very large high nucleic acid bacteria (vLHNA) for all additions at sampled depths for experiments at OOI-1 and OOI-3, TS-1 and TS-2, TN-3 and P3 at SG after 6 days incubation (4 days for SG). * indicates that the corresponding leucine uptake was significantly different from the control using an ANOVA with Bonferroni multi comparison tests ($p<0.05$).

5.3.6 Results Summary

Seventeen out of 32 combined +Fe+C additions resulted in a significant difference (ANOVA with Bonferroni) in Leucine uptake (as a proxy for bacterial production) compared to the control with the greater increase in leucine uptake at depth (Table 10). Four out of 32 incubations for the sole +C additions and 2 out of 32 sole +Fe incubations resulted in a significant difference (ANOVA with Bonferroni) in Leucine uptake compared to the control. In the sole +C additions, similarly to +Fe+C, the greater increase in leucine uptake was at depth whilst the sole +Fe additions were only significant in the 20 m samples (Table 10).

Table 10: Significant (ANOVA and post hoc Bonferroni) fold increase from the control for each treatment at each experimental site occupation per depth and incubations time. Grey shading represents no significant difference from the control. +Fe is the sole Fe addition, +C is the sole C addition and +Fe+C is the combined Fe and C addition.

			Significant Leuince fold increase from control		
Location	Depth (m)	Incubation time (days)	+Fe	+C	+Fe+C
OOI-1	20	2		1.5	
		6			
	60	2			1.3
		6			2.3
	500	2			
		6			
OOI-2	20	2			
		6			
	150	2			
		6			48.4
OOI-3	20	2	1.4	1.5	1.4
		6			
	150	2			
		6			213
TS-1	20	2			
		6			4.3
	60	2			
		6		2	5.9
	500	2			
		6		69	81.0
TS-2	20	2			1.5
		6			
	150	2			
		6			73.7
TS-3	20	2			1.7
		6			4.5
	150	2			
		6			5.8
TN-3	20	2	1.5		1.9
		6			8.4
	150	2			1.9
		6			19.1

5.4 Discussion

It is well known that HNLC phytoplankton are Fe limited (Martin et al., (1990); this thesis, section 3.3.2). Our results in this chapter alongside previous experiments (Table 9) show that surface bacteria can be limited by Fe alone and to a greater extent by combined Fe and Corg. These experiments are the first (to our knowledge) that also consistently demonstrate Fe and Corg (co-) limitation in mesopelagic bacterial populations.

5.4.1 Upper mesopelagic bacterial Fe and C (co-) limitation response dominated by community composition change

Within the 19 experiments performed across the 4 sites, we found consistent evidence of strong enhancement of leucine uptake (bacterial production) to combined +Fe+C addition for upper mesopelagic depths (Figure 18). These responses appeared to be dominated by a strong growth response by the sub-group of free-living bacteria with the largest observed cell sizes and nucleic acid contents (Figure 19). These mesopelagic results follow a similar trend to surface bacteria nucleic acid cell fractions, with higher nucleic acid (HNA) cells dominating in a nutrient rich region compared to smaller nucleic acid cells dominating in a nutrient poor region with increased bacterial production correlating with increased HNA cells, although interestingly no correlation was found between HNA cells and increased bacterial respiration (Obernosterer et al., 2008).

In the upper mesopelagic at 150 m, all experiments in the South Pacific resulted in consistently large increases in leucine uptake when combined +Fe+C were added (Figure 18). These statistically significant increases in leucine uptake in the +Fe+C additions at the HNLC sites are likely a result of a shift in community composition from large high nucleic acid (LHNA) to the very large high nucleic acid (vLHNA) bacteria (Figure 19). The +Fe+C additions that resulted in a large leucine uptake increase relative to the control sample both at 150 and 500 m show a corresponding large increase in the vLHNA fraction of the community (Figure 20). At depth the vLHNA bacteria initially have low cell abundance and low relative nucleic acid abundance (Figure 19). Enhanced growth relative to their low initial abundance correlates with the significant increase in leucine uptake (Figure 20), with the larger cells contributing to larger bacterial production (Obernosterer et al., 2008). The significant increases in leucine uptake in the samples from the surface (20 and 60 m) were not accompanied by a shift in bacterial

community composition from the control sample, with the dominant bacterial fraction remaining as the LHNA cells. This lack of response in the surface compared to a change in community composition at depth would suggest different bacterial communities at different depths (Figure 19 and Figure 30 in Appendix F), (Cram et al., 2015; Luna et al., 2016; Mestre et al., 2018; Richert et al., 2019; Baumas et al., 2021; Wenley et al., 2021).

We estimated the Fe and C demand of the vLHNA bacteria to determine how the *in-situ* standing stocks of dFe and DOC might have related to the observed limiting status of these stocks for at least a subset of the free-living bacterial community. From the difference in cell counts between the control and combined +Fe+C amended treatments and a low assumed carbon content per vLHNA bacterial cell of 6.5 fg C $cell^{-1}$ (Fukuda et al., 1998) and 6 pmol Fe / µmol C (Tortell et al., 1999), we calculate that only a small amount of between 0.006 and 0.43 pM of the 2 nM added Fe is converted into intercellular bacterial Fe within the experiments. Conversely, considering our cells are classified as very large high nucleic acid bacteria, using a greater assumed carbon content per vLHNA bacterial cell of 52 fg C $cell^{-1}$ (Bjørnsen and Kuparinen, 1991) and 41 pmol Fe / µmol C (Fourquez et al., 2020), we calculate that still only a small amount of between 0.3 and 23.5 pM of the 2 nM added Fe is converted into intercellular bacterial Fe within the experiments. Thus, the *in-situ* pool sizes of dFe (Figure 17 c) could potentially be adequate to support bacterial uptake demands if fully bioavailable. However, the few statistically significant responses and lack of strong response when highly bioavailable DOC (as glucose) was added alone (Figure 18), indicates that a large proportion of the ambient dFe must not be bioavailable. Similarly, the lack of strong responses in the mesopelagic when Fe was added alone compared to the strong responses when Fe and highly labile DOC were added together, suggests that the bioavailable standing stocks of DOC and POC could not satisfy any potential Fe enhanced bacterial C demands. A rough estimate of the vLHNA bacterial carbon demand using a leucine to carbon conversion factor of 0.81 (Pedros-Alio et al., 2002) and a bacterial growth efficiency from an empirical relationship from Del Giorgio and Cole (1998) from a dataset on bacterial respiration and production, results in an estimated bacterial carbon demand ranging from 0.2 – 2.5 µM d^{-1} which can be compared to standing stocks of *in-situ* DOC of ~50 µM (Hansell (2013)), much of which must again presumably be non-available over short timescales to the sub-communities responding in the experiments (Figure 18).

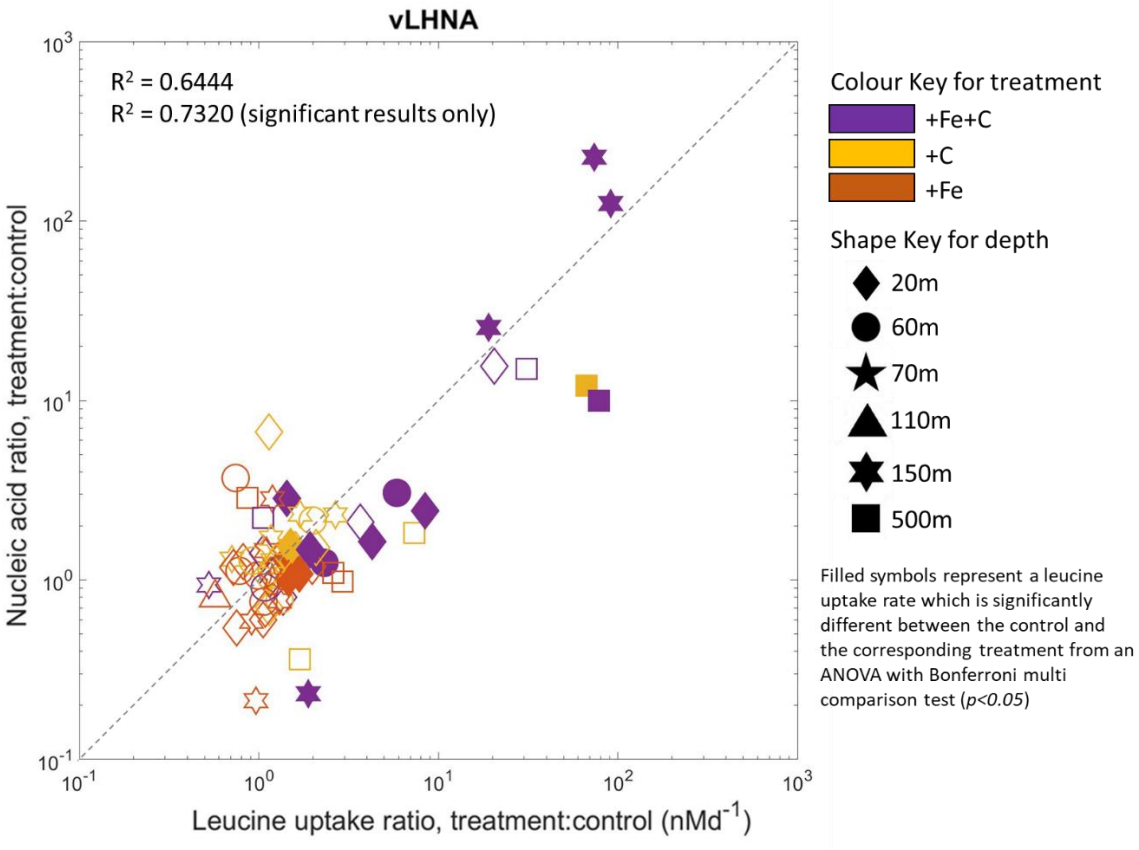

Figure 20: Relationship between average leucine uptake (nMd^{-1}) ratio of treatment to control and very large high nucleic acid (vLHNA) bacteria ratio of treatment to control for both time points. Filled symbols represent a leucine uptake rate which is significantly different between the control and the corresponding treatment from an ANOVA with Bonferroni multi comparison test ($p<0.05$). Colours represent the different additions, +Fe+C purple, +C orange, +Fe red. Symbol shapes represent the different sampled depths, 20 m diamond, 60 m circle, 70 m pentagram, 110 m triangle, 150 m star and 500 m square. Note; the small significant leucine uptake at 150 m in the +Fe+C sample (filled purple star) that has a very low nucleic acid ratio is a time point 1 sample where the minimal (but still significant) leucine uptake was not from the vLHNA cells within the timeframe.

Wenley et al. (2021) investigated seasonal prokaryotic community linkages between surface and deep (500 m) waters in the South Pacific Ocean and found that depth was the main driver for community differences, deeper communities were most diverse and the community composition changing seasonally. Increasing species number could result in more mixed communities of prokaryotic species with more contrasting ecological functions enabling them to use the limiting resources more efficiently (Waide et al., 1999). There is however contrasting evidence as to whether a more diverse mesopelagic prokaryotic community has increased bacterial production rates (Baumas et al., 2021 and references therein).

5.4.2 Increasing higher primary productive sites show greater Fe and C bacterial production limitation

The more productive sites of SG (P3), TS and TN had higher initial control sample surface bacterial leucine uptake as a proxy for bacterial production (0.80 ±0.46, 0.72 ±0.10 and 0.50 ±0.03 nMd^{-1} respectively) than the less productive OOI site (0.22 ±0.008 nMd^{-1}), consistent with elevated chlorophyll-*a* and elevated primary production supporting elevated heterotrophic bacterial production (Wenley et al., 2021). However, the surface combined +Fe+C limitation of heterotrophic bacteria was more prevalent at sites with higher primary productivity (Figure 17 a, b; Figure 18). It can be speculated that the more productive sites may be characterised by increased release of DOC derived from the primary production which could increase the Fe demand of the heterotrophic bacteria to utilise this labile C source (Fourquez et al., 2015). However, it is unlikely that the increased bacterial Fe demand was satisfied by the *in-situ* low surface bioavailable dFe concentrations (section 5.4.1; Figure 17 c). Increased *in-situ* DOC may also have not had high enough lability to alleviate limitation, as sole Fe additions did not result in a positive response, thus indicating limited bacterial growth and (secondary) bacterial production.

It is commonly reported that bacteria are highly competitive over phytoplankton for Fe due to the production of siderophores (Braun and Killmann, 1999; Armstrong et al., 2004) combined with small cell sizes and hence a low potential for diffusion limitation. However, more recent studies have found that when DOC is no longer a limiting resource autotrophic pico- and nanoplankton can outcompete heterotrophic bacteria for Fe (Fourquez et al., 2015; Fourquez et al., 2020). In contrast, a modelling study by Ratnarajah et al. (2021) found that bacteria can outcompete phytoplankton for Fe leading to a decrease in phytoplankton biomass if sufficient

labile DOC is available. The increase in DOC supplied via phytoplankton exudation leads to an increase in bacterial growth rate but is insufficient to stimulate bacterial biomass to an extent that bacteria outcompete phytoplankton (Ratnarajah et al., 2021).

Our study sites were however dominated by larger phytoplankton (Table 4, Table 6), which are presumably poor competitors for dFe. The competition for resources could be greatest at the higher productivity sites resulting in Fe limitation of all autotrophic and heterotrophic cells as the nutrients are drawn down, perhaps exacerbated by the increased bacterial Fe demand due to increased DOC (Fourquez et al., 2015). Thus the natural *in-situ* system was potentially on the edge of Fe limitation with the addition of Corg tipping the heterotrophic bacteria into Fe limitation as the addition of both nutrients resulted in the strongest response.

The relationship between increased primary productivity and increased Fe and C bacterial limitation could also be possibly attributed to different phases and composition of the bloom at each site. South Georgia (with the highest primary production) was in the declining phase of a strong diatom bloom with potentially enhanced bioavailable DOC (Landa et al., 2018) from cell senescence and minimal regenerated surface dFe from remineralisation of large cells (Fourquez et al., 2020) retaining low dFe surface concentrations (Table 4). The more bioavailable diatom derived DOC may have alleviated the C limitation of the surface bacteria as an adequate supply of organic C, promoting sequential limitation of Fe (Fourquez et al., 2020) that was observed at South Georgia. The same extensive depth resolved experiments were not performed at South Georgia, but it could be hypothesised that due to pulses of C export to depth at this more productive site and higher concentrations of sub surface dFe (Figure 17), it was harder to tip the system into Fe limitation at depth compared to the HNLC sites with low C export and low dFe concentrations at depth (Figure 17).

5.4.3 Nutrient regimes influence mesopelagic bacterial recycling of carbon and sequestration depth?

We hypothesise that the subsurface concentrations of Fe and N, influenced by differing recycling regimes, could influence the bacterial recycling of carbon and carbon sequestration depth.

This section lays out a sequence of nutrient limitation scenarios that expands on our hypothesis but will require further exploration outside of this thesis.

Nutrient limited phytoplankton and nutrient and C limited bacteria reside in the euphotic zone (conceptual Figure 21) with limitation intensifying with increasing production due to draw down of the key nutrients; Fe in HNLC regimes (this thesis section 3.3.2 and 5.3.4) and N in subtropics (Mills et al., 2008). Bacteria can contribute to the remineralisation of surface phytoplankton (Figure 21.1) and release CO_2 through respiration of POC/DOC (Ducklow et al., 1993; Cole et al., 1988; Boyd et al., 2019) (Figure 21 .2), possibly to a greater extent if bacterial growth and production limitation was alleviated. Irrespective of the identity of the surface limiting nutrient, phytoplankton whole and detrital cells might be expected to be exported out of the euphotic zone with a high C:nutrient ratio (Figure 21 .3) due to the nutrient being at limiting concentrations in surface waters.

A key difference across the different nutrient regimes from the N limited (sub-)tropics (Moore et al., 2013) to Fe limited HNLC regions occurs within the mesopelagic zone. In an Fe limited system such as the South Pacific HNLC region (Wyatt et al., in press), the upper mesopelagic has low standing stock of Fe partly due to deep ferriclines generated by deep winter mixing setting the depth region of Fe C (co-) limitation (Figure 17 c; Twining et al., 2014; Rigby et al., 2020). The lack of Fe (co-) limitation in the mesopelagic at South Georgia and below the ferricline depth at TS where sole Corg and combined +Fe+C additions at 500 m are equivalent (Figure 18) (indicating C as the limiting nutrient) was consistent with higher *in-situ* dFe concentrations in these regions and depths (Figure 17 c). In addition, the availability of organic C and bioavailable Fe in the mesopelagic will depend on standing stocks, supply from the euphotic zone (to an extent via remineralisation and dissassociation from sinking material (Boyd and Ellwood, 2010)) combined with potentially low Fe content in sinking cells and sub-surface scavenging of any released dFe (see Figure 21, Fe depth profile). The Fe and C limited mesopelagic bacteria will hence potentially be restricted in their ability to remineralise mesopelagic organic carbon sources (Figure 21 .4) with limited release of CO_2 (Figure 21 .5)

due to the observed Fe C (co-) limitation in the mesopelagic of this system (Figure 18). As bacterial growth is limited, a knock on consequence may be a slowing of the rate of remineralisation of organic carbon in the sinking material, thus potentially increasing the sequestration depth of the C and associated nutrients (Figure 21 .6). This could then be hypothesised to also deepen the depth of remineralisation of dFe, reinforcing the tendency for the ferricline to remain deep, while also resulting in deeper C remineralisation and hence the less carbon being locally returned to the surface ocean and atmosphere (Figure 21 .7).

Our sampling was during the decline of a bloom period with the potential for sinking particles to transport microbes to the deep ocean connecting surface and deep microbial communities (Wenley et al., 2021). The sinking particles might be expected to have relatively high C:Fe ratios as the material resulted from Fe limited surface phytoplankton communities (Ainsworth et al., COMICS SI; Wyatt et al., In press). The stoichiometry of the sinking material may then influence the Fe availability for the attached microbes and the source of Fe to the deeper free living microbial community, thus it could be hypothesised that Fe limited surface microbial communities could be a driver in setting Fe limitation in deeper communities. During winter months the prokaryotic community will be influenced by overturning via vertical convection, transporting bacteria between depth layers (Wenley et al., 2021) of potentially different Fe concentrations as the ferricline deepens with winter mixing. Regions, such as the Southern Ocean, can have deep ferriclines, often found below the maximum winter mixed-layer depth (Tagliabue et al., 2014) setting permanent low dFe concentrations in the upper mesopelagic (Figure 29) contributing to reduced bacterial production and influencing mesopelagic bacterial community structure (5.3.4, 5.3.5).

Conversely, in low latitude regions within a N limiting regime (Mills et al., 2008), mesopelagic bacteria are unlikely to be N limited due to large *in-situ* pools of remineralised N in the upper mesopelagic just below the surface (see Figure 21, N depth profile), that could provide adequate N and potentially adequate C for bacterial growth and production. We therefore hypothesise that the non N limited bacteria can contribute to the shallow remineralisation of particulate matter in the mesopelagic (Ducklow et al., 2001) (Figure 21 .7) with respiration of the CO_2 (Figure 21 .8) proceeding without any restriction due to substrate availability, thus supporting rapid and relatively shallower remineralisation of organic carbon by bacteria in these regions and hence with a greater potential for local C return to the surface (Figure 21. 9, 10).

This thought experiment focuses on the primary limiting nutrient in each regime and the difference in remineralisation profiles in the mesopelagic influencing the supply of that nutrient. It is recognised that the cycling of both Fe and N happens in both regimes, for example iron availability does play a role in nitrogen fixation in diazotrophs in low latitude systems (Mills et al., 2004) but the bulk heterotrophic bacterial community are not Fe limited in N limitation regimes (Mills et al., 2008).

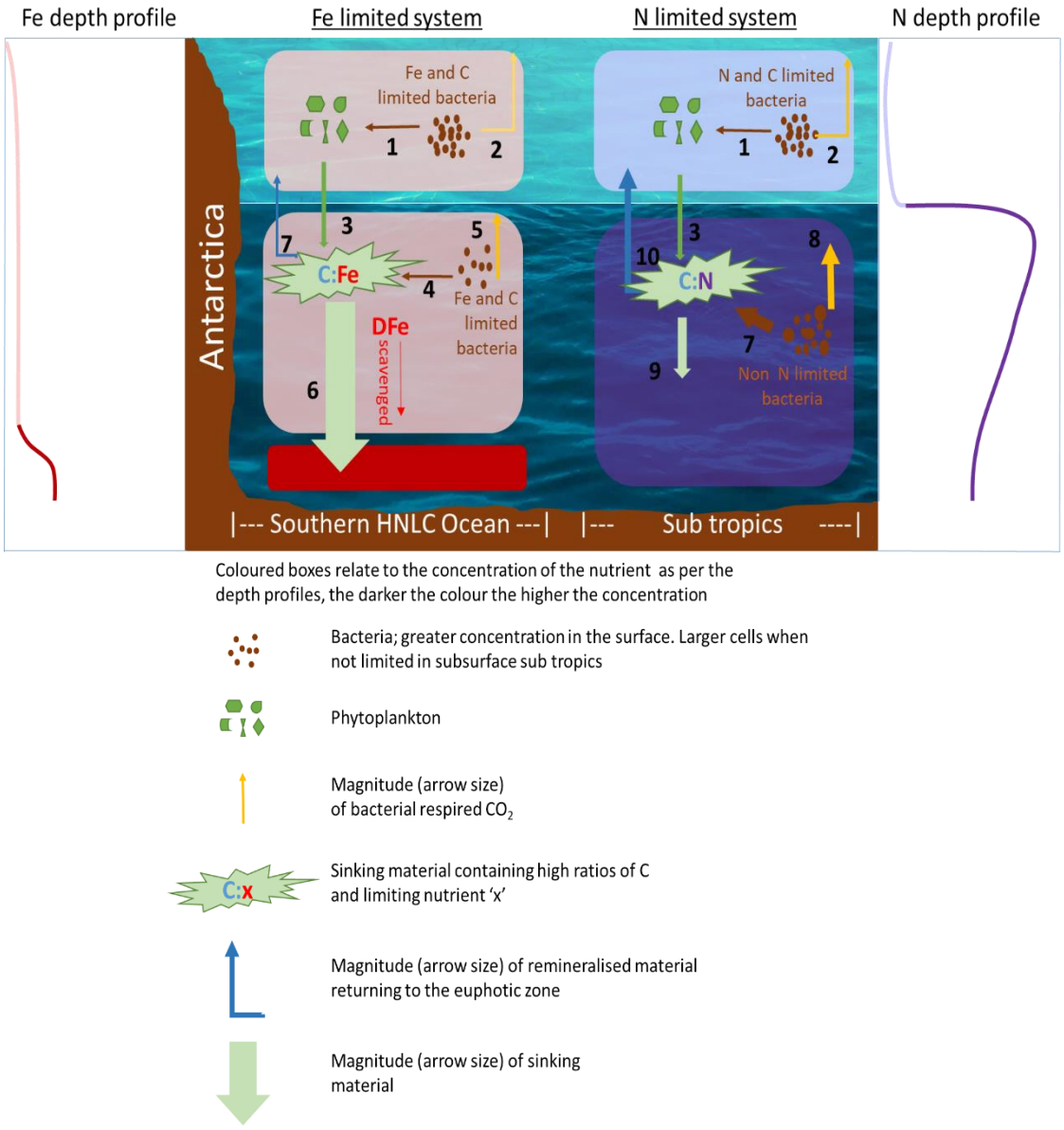

Figure 21: Conceptual comparison of the remineralisation of sinking material via Fe limited and non N limited mesopelagic bacteria in HNLC Fe and sub tropic N limited regimes. The numbers define stages of the process for reference in the text. Other processes contributing to the remineralisation of C are not shown to allow clarity of the processes under discussion.

5.5 Conclusion

The increase in cell abundance of the very large high nucleic bacteria when combined Fe and Corg were added to mesopelagic waters from 150 and 500 m supported a large (1-2 order of magnitude) increase in bacterial production indicating the (co-) limitation of a sub-population of the free-living bacteria at depth. Total cell count alone did not provide such a strong pattern of response in bacterial production. Comparing *in-situ* concentrations of dFe and DOC with the magnitude of observed responses and corresponding estimated C and Fe uptake suggested that much of the *in-situ* nutrient pool was not readily bioavailable to the larger sized free-living bacterial populations at depth.

The region of Fe C (co-) limitation sits within the upper mesopelagic above the ferricline with the limited experiments below the ferricline indicating sole Corg limitation. Consequently, the controls on ferricline depth and mesopelagic standing stocks of Fe (winter mixing, scavenging, Fe associated with sinking material) will be important in determining the extent of ocean Fe C (co-) limitation of mesopelagic bacterial growth and production and will be a driver in bacterial community composition at depth, where much of the downward particle flux is attenuated via a combination of zooplankton and bacterial respiration (Ducklow et al., 2001). Nutrient limitation in the mesopelagic bacteria has potentially important consequences if it also reduces the overall rate of remineralisation and thus both generates a potential reinforcing feedback on the maintenance of a deep ferricline and increases the remineralisation depth and hence long-term storage of carbon in the ocean. More broadly, differences in nutrient limitation regimes could hence potentially influence the rate of remineralisation in the mesopelagic by bacteria and thus carbon sequestration.

Chapter 6 Synthesis and future work

6.1 Introduction

Most (~80 %) of the organic C produced by phytoplankton is remineralised in the surface ocean, with the resulting recycled inorganic CO_2 then being available for release back into the atmosphere, while the majority of the remaining fraction which leaves the surface is remineralised at relatively shallow depths in the upper ~1000 m (Eppley and Peterson, 1979). Bacteria directly process around one-sixth of the C that is fixed by phytoplankton in the surface ocean (Ducklow et al., 1993; Cole et al., 1988; Boyd et al., 2019) and numerically dominate surface microbial communities (Kirchman, 2008). The organic C content of the sinking particles in the upper 1000 m is mainly remineralised by heterotrophic microorganisms (Cho and Azam, 1988; Azam and Long, 2001). The POC flux is attenuated with depth through zooplankton activity and abiotic processes, but the final remineralisation step (releasing dissolved CO_2) is mainly performed by heterotrophic bacteria (Giering et al., 2014; Burd et al., 2010). The transfer efficiency of the BCP is determined in the subsurface ocean (Buesseler and Boyd, 2009), so that understanding the controls on C remineralisation and the influence of Fe on these processes in the mesopelagic zone is thus important for understanding the operation of the BCP and therefore potentially the regulation of atmospheric CO_2. This study investigated biotic and abiotic processes influencing the parallel remineralisation of C, Fe and Si in natural phytoplankton assemblages resuspended in whole upper mesopelagic waters from a naturally Fe fertilised HNLC region and a productive upwelling system to examine the relative remineralisation of macro and micronutrients in the upper mesopelagic (Chapters 3 and 4). The reciprocal influence of Fe availability in the sub-surface on bacterial processes and hence remineralisation was further investigated through examining Fe and Fe C (co-) limitation on microbial bacterial production and cell abundance in the surface and subsurface of two contrasting Southern Ocean sites. The growth limiting factors and community composition changes due to the availability of key nutrients and the potential influence on mesopelagic remineralisation rates and C storage was thus explored (Chapter 5).

6.2 Synthesis

Objective 1, investigating the biotic and abiotic factors influencing Fe cycling in the mesopelagic zone and the (de-) coupling of Fe and macronutrients at depth, resulted in the remineralisation experiments using whole live diatoms (detailed in Chapters 3 and 4) repeated a number of times at different oceanic regions. These regions are compared in the following section 6.2.1 to gain an understanding of oceanographic differences and their potential influence on the remineralisation of Fe, C and Si in the mesopelagic.

The overarching aim of this thesis is "what are the potentially reciprocal feedback processes which influence Fe cycling and consequently C cycling in the mesopelagic zone?" The 2 main objectives that approached this question (see below) can be conceptually synthesised to focus on the reciprocal feedback process between bacterial limitation and subsequent influence on Fe and C remineralisation, this is detailed in section 6.2.3

1. Differentiating the biotic and abiotic factors influencing Fe cycling in the mesopelagic zone and the (de-) coupling of Fe and macronutrients at depth.
2. Investigating the potential for Fe and C (co-) limitation of mesopelagic bacteria with the hypothesis being; "upper mesopelagic bacteria are Fe and C limited, reducing their bacterial production and therefore decreasing the remineralisation rate of C in the mesopelagic zone".

6.2.1 South Georgia and Benguela; Fe, C and Si remineralisation comparison

Overall, between the two COMICS cruises to South Georgia (P3A, P3B and P3C) and the Benguela upwelling (BN.1 and BN.2), the remineralisation experiments with resuspension of the >5 µm particulates in upper mesopelagic water to observe the relative distribution of ^{14}C, ^{32}Si and ^{55}Fe were performed 7 times (including the detrital experiments). Table 11 summarises the significant ($p<0.05$) presence of the <5 µm fraction and the dissolved fraction at each time point for each radio isotope and provides a total and percentage presence per time point at each site in bold.

Table 11: Summary results of significant presence of the radio isotope fraction at each time point and the sum and percentage presence for each region.

	Fe		**Si**		**C**	
	<5 µm	diss	<5 µm	diss	<5 µm	diss
P3A	0/3	2/3	1/3	0/3	1/3	0/3
P3B	2/3	1/3	0/3	3/3	1/3	0/3
P3C	1/3	3/3	0/3	1/3	0/3	1/3
	3/9 (33 %)	**6/9 (66 %)**	**1/9 (11 %)**	**4/9 (44 %)**	**2/9 (22 %)**	**1/9 (11 %)**
BN.1 whole	3/5	5/5	1/5	1/5	0/5	4/5
BN.2 whole	3/3	3/3	0/3	3/3	1/3	3/3
	6/8 (75 %)	**8/8 (100 %)**	**1/8 (13 %)**	**4/8 (50 %)**	**1/8 (13 %)**	**7/8 (88 %)**
BN.1 detrital	3/5	5/5	0/5	5/5	0/5	5/5
BN.2 detrital	2/3	3/3	0/3	2/3	0/3	3/3
	5/8 (63 %)	**8/8 (100 %)**	**0/8 (0 %)**	**7/8 (88 %)**	**0/8 (0 %)**	**8/8 (100 %)**

Across all experiments, the most consistent evidence of transfer of activity from the resuspended larger particulates to the smaller particulates and the dissolved fraction was found in the ^{55}Fe samples (Table 11, Figure 22). At South Georgia, the most signifcant transfer of ^{55}Fe we observed was via the (re-)mobilisation of the adsorbed (extra cellular) pool into the dissolved phase and it was determined that the ^{55}Fe activity associated with the smaller particles was in the majority extracellular, indicating adsorption rather than uptake of activity (section 3.3.4.2 Figure 12). For Benguela, the intra- vs extra-cellular ^{55}Fe could not be determined but the similar results of a consistent dissolved ^{55}Fe and <5 µm ^{55}Fe fraction (Figure 22) could suggest similar abiotic transfer of ^{55}Fe.

There were also some observable differences between the two regions experimental results. The BN experiments for both whole and detrital resuspensions resulted in a greater presence of activity in the dissolved fraction for all isotopes, most notably in the ^{14}C and ^{32}Si experiments (Table 11, Figure 22). The increase in presence of the dissolved fraction at BN compared to P3 was not accompanied by an increased presence of ^{14}C or ^{32}Si in the smaller (<5 µm) particulate fraction (Table 11, Figure 22) which indicates that cell break down or uptake and conversion to biomass by smaller biota did not occur. However bacterial respiration contributing to the DI^{14}C pool may have been present at BN and confirmed not present at P3. For ^{55}Fe at BN, the increased presence of activity in the dissolved fraction was accompanied by an increased presence of activity associated with the smaller <5 µm particulates (Table 11, Figure 22), suggesting that the abiotic movement of ^{55}Fe from the particulate to the dissolved fraction and then back (re-)adsorbed to the smaller particles is the most likely process resulting in the observed transfers and is consistent with the particle reactive nature of Fe leading to significant de-absorption which has also been observed with Zn (Weber et al., 2018) and Chromium (Janssen et al., 2021).

Different species of diatom under different conditions can display a lag time before the onset of dissolution (Passow et al., 2011). Viable cells can take up to 9-14 days before the onset of dissolution while detrital cells can dissolve rapidly (Passow et al., 2011). The viable cells at South Georgia were only incubated for up to 5 days which may have prevented detection of Si dissolution. At BN.1 whole cells were incubated for up to 10 days which still didn't result in a significant consistent dissolved ^{32}Si fraction, however the second stage of the BN.2 experiment was only incubated for up to 6 days and did observed Si dissolution. Other factors such as the concentrations of transparent exopolymer particles (TEP) which aid in aggregation and would provide a labile C source for the bacteria, will also slow down dissolution (Passow

et al., 2011) but TEP concentrations are unknown for these experiments. A recent study by Alcolombri et al. (2021) has shown that the act of sinking itself influences the rate at which bacteria degrade particles with even modest sinking rates of 8 m d^{-1} enhancing degradation rates 10- fold compared with non-sinking particles. Our experiments did not simulate sinking and hence may have limited observable particle degradation by bacteria in the experimental time frames.

BN had an order of magnitude warmer mesopelagic waters used for resuspension than SG (Table 4, Table 5) which may have contributed to the increased dissolution of Si as bacteria mediated selective preservation of Si over C increases with decreasing temperature (Bidle et al., 2002) as well as low temperatures reducing the Si dissolution rate (Passow et al., 2011). Additionally, the BN site was characterised by 5 orders of magnitude greater mesopelagic bacteria cell abundance than P3 (Table 4, Table 5). This may have enhanced the ^{14}C and ^{32}Si dissolution with bacterial respiration dominating over bacterial production resulting in dissolved ^{14}C and ^{32}Si as well as DI^{14}C rather than accumulating ^{14}C or ^{32}Si in their biomass which was not detected in the smaller particulate fraction. The greater abundance of small biota may explain the greater presence of <5 µm particulate ^{55}Fe at BN due to scavenging of dissolved ^{55}Fe onto these smaller particles.

Turnover rates for each isotope were calculated by the loss in particulates over time. At South Georgia P3, ^{14}C averaged a turnover rate of 0.03 d^{-1} (turnover only measurable at a single experiment) and ^{32}Si averaged a turnover rate of 0.030 ± 0.006 d^{-1}, whilst ^{55}Fe turned over at an average rate of 0.06 ± 0.03 d^{-1}. For the comparable <5 µm resuspended live cells at Benguela BN.1, ^{14}C turned over at a higher rate of 0.05 d^{-1}, ^{32}Si turned over at a similar rate of 0.03 d^{-1} and ^{55}Fe turned over at a similar rate of 0.06 d^{-1} than at P3. BN.2 had the highest turnover rates of all sites with ^{14}C turned over at a rate of 0.09 d^{-1}, ^{32}Si turned over at a rate of 0.08 d^{-1} and ^{55}Fe turned over at a rate of 0.10 d^{-1}. BN.2 was dominated by smaller, less silicified cells than both BN.1 and P3, also with a high mesopelagic bacterial abundance (Table 4, Table 5) which may contribute to the highest turnover rate of all isotopes out of all of the sites (Bidle and Azam, 1999).

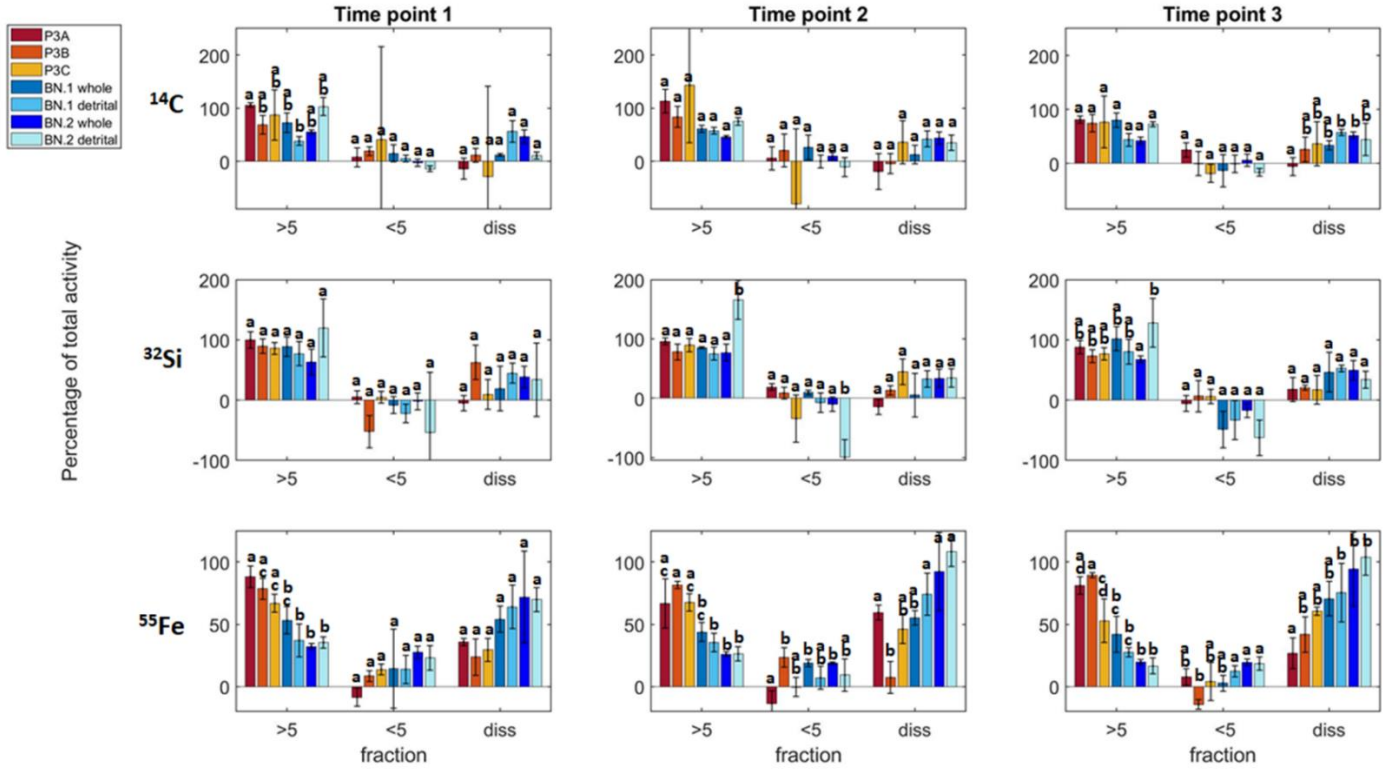

Figure 22: Distribution of >5 particulates, <5 particulates and dissolved (+wall wash for Fe) radio isotope activity as a percentage of total activity from South Georgia (P3A, P3B, P3C) in hot colours and Benguela whole and detrital (BN.1 and BN.2) in cool colours remineralisation experiments. ^{14}C (top), ^{32}Si (middle) and ^{55}Fe (bottom) panels with 3 comparable time points. Time points in days from resuspension are: P3A 2 days, 4 days, 6 days; P3B 1 day, 4 days, 8 days: P3C 1 day, 3 days, 5 days; BN 2 days, 4 days, 6 days. Error bars are standard deviation from triplicate samples, results of ANOVA with Bonferroni multi comparison test ($p<0.05$) shown as lowercase letters: levels not connected by the same letter are significantly different between different sites per fraction.

6.2.2 Summary of key findings

The two contrasting regions the remineralisation experiments were performed at, a naturally Fe fertilised productive region at South Georgia and a less productive but higher bacterial abundance and warmer mesopelagic waters of the Benguela upwelling system, resulted in different de-coupling processes driving remineralisation of Fe, C and Si.

In the South Atlantic sector of the Southern Ocean near South Georgia, mesopelagic bacterial communities did not strongly remineralise the healthy diatom cells which characterised much of the surface microbial populations in this regions. The diatoms remained metabolically active after being incubated in the dark for up to 6 days in upper mesopelagic water, with respiration not attributable to bacteria but the diatoms themselves. Lack of bacterial respiration of the labelled C coupled with minimal transfer of labelled C, Si or Fe into smaller particles (bacteria or cell fragments) indicated a general lack of remineralisation and thus would imply that export of C and nutrients to depth would likely be efficient if remineralisation were dominated by microbial processes. The differences in cycling of the different elements (C, Si, Fe) within the experiments at South Georgia suggest that remineralisation length scales of each of the elements may be decoupled due to both biotic and abiotic processes. The Si was retained intracellularly (i.e. within the diatom frustules), some proportion of the cell C was respired, and the Fe associated with the exterior of the cells (adsorbed extracellularly) was rapidly lost. With modest *in-situ* sinking rates of 18 to 60 m d^{-1} for large diatoms (Villa-Alfageme et al., COMICS SI) the experimental timescale used could translate to a sinking depth range of 100-300 m (see section 3.4.3) releasing dFe into the mesopelagic abiotically. Although it should be noted that this may be accompanied by subsequent re-uptake through a de-absorption process. Ultimately, the kinetics and equilibrium conditions of Fe exchange will be influenced by ligand binding site density on cell surfaces of phytoplankton and bacterial cells, as well as the dissolved ligand pool. Intracellular pools of Fe (along with C and Si) could be exported to deeper depths than extracellular Fe, with a slow remineralisation rate, if physical processes such as grazing or cell lysis do not act to break cells up and speed up remineralisation. Such a lack of microbe-mediated respiration, dissolution and cell breakdown would tend to increase the remineralisation length scale of the intra-cellular Fe, C and Si.

Within the Benguela system, the remineralisation signal of all the isotopes were stronger. The transfer of Fe from particulate to dissolved fractions likely followed the same processes as around South Georgia, with scavenging/ de-absorption of the extra-cellular adsorbed Fe. The warmer waters and greater mesopelagic bacterial abundance at the Benguela upwelling are likely to have enhanced the Si dissolution of the cell frustules and bacterial respiration of the C without an

increase in bacterial biomass. The experiments performed with detrital material indicated some enhanced Si and C dissolution, potentially associated with removal of the diatom outer protective coating and cell leakage of DOC that the bacterial community ultimately respired as DIC with no measurable bacterial production.

Bacterial production and cell growth were found to be (co-) limited by Fe and Corg, with strongest responses from the mesopelagic bacteria assemblages in the HNLC Pacific sector of the Southern Ocean. The addition of combined Fe and Corg stimulated a change in bacterial community composition within the upper mesopelagic above the ferricline towards larger celled bacteria that contributed to an overall increase in bacterial production. Consequently, the controls on ferricline depth and mesopelagic standing stocks of Fe (winter mixing, scavenging, Fe associated with sinking material) will be important in determining the extent of ocean Fe C (co-) limitation of mesopelagic bacterial growth and production and will be a driver in bacterial community composition at depth, where much of the downward particle flux is attenuated via zooplankton and bacterial respiration (Ducklow et al., 2001).

6.2.3 Experiment synthesis; the reciprocal feedback processes which influence Fe cycling and consequently C cycling in the mesopelagic zone

The results from the two main experiment types in this study of relative mesopelagic remineralisation of C, Si and Fe and mesopelagic bacterial limitation, performed across the 3 different cruises, can be conceptually synthesised, alongside known processes (Boyd and Ellwood, 2010) to assess the potential combined impact on the sequestration of C. Figure 23 builds upon both of the objectives in this thesis with the conclusions from bacterial limitation in section 5.4.3 to also include the remineralisation results from sections 3.4.3 (South Georgia remineralisation results) and 4.4.1 (Benguela whole and detrital remineralisation results).

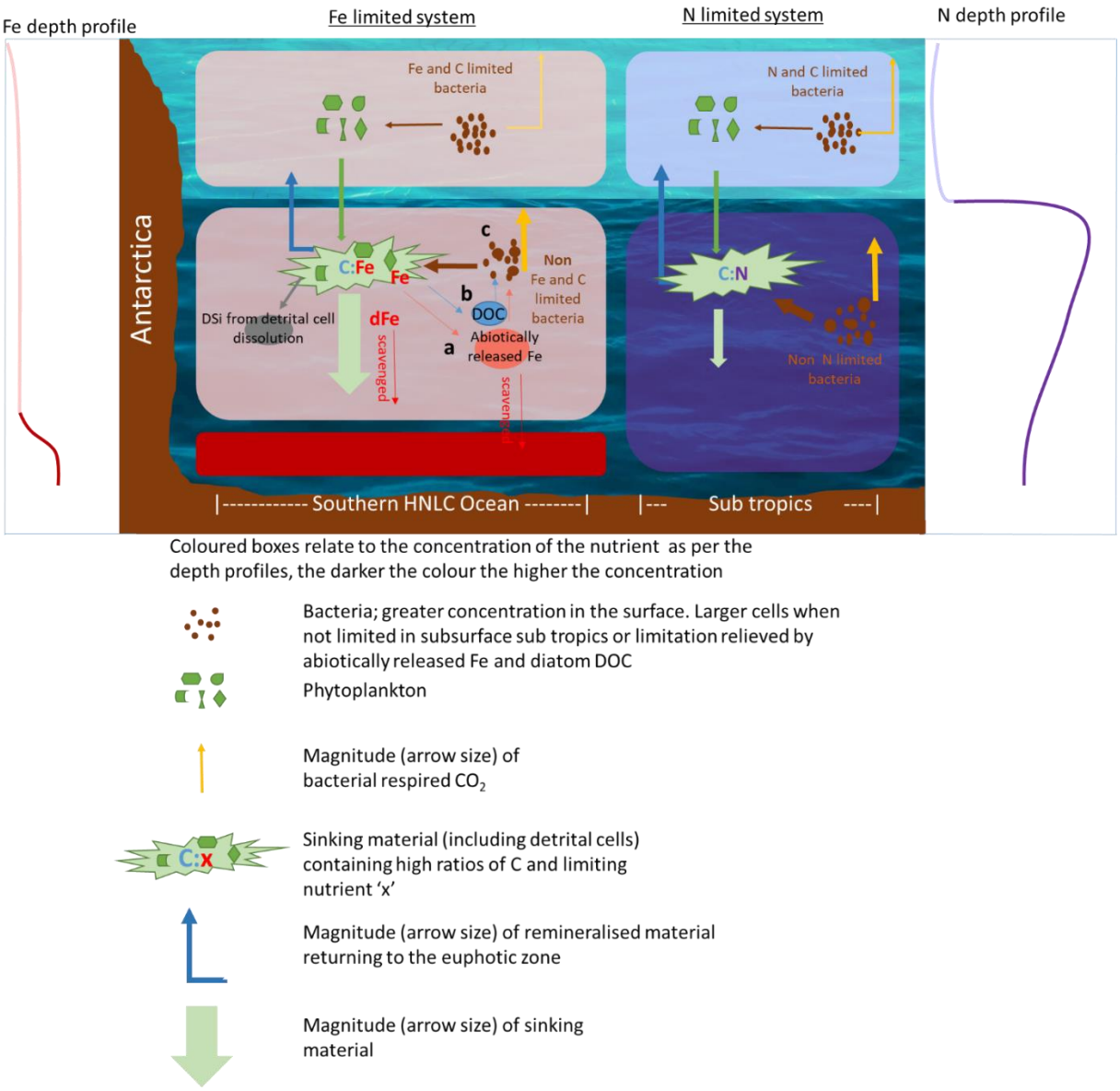

Figure 23: Conceptual influence of the combined mesopelagic bacterial remineralisation and bacterial limitation results on carbon sequestration. The letters define stages of the process for reference in the text. Other processes contributing to the remineralisation of C are not shown to allow clarity of the processes under discussion.

Section 5.4.3 hypothesised how nutrient limited mesopelagic bacteria may influence the C sequestration depth in two different nutrient regimes. In addition, the results from the remineralisation experiments from South Georgia at P3 indicate how abiotic processes may influence the Fe associated with and released from sinking particles and hence contribute to the mesopelagic Fe standing stocks which in turn may influence mesopelagic bacterial growth and production. The results from the detrital cell resuspension of release of DOC and subsequent respiration by the bacteria into the DIC pool may also influence the mesopelagic bacterial community.

The finding of the abiotic movement of adsorbed extra-cellular Fe into the water as the main transfer of Fe from particulate phases to the dissolved fraction in the remineralisation experiments could in part replenish scavenged dFe (but will depend on the balance and rate between abiotic Fe release and further scavenging) and contribute towards alleviating the limitation of mesopelagic bacteria if enough labile organic C is bioavailable (Figure 23).

In our remineralisation experiments, the surface community was dominated by diatoms and the resuspended whole live diatoms were still respiring the labelled C into the DIC pool and contributing to the abiotic transfer of PFe to dFe after 6 days incubation in the dark. With modest sinking rates of 18 to 60 m d^{-1} for large diatoms this could translate to a sinking depth range of 100-300 m (see section 3.4.3) releasing dFe into the mesopelagic increasing the dFe pool available to the bacteria (Figure 23 a). The detrital diatom cells were possibly more prone to dissolution in the mesopelagic (see section 4.4.1) releasing Si and DOC subsequently taken up and released by bacteria as DIC into the water column, as well as the abiotic transfer of adsorbed PFe to dFe (Figure 23 a and b). The amount of dFe released by sinking whole or detrital diatoms and higher diatom DOC bioavailability (Landa et al., 2018) could contribute towards alleviating Fe and Corg (co-) limitation in mesopelagic bacteria. This has created two opposing gradients between sinking diatoms as a transport vector of C and deep C sequestration and diatom derived DOC and abiotically released dFe increasing bacterial growth of large cells, increasing secondary bacterial production, so potentially enhanced remineralisation rate (Figure 23 c). Thus shallowing the remineralisation length scale of the nutrients and ultimately the C sequestration. From our experiments the dominance of these two opposing processes are unknown.

6.3 Future Experimental Work

6.3.1 Influence of detrital cells on remineralisation rates

Future experimental work of the type performed in chapters 3&4 could consider further modifications. The freeze thaw of stage 1 surface material (Chapter 4) should be repeated to confirm the weak signal of greater Si dissolution with detrital cells than whole cells when resuspended in mesopelagic water. The dissolved fraction should be measured rather than calculated, with a large enough dissolved sample volume to accurately count on the scintillation counter. The experiments could be performed in the surface as well as the mesopelagic to provide the potential for stronger comparison with Bidle and Azam (1999) Si dissolution experiments.

6.3.2 Influence of cells size on remineralisation rates

A greater difference in cell size should be used for stage 1 resuspension to assess how cell size could influence the remineralisation rate and de-coupling of Fe, C and Si in the mesopelagic. Cell size may influence the Fe adsorption/de absorption rates as a larger surface area would provide more ligand binding sites (Hou et al., 2020). Smaller cells could be degraded more rapidly as the larger surface area to volume ratio will result in more rapid colonization of free living bacteria, resulting in higher remineralisation rates of C and Si compared with larger fast-sinking particles (Hargrave, 1972; Cavan et al, 2017b). The difference in cell size may therefore further decouple the abiotic Fe transfer mechanism and the biotic C and Si remineralisation pathways.

6.3.3 Mesopelagic bacterial limitation

Although clear evidence for the limitation responses observed being driven by a sub-population of the bacterial community were presented in Chapter 5 (Figure 19, Figure 20), further work could provide more information on the taxonomic response. Sterivex samples for 16S - DNA sequencing corresponding to flow cytometer samples were collected within the same set of experiments and could be analysed from the experiments performed around South Georgia and in the Pacific sector of the Southern Ocean. This would provide more information on the community composition change in response to the different additions in the bacterial limitation experiments. The plan is to

add these results to those presented in Chapter 5 of this thesis in preparation as a manuscript for publication.

To further expand the dataset of mesopelagic bacteria limitation a fuller suite of experiments could be performed at contrasting naturally Fe fertilised, HNLC and N limited sites with experimental depths designed to sample above and below the ferricline and nitracline. Wider contextual data of Fe content in sinking material as well as mesopelagic standing stocks of dFe could also provide further context to understand the global extent and potential consequences of the Fe C (co-) limitation of mesopelagic bacteria we observed. Obernosterer et al. (2008) found no correlation between the abundance of HNA cells and bacterial respiration. Further data on bacterial respiration as well as bacterial production could be collected during the experiments to determine if bacterial respiration correlated with nucleic acid content and cell size under different treatments as it is bacterial respiration that ultimately influences the cycling of C back into the water column.

Additionally, other trace metals could be further explored to examine their potential to play a role in mesopelagic bacterial limitation. For example, Baltar et al. (2018) found limited evidence of Zn as well as Fe limitation of bacterial production at 500 m but did not explore the role of organic C availability. If organic C limitation is alleviated it would be interesting to determine whether the sequential limitation of Zn (which has physiological importance in enzymes for redox reactions (Morel et al., 2003)) could influence bacterial production, cell abundance and community composition. However, in the context of the developed conceptual models (Figure 23), Zn would be expected to increase rapidly with depth in the mesopelagic due to a 'nutrient like' depth profile (Figure 25 in Appendix A). It would thus also be interesting to explore whether other scavenged type metals (e.g. Mn, Co) might have some potential to influence mesopelagic biological processes.

6.3.4 Mesopelagic bacterial limitation influencing remineralisation

Further in field experiments could be performed that combine aspects of the remineralisation and bacterial limitation experiments. Stage 2 of the remineralisation experiments could be enhanced by adding cold Fe and cold Corg to the water used for resuspension (from multiple depths) to determine whether this potential alleviation of bacterial production limitation would enhance the relative remineralisation rates of the ^{14}C, ^{32}Si and ^{55}Fe. Finally, running the experiments for longer (>14 days; Passow et al., 2011) would potentially allow for a stronger remineralisation signal.

6.4 Future Broader Work

Climate change is predicted to alter ocean circulation with implications on the distribution of bioavailable Fe and N (Buchanan et al., 2021). The altering of substrate availability due to climate change is a contributing factor of twenty-first century increases in nitrogen limitation, resultant primary productivity declines and shifts in the sources and sinks of nitrogen (Buchanan et al., 2021). The IPCC report (Bindoff et al., 2019) modelling predicts that the upper 100 m nitrate concentrations are very likely (with medium confidence) to decline in response to increased stratification however there is low confidence regarding the projected increases in surface ocean iron levels due to systemic uncertainties in the CMIP5 (Coupled Model Intercomparison Project) models used, therefore greater understanding of Fe cycling could benefit future predictions. Iron cycling in the oceans' interior represents a major unknown and critically is hindering model development (Boyd et al., 2017).

Free living carbon oxidising bacteria are the most abundant type of bacteria in the open ocean (Giovannoni, 2017) and modelled to play a significant role in Fe cycling (Pham et al., 2021) however limited models explicitly represent free living bacteria and their impact on the Fe, N and C cycles (Tagliabue et al., 2016). Some recent model studies are exploring the interactions between free living bacteria, Fe and phytoplankton bloom dynamics (Pham et al., 2021) including bacterial activity in the mesopelagic zone, however the model likely underestimates the role of free living bacteria in the Fe cycle at this depth (Pham et al., 2021). An increasing knowledge of internal Fe recycling, speciation and influence of different bacterial groups on Fe cycling could enhance understanding of Fe availability to bacteria and phytoplankton and distribution feedbacks to the C cycle and climate, especially in the mesopelagic zone which is an understudied region and can be a key junction of water masses that in part determine the fate of the Fe and C storage (such as at the OOI site, Figure 6a). The increased knowledge can come through a combination of experimental and modelling work.

The conceptual comparison of the role nutrient limited mesopelagic bacteria play on remineralisation rates of sinking material in different nutrient limitation regimes (Figure 23) could be explored further using numerical modelling. Modelling could help test the hypothesis that in low latitude N limited systems mesopelagic bacteria are not N limited and would thus increase the rate of remineralisation of sinking particles (leading to shallow remineralisation), whilst high latitude mesopelagic bacteria are Fe and C limited, reducing the rate of remineralisation (leading to deep remineralisation and longer term storage). This would allow further testing of the hypothesised feedback whereby a deep ferricline may be stabilised through de-absorption of Fe from the outer surfaces of sinking particles (transfer of PFe to dFe), combined with any influence of Fe C (co-)

limitation of heterotrophic activity on remineralisation restricting biotic release of both C and Fe above the ferricline. Physical effects of winter mixing on ferricline depth and hence mesopelagic dFe concentrations could also be investigated.

In addition, our experimental results of Fe C (co-) limitation of free living bacteria at depth with larger bacteria responding to a greater extent to nutrient addition than smaller bacteria, thus increasing the overall population bacterial production (see Chapter 5), could be numerically modelled to assess the feedbacks of different bacterial groups and community structure to Fe and C remineralisation as the bacteria size class dominance alters as nutrient limitation is alleviated.

Enhanced experimental work of the combination of the bacterial limitation and remineralisation experiments (see section 6.3.4) could have a broader dataset gathered to feed into model parameters. The community structure of the bacterial population during the limitation sampling (via sterivex samples for DNA analysis) could be assessed to understand if the mesopelagic bacterial community structure plays a role in the de-coupling of Fe from macronutrients measured during the remineralisation experiments.

Practical experimental limitations will have to be considered but a further factor to consider is how different forms of iron (e.g. organically complexed or lithogenic; affecting bioavailability) could influence the alleviation of bacterial production limitation and subsequent remineralisation and de-coupling of Fe and C at depth.

Further enhanced knowledge of biotic and abiotic factors that influence the vertical profiles of Fe and C in the mesopelagic zone relative to water masses could contribute to a broader understanding of basin distributions of Fe and C and resupply to surface biota.

Increased modelling of the linkages between bacteria and Fe, N and C cycling based on enhanced experimental data could help reduce the uncertainty of future climate change predictions.

Appendix A South Georgia iron cycling supplementary data

Table 12: P3 experimental metadata at time of collection of phytoplankton cells for each experiment, either iron limitation or remineralisation. N/A indicates not available

Station	**P3A**		**P3B**			**P3C**	
Expt.	Iron limitation	Remineralisation (stage 1 cell collection)	Iron limitation	Remineralisation (stage 1 cell collection)	Iron limitation	Remineralisation (stage 1 cell collection)	Iron limitation
Cast	CTD003/004		CTD015		CTD024	CTD026	CTD029
Date	16/11/17		29/11/17		05/12/17	09/12/17	11/12/17
Depth (m)	30		30		20	18	20
Temp (^{o}C)	2.3		2.9		3.4	3.3	3.4
$Si(OH)_4$ (µM)	4.16		0.46		0.18	1.02	0.68
NO_3 (µM)	19.17		17.74		17.01	16.80	16.84
Chl-*a* (mg m^{-3})	4.4		4.30		1.74	2.81	1.59
dFe (nM)	0.03		0.17		N/A	N/A	0.15

Appendix A

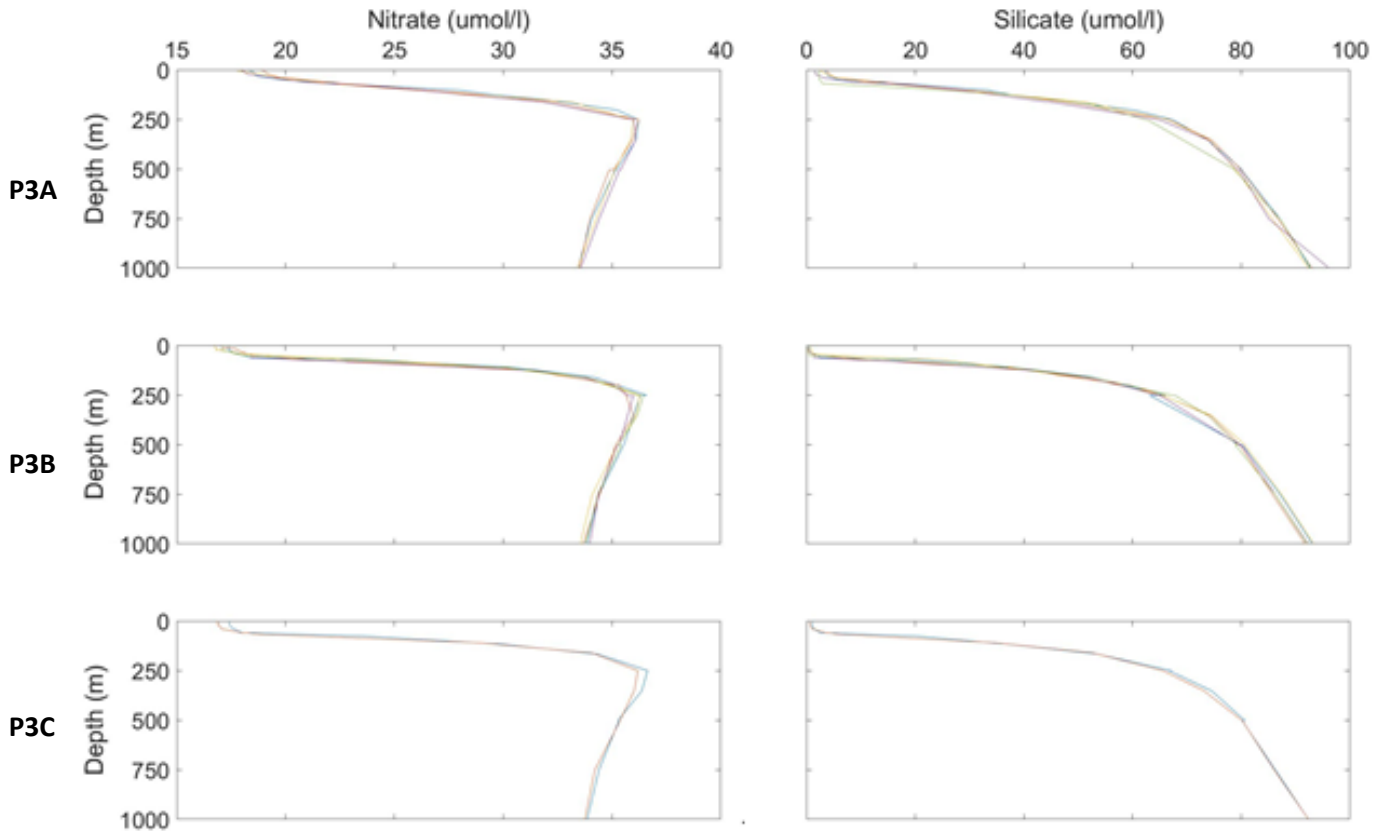

Figure 24: Depth profiles of all stainless steel CTD casts for Nitrate (µmol/L) and Silicate (µmol/L) of each P3 occupation at 52S, 40W. P3A (15th to 22nd November 2017), P3B (29th November to 5th December 2017) and P3C (9th to 15th December 2017).

.

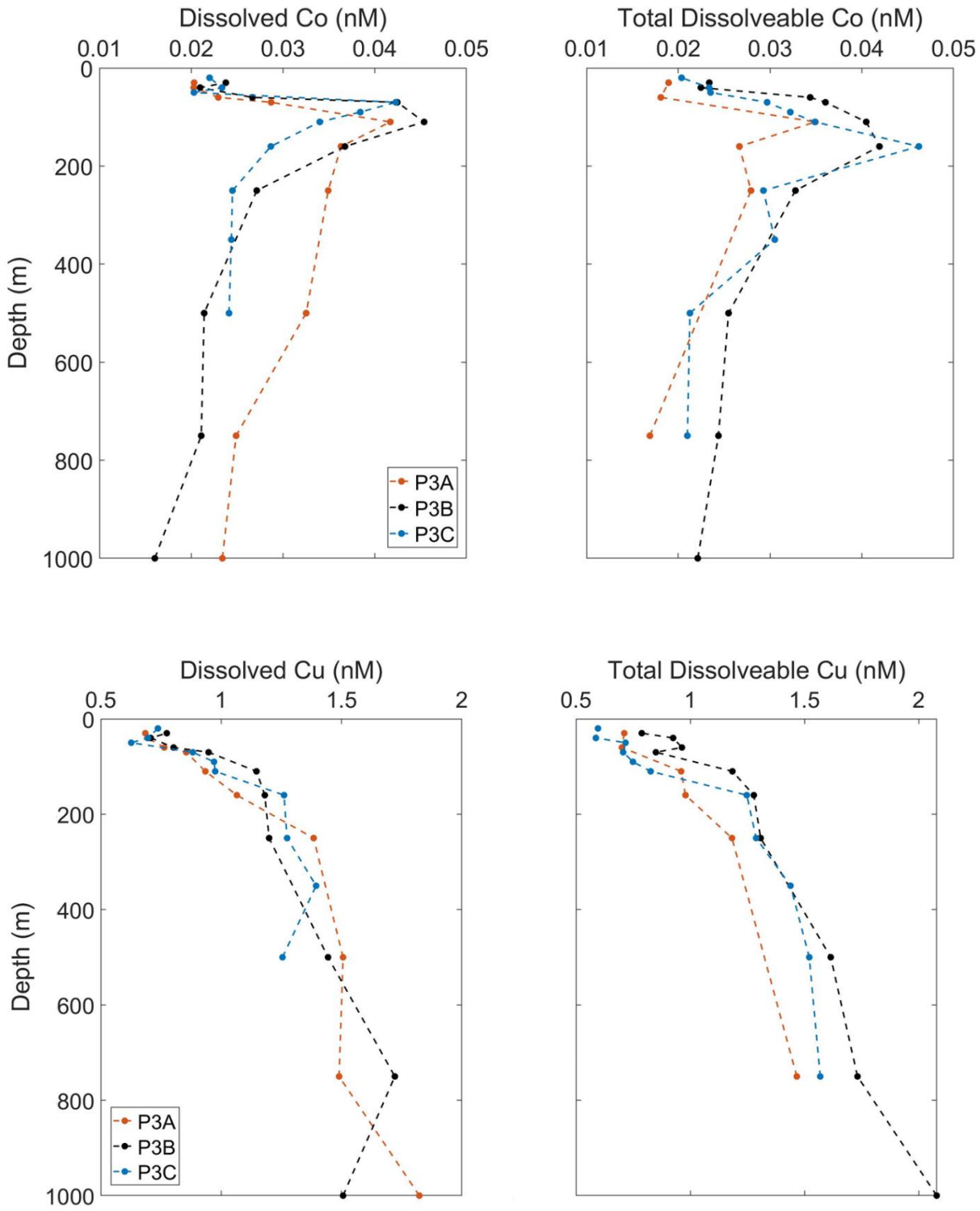
Dissolved Co (nM)
Total Dissolveable Co (nM)
Dissolved Cu (nM)
Total Dissolveable Cu (nM)
Depth (m)
P3A
P3B
P3C

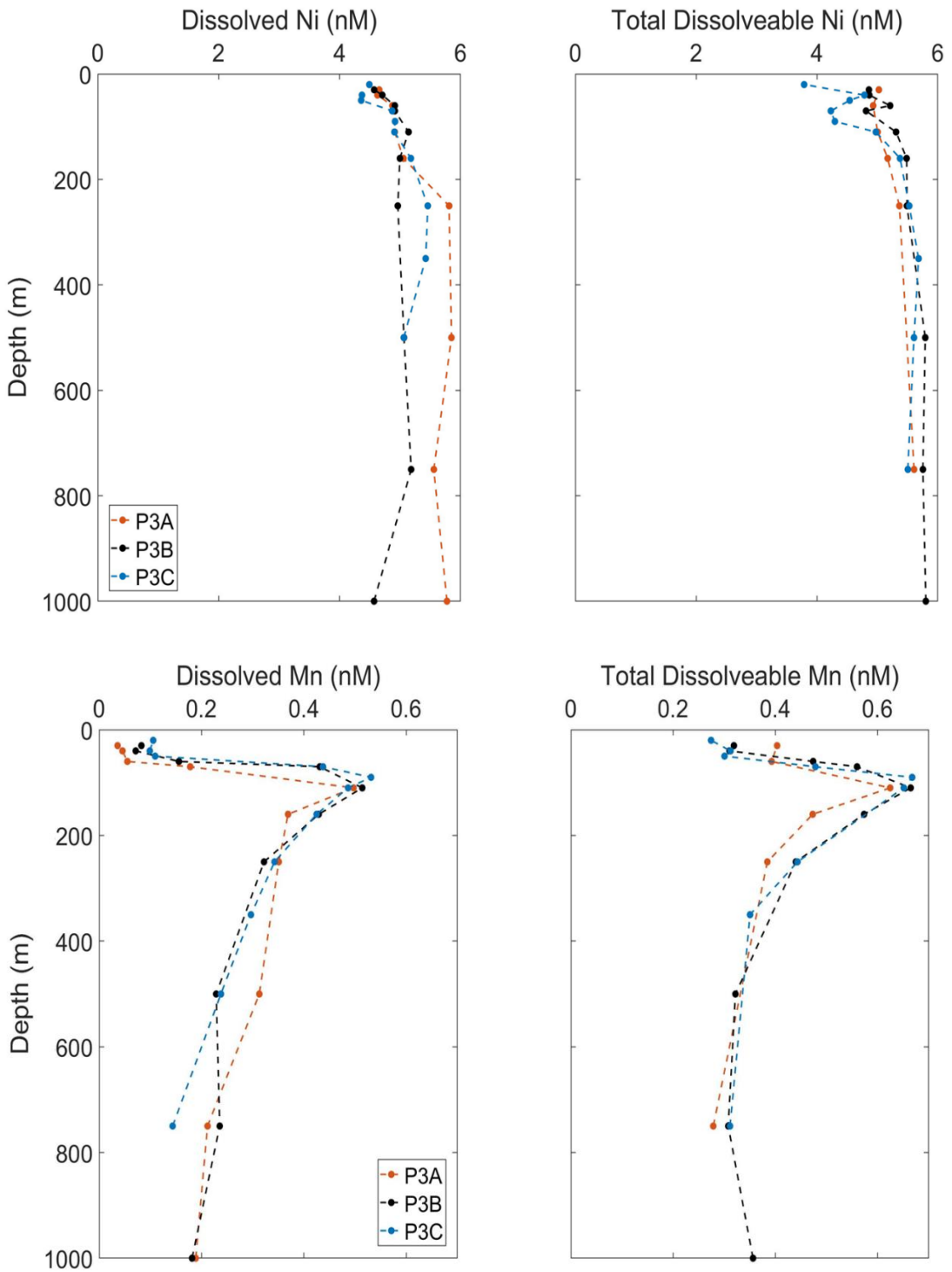
Dissolved Ni (nM)
Total Dissolveable Ni (nM)
Dissolved Mn (nM)
Total Dissolveable Mn (nM)
Depth (m)
P3A
P3B
P3C

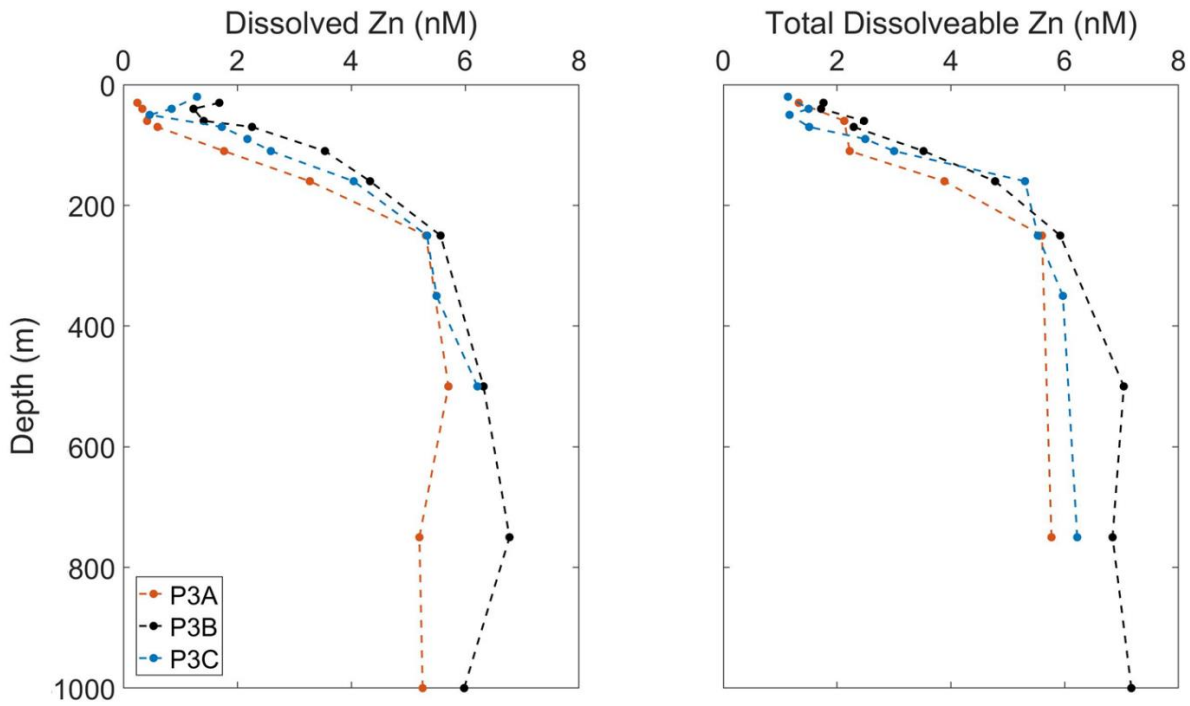

Figure 25: Trace metal depth profiles of dissolved and total dissolvable Cobalt (Co), Copper (Cu), Nickel (Ni), Manganese (Mn) and Zinc (Zn).

Appendix B BN.2 whole vs detrital remineralisation experiment

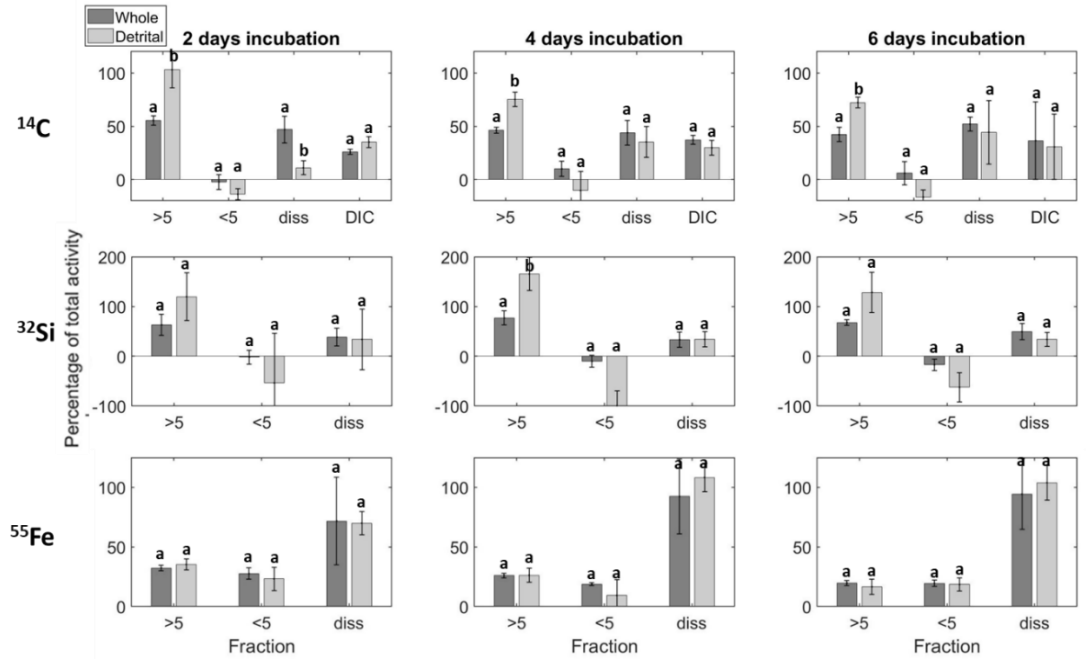

Figure 26: Distribution of >5 µm particulates, <5 µm particulates, dissolved (+ wall wash for Fe) and DI^{14}C radio isotope activity as a percentage of total activity in whole live (dark grey) and detrital (light grey) remineralisation experiments at BN.2. ^{14}C (top), ^{32}Si (middle) and ^{55}Fe (bottom) panels for expt. 2 at BN.2 with 3 time points from 2 to 6 days incubation from resuspension. Error bars are standard deviation from triplicate samples, results of ANOVA with Bonferroni multi comparison test ($p<0.05$) shown as lowercase letters: levels not connected by the same letter are significantly different between whole and detrital incubations per fraction.

Appendix C Zooplankton grazing influence on remineralisation potential

Zooplankton play fundamental roles in the cycling and export of C and nutrients in the ocean as the C and nutrients can be ingested, absorbed, egested, metabolized, and made available to higher trophic levels through growth and reproduction (Steinberg and Landry, 2017). Zooplankton community structure can increase C remineralisation through the fragmentation of particles that are subsequently rapidly colonised and degraded (Giering et al., 2014; Mayor et al., 2014) as well as increasing the transfer of C into deeper waters via vertical migration and the production of faecal pellets containing POC that sink through the mesopelagic (Steinberg et al., 2000). In the Southern Ocean, calanoid copepods contribute substantially to zooplankton biomass (Boysen-Ennen et al., 1991; Hopkins et al., 1993). *Calanoides acutus* was dominant at the South Georgia P3 site forming nearly 80 % of the mesozooplankton surface community (Cook et al., COMCIS SI) and is a large herbivorous species with its diet consisting of 45 – 61 % Diatoms at P3 (Cook et al., COMICS SI), which overwinters in diapause at depth (Hopkins, 1985; Hopkins and Torres, 1989).

C.1 Material and Methods

The remineralisation experiments followed the method detailed in section 2.5 with the following additions. At the final occupation of P3, a parallel experiment was set up such that during stage 2 resuspension of surface material in whole community mesopelagic water, a single picked zooplankton (*Calanoides acutus*) was added to investigate differential uptake and re-distribution of the radio isotopes by the zooplankton. Quantification of activity within each phase (size fractionated particulate, adsorbed, dissolved, wall wash, DIC) used methods similar to the end-point measurements at the termination of stage 2 in the experiments described in Chapter 3, with the addition of the picked zooplankton being placed in a vial with 6 mL Ultima Gold scintillation cocktail before being counted on a liquid scintillation counter (Perkin Elmer TriCarb 3180 TR/SL) to determine isotope uptake/adsorption by the zooplankton itself.

C.2 Results

The South Georgia experimental remineralisation results indicate that mesopelagic microbial communities are likely not the primary process acting on sinking healthy, diatom cells, suggesting that other processes such as zooplankton grazing could be important in contributing to remineralisation in that system. In order to test this extended hypothesis, a parallel experiment at P3C was performed that included a picked zooplankton (see methods section 2.5).

Following stage 1 resuspension of the >5 µm particulates, the activity associated with these particulates becomes the carried over total activity for stage 2. The retention or redistribution of the carried over total activity into size fractionated particulates or the dissolved fraction were then assessed for both the non-zooplankton and zooplankton addition samples as well as activity associated with the zooplankton itself. If the addition of the zooplankton enhanced the remineralisation of the C, Si and Fe it would result in the zooplankton experiment having a greater proportion of radio isotope in the smaller size fraction and/or the dissolved fraction than the non zooplankton experiment, with activity associated with the zooplankton itself. In the case of ^{55}Fe, the activity associated with the wall wash has been considered a part of the dissolved fraction.

Comparison of the activity within the carried over total from stage 1 to the retention of activity in the measured particulate (all particulates, >0.2 µm) within stage 2 for ^{14}C were statistically ($p<0.05$) indistinguishable (i.e. no presence of dissolved activity) for all but a single time point after 5 days incubation in the non-zooplankton samples (Figure 27). For the zooplankton parallel experiment an additional time point (1 day and 5 days incubation) resulted in significant ($p<0.05$) measurable dissolved fraction (Figure 27). At the time point after 5 days of incubation that resulted in the dissolved fraction in both the non zooplankton and parallel zooplankton experiment, the fraction of dissolved activity as a percentage of the total activity were indistinguishable ($p<0.05$) (Figure 27). The minimal increase in presence of dissolved ^{14}C within the zooplankton addition experiments were not due to DI^{14}C respired by the zooplankton as the level of ^{14}C activity in the DIC pool was significantly less in the zooplankton experiment than the non zooplankton experiment (Figure 27).

For the zooplankton experiment there were no statistically distinguishable ($p<0.05$) difference between the carried over ^{32}Si total activity from stage 1 to the retention of ^{32}Si activity in the measured particulate (all particulates, >0.2 µm) within stage 2 (i.e. no dissolved

fraction) compared with a single time point after 3 days of incubation for the non-zooplankton experiment (Figure 27). Similarly to ^{14}C, the majority of ^{32}Si activity remained in the particulate fraction for 5 days in the dark for both parallel experiments. Neither ^{14}C or ^{32}Si activity were significantly (*p<0.05*) measurable associated with the zooplankton itself or in any smaller <5 µm particulates (Figure 27).

For ^{55}Fe, both experiments resulted in all time points having the carried over total and particulates being statistically different (*p<0.05*), indicating a consistent dissolved fraction in both experiments, but the amount transferred from particulate to dissolved phase was not significantly different between experiments (Figure 27). Only the first time point after 1 day incubation resulted in ^{55}Fe activity in the <5 µm particulates for both experiments (again not significantly different between experiments) and only the second time point after 3 days incubation had significantly measurable activity associated with the zooplankton itself (Figure 27).

For all isotopes in all time points, the activity in the <5 µm particulates and dissolved fractions were indistinguishable (*p<0.05*) between the zooplankton and non zooplankton experiments.

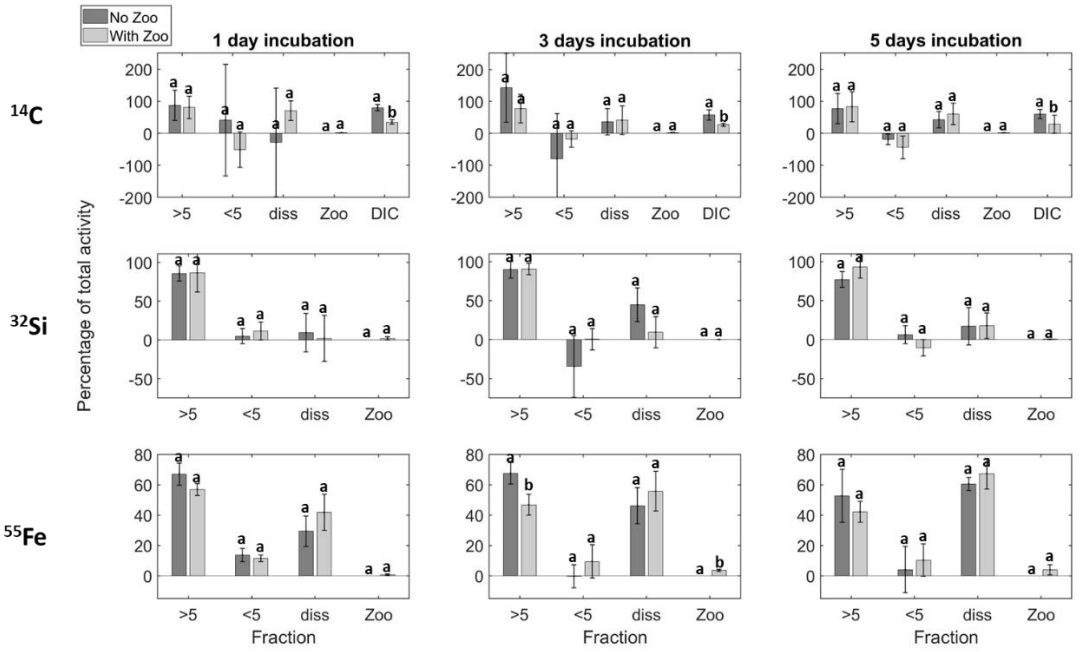

Figure 27: Distribution of >5 µm particulates, <5 µm particulates, dissolved (+ wall wash for Fe), zooplankton (zoo) and DI^{14}C radio isotope activity as a percentage of total activity in non-zooplankton addition (dark grey) and zooplankton addition (light grey) remineralisation experiments. ^{14}C (top), ^{32}Si (middle) and ^{55}Fe (bottom) panels at P3C with 3 time points from 1 to 5 days incubation from resuspension. Error bars are standard deviation from triplicate samples, results of ANOVA with Bonferroni multi comparison test (*p<0.05*) shown as lowercase letters: levels not connected by the same letter are significantly different between non zooplankton and zooplankton incubations per fraction.

C.3 Discussion

The common diatom taxa present at P3 around South Georgia were *Chaetoceros spp*., *Thalassionema nitzschioides*, *Fragilariopsis kerguelensis*, *Eucampia antarctica*, and *Pseudo-nitzschia spp* and these taxa remained consistent throughout the P3 occupation, with no succession observed (Poulton et al., COMICS SI). *Calanoides acutus* was the zooplankton species added to the resuspension experiments and were observed to graze upon diatoms at P3, with specific grazing experiments from P3 showing a *Calanoides acutus* diet comprising of diatoms (*Eucampia* sp.) (45-61%), phytodetritus and planktonic ciliates (Cook et al., COMICS SI). Independent measurements of silica cycling at P3 showed a reduction in the Si:N ratio from 2.5 to 1.3 mol mol^{-1} from P3A to P3C (Poulton et al., COMICS SI) indicating less silicification, which could encourage grazing of the diatoms resuspended in the remineralisation experiments by the picked zooplankton at P3C. However, it is possible that the similarity between the zooplankton and non-zooplankton remineralisation results, with no consistent transfer of radio isotope between the diatom particulate and the fragmented smaller particulates and the dissolved fraction could have been due to the diatoms settling at the base of the sample bottles making them less available for grazing by *Calanoides acutus.*

Appendix D Remineralisation potential of different particle sizes

D.1 Smaller phytoplankton remineralisation potential

Cells that avoid zooplankton ingestion or fragmentation can directly sink transferring POC and nutrients through the mesopelagic. Smaller cells can be degraded more rapidly than larger cells as the larger surface area to volume ratio will result in more rapid colonization by free living bacteria, resulting in higher remineralisation rates compared with larger fast-sinking particles (Hargrave, 1972; Cavan et al., 2017b).

The Benguela cruise consisted of 2 stations with the southerly station (BS) only visited once (Table 5). This station was dominated by <10 µm phytoplankton (Table 5) and so could be used to test the extended hypothesis from the results of the South Georgia cruise that limited remineralisation occurred due to large diatoms resisting bacterial degradation (Chapter 3), with smaller phytoplankton being more prone to remineralisation (Hargrave, 1972; Cavan et al, 2017b). The hypothesis based on the results of the South Georgia experiments that small cells may be easier to remineralise than large cells would be expected to result in the >2 µm resuspended phytoplankton having a greater proportion of radio isotope in the dissolved and/or smaller size fraction than for the >5 µm resuspended phytoplankton. In the case of ^{55}Fe, the activity associated with the wall wash has again been considered a part of the dissolved fraction. The small >2 µm cells used in the remineralisation experiments of the southern station BS can be compared to the first occupation of the northern station BN.1, where large >10 µm cells dominated the phytoplankton community (Table 5) and were used for resuspension in the remineralisation experiments.

D.2 Results

The retention or redistribution of the carried over total activity from stage 1 into size fractionated particulates or the dissolved fraction at stage 2 were assessed to determine evidence of remineralisation and compared between the particulate size fractions resuspended.

The ^{14}C experiments at both BS (>2 µm phytoplankton) and BN.1 (>5 µm phytoplankton) resulted in 80 % of time points with significant (*p<0.05*) presence of activity in the dissolved fraction. Of these, the >2 µm resuspended cells dissolved ^{14}C activity as a proportion of the total activity was significantly greater (*p<0.05*) than the >5 µm resuspended cells dissolved ^{14}C proportion in a single time point (after 4 days incubation). Silica-32 experiments showed less presence of activity in the dissolved fraction than the ^{14}C experiments at both stations. BS (dominated by >2 µm phytoplankton) had measurable dissolved phases for 60 % of time points while BN.1 (>5 µm phytoplankton) had only 20 % of time points with significant (*p<0.05*) ^{32}Si activity in the dissolved fraction, however the proportion of dissolved ^{32}Si between the parallel experiments were again statistically indistinguishable (*p<0.05*) (Figure 28).

Both ^{32}Si and ^{14}C experiments at BS showed significant (*p<0.05*) presence of activity within the <2 µm particulate fraction, with ^{32}Si present in 20 % of time points (after 2 days incubation) and ^{14}C at 40 % of time points (after 2 and 6 days incubation) whilst BN.1 had no significant ^{14}C activity in the <5 µm particulate fraction and 20 % of time points resulted in significant ^{32}Si activity in the <5 µm particulate fraction (after 4 days incubation). Again, the proportion of smaller particulate ^{32}Si and ^{14}C between the parallel experiments were indistinguishable (*p<0.05*) (Figure 28).

For the distribution of ^{55}Fe activity between the different fractions, BN.1 (>5 µm phytoplankton) results indicated that all time points had a carried over total and particulates being statistically different (*p<0.05*), indicating a consistent dissolved fraction, with 60 % of the time points having activity transferred to the smaller <5 µm particulates (after 4, 8 and 10 days incubation). In contrast, at BS (>2 µm phytoplankton) 40 % of the time points resulted in significant (*p<0.05*) dissolved activity (after 6 and 8 days incubation) and 60 % of the time points resulted in ^{55}Fe in the smaller <2 µm particulates (also after 4, 6 and 8 days incubation). None of the presence of dissolved ^{55}Fe or ^{55}Fe in the smaller particulates were significantly (*p<0.05*) different between the two parallel experiments (Figure 28).

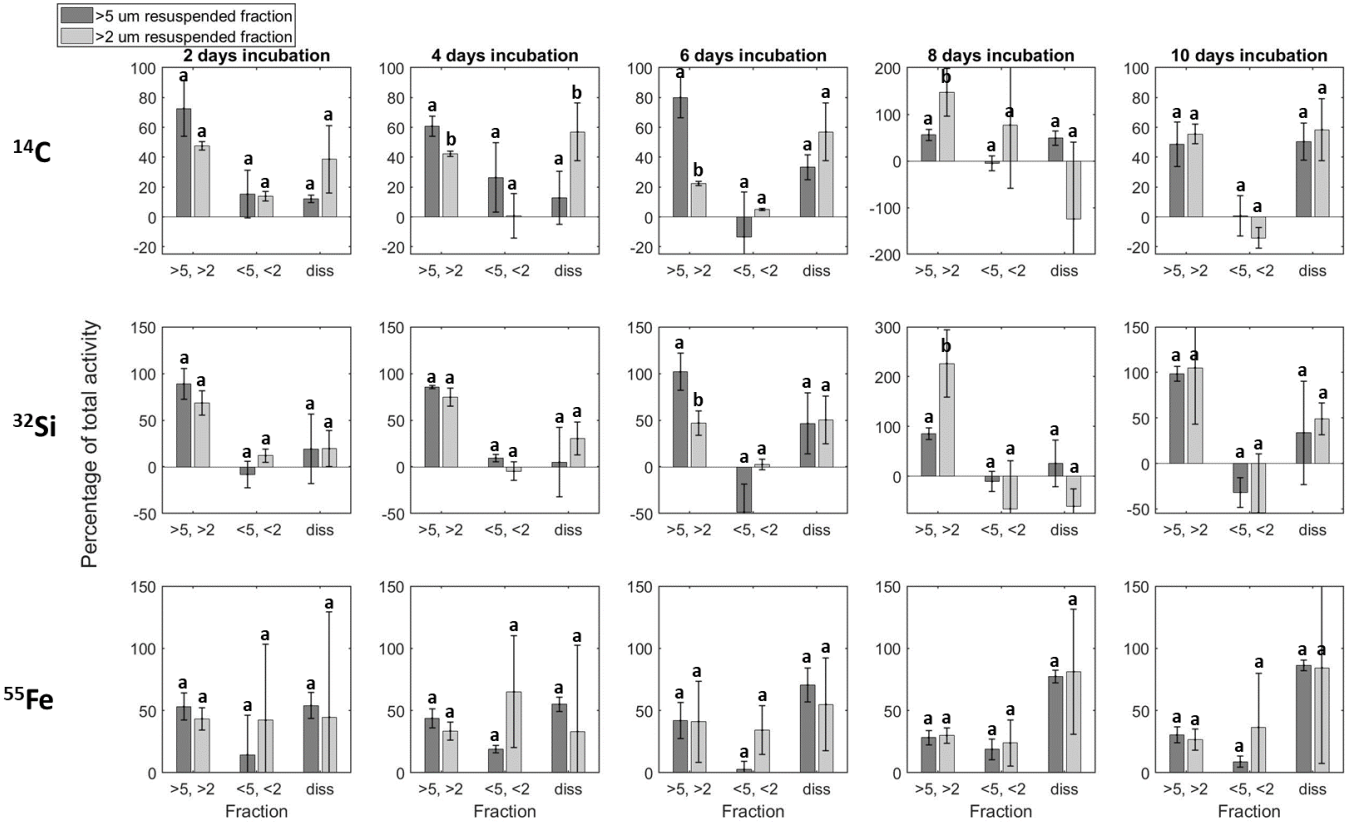

Figure 28: Distribution of >5 or >2 µm particulates, <5 or <2 µm particulates and dissolved (+ wall wash for Fe) radio isotope activity as a percentage of total activity in >5 µm sized particulate resuspension (dark grey) and >2 µm sized particulate resuspension (light grey) remineralisation experiments. ^{14}C (top), ^{32}Si (middle) and ^{55}Fe (bottom) panels from BS and BN.1 with 5 time points from 2 to 10 days incubation from resuspension. Error bars are standard deviation from triplicate samples, results of ANOVA with Bonferroni multi comparison test ($p<0.05$) shown as lowercase letters: levels not connected by the same letter are significantly different between different size particulate resuspensions per fraction.

D.3 Discussion

The dominance of small phytoplankton at BS compared to large phytoplankton at BN.1 presented the opportunity to observe if this size difference affected the amount of remineralisation of each radioisotope by mesopelagic communities. Smaller particles have a greater surface area to volume ratio so can be colonised by free-living bacteria more rapidly, potentially resulting in higher remineralisation rates compared with larger particles (Hargrave, 1972; Cavan et al, 2017b). BS was dominated by the >2 to <10 µm phytoplankton size fraction while BN.1 was dominated by the >10 µm size fraction (Table 5).

The repeated remineralisation experiments of both resuspended cell size fractions showed limited consistent evidence of microbe mediated remineralisation of the particulate material labelled with radioisotopes, similar results to the original South Georgia P3 remineralisation experiments (section 3.3.4), with no clear consistent difference between the size fractions. The resuspended large sized particles at BN.1 in the ^{55}Fe experiments showed consistent transfer from the particulate fraction to the dissolved fraction and smaller particulate fraction, but the lack of similar observable transfer of ^{14}C or ^{32}Si indicated that abiotic extra-cellular release of the ^{55}Fe is likely the mechanism of transfer, rather than biotic microbe mediated remineralisation, again similar to the results obtained north of South Georgia at P3.

D.3.1 Phytoplankton size indistinguishable

The two different size fractions resuspended may have been too similar in size (>2 vs >5 µm) to draw firm conclusions on the differences in the remineralisation of the 3 radioisotopes. Other studies classified 11–64 µm particles as “small” within an overall particle size spectrum ranging from 11-1000 µm (Durkin et al., 2015). Thus this suite of experiments reinforces the results obtained from P3 but may not be able to conclude the influence of phytoplankton particle size on remineralisation rate in the mesopelagic.

Appendix E OOI, TN and TS full depth dFe profiles

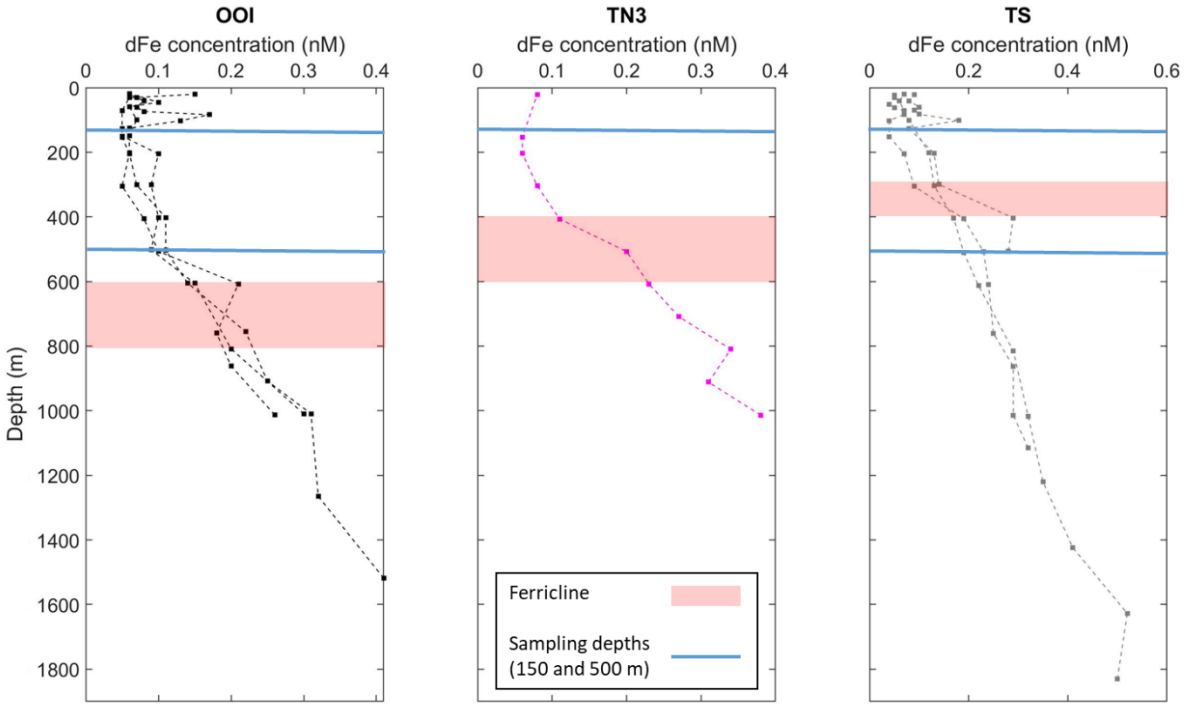

Figure 29: Full depth dFe concentrations (nM) profiles at OOI, TN3 and TS with ferricline depth (light red fill) and mesopelagic sampling depth (blue line). Ferricline defined for this study as the depth region at which the change in dFe with depth is the greatest (Tagliabue et al., 2014).

Appendix F LHNA and SLNA nucleic acid size fractions leucine uptake

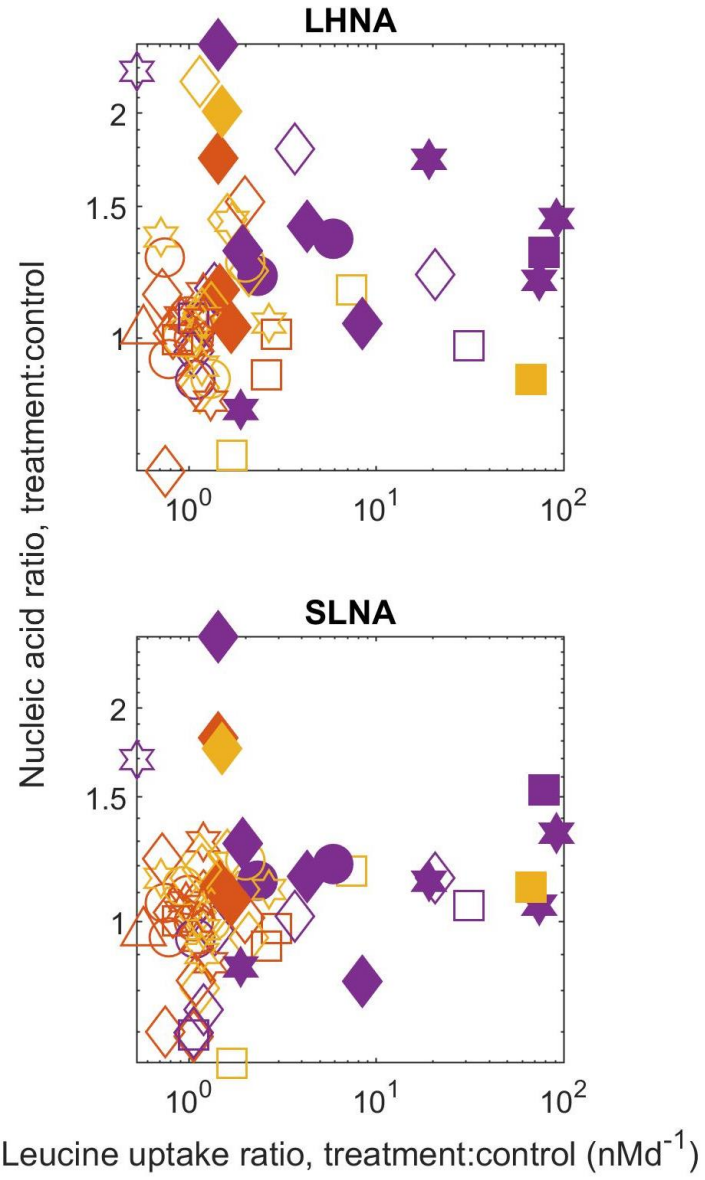

Figure 30: Relationship between average leucine uptake (nMd^{-1}) ratio of treatment to control and large high nucleic acid (LHNA) and small low nucleic acid (SLNA) bacteria ratio of treatment to control. Filled symbols represent a leucine uptake significant difference between the control and the corresponding treatment from an ANOVA with Bonferroni multi comparison test ($p<0.05$). Colours represent the different additions, +Fe+C purple, +C orange, +Fe red. Symbol shapes represent the different sampled depths, 20 m diamond, 60 m circle, 70 m pentagram, 110 m triangle, 150 m star and 500 m square.

List of References

Alcolombri, U., Peaudecerf, F. J., Fernandez, V. I., Behrendt, L., Stocler, L and R., 2021, 'Sinking enhances the degradation of organic particles by marine bacteria', *Nature Geoscience*, 31.

Allnutt, F. C., and Bonner, W. D., 1987, 'Evaluation of Reductive Release as a Mechanism for Iron Uptake from Ferrioxamine B by Chlorella vulgaris'. *Plant Physiology*, 85, 751-756.

Amin, S., Parker, M. S., Armbrust, E. V., 2012, 'Interactions between Diatoms and Bacteria, *American Society for Microbiology, Microbiology and Molecular Biology Reviews,* 76, 3.

Andrews, S. C., Robinson, A. K., Rodríguez-Quiñones, F., 2003, 'Bacterial iron homeostasis', *FEMS Microbiology Review*, 27, 215–237.

Armstrong, R., Lee, C., Hedges, J., Honjo, S., Wakeham, S., 2002, 'A new, mechanistic model for organic carbon fluxes in the ocean based on the quantitative association of POC with ballast minerals', *Deep Sea Research*, 49, 219–236.

Armstrong, E., Granger, J., Mann, E. L., Price, N., 2004, 'Outer-membrane siderophore receptors of heterotrophic oceanic bacteria', *Limnology and Oceanography,* 49, 579-587.

Arrigo, K. R., 2005, 'Marine microorganisms and global nutrient cycles', *Nature*, 437, 349–355.

Assmy, P., Smetacek, V., Montresor, M., et al., 2013, 'Thick-shelled, grazer-protected diatoms decouple ocean carbon and silicon cycles in the iron-limited Antarctic circumpolar current', *Proceedings of the National Academy of Sciences*, 110, 20633–20638.

Atkinson, A., Whitehouse, M., J., Priddle, J., Cripps, G., C., Ward, P., Brandon, M., A., 2001, 'The pelagic ecosystem of South Georgia, Antarctica'*, Marine Ecology Progress Series*, 216, 279–308.

Atkinson A. and Guerinot, M.L., 2011, 'Metal Transport', *In: Murphy A., Schulz B., Peer W. (eds) The Plant Plasma Membrane. Plant Cell Monographs*, vol 19. Springer, Berlin, Heidelberg.

Azam, F. and Long, R. A., 2001, 'Sea snow microcosms', *Nature*, 414, 495-498.

Balch, W. M., Drapeau, D. T., Fritz, J. J., 2000, 'Monsoonal forcing of calcification in the Arabian Sea', *Deep Sea Research II,* 47, 1301-1337.

Baltar, F., Gutiérrez-Rodríguez, A., Meyer, M., Skudelny, I., Sander, S., Thomson, B., Nodder, S., Middag, R., Morales, S., E., 2018, 'Specific Effect of Trace Metals on Marine Heterotrophic Microbial Activity and Diversity: Key Role of Iron and Zinc and Hydrocarbon-Degrading Bacteria, *Frontiers in Microbiology,* 9, 3190.

Baumas, C. M. J., Le Moigne, F. A. C, Garel, M., Bhairy, N., Guasco, S., Riou, V., Armougom, F., Grossart, H., Tamburini, C., 2021, 'Mesopelagic microbial carbon production correlates with diversity across different marine particle fractions', *ISME Journal*, 15, 1695-1708.

Berges, J. A. and Falkowski, P. G., 1998, 'Physiological stress and cell death in marine phytoplankton: induction of proteases in response to nitrogen or light limitation'. *Limnology and Oceanography*, 43.

Bertrand, E. M., Saito, M., Lee, P., Dunbar, R. B., Sedwick, P. N., DiTullio, G. R., 2011, 'Iron limitation of a springtime bacterial and phytoplankton community in the Ross Sea: implications for vitamin B12 nutrition', *Frontiers in Microbiology*, 2.

Bianchi, D., Galbraith, E. D., Carozza, D. A., Mislan, K. A. S., Stock, C. A., 2013, 'Intensification of open-ocean oxygen depletion by vertically migrating animals', *Nature Geoscience*, 6, 545–54.

Biddanda, B., and Benner, R., 1997, 'Major contribution from mesopelagic plankton to heterotrophic metabolism in the upper ocean'. *Deep Sea Research I*, 14, 2069–2085.

Bidle, K. D. and Azam, F., 1999, 'Accelerated dissolution of diatom silica by marine bacterial assemblages', *Nature*, 397, 508-512.

Bidle, K. D. and Azam, F., 2001, 'Bacterial control of silicon regeneration from diatom detritus: significance of bacterial ectohydrolases and species identity', *Limnology and Oceanography*, 46, 1606–1623.

Bidle, K. D., Manganelli, M., Azam, F., 2002, 'Regulation of oceanic silicon and carbon preservation by temperature control on bacteria', *Science*, 298, 1980-1984.

Bidle, K. D., Brzezinski, M. A., Long, R. A., Jones, J. L., Azam, F., 2003, 'Diminished efficiency in the oceanic silica pump caused by bacteria-mediated silica dissolution', *Limnology and Oceanography,* 48, 5, 1855-1868.

Bindoff, N.L., W.W.L. Cheung, J.G. Kairo, J. Arístegui, V.A. Guinder, R. Hallberg, N. Hilmi, N. Jiao, M.S. Karim, L. Levin, S. O'Donoghue, S.R. Purca Cuicapusa, B. Rinkevich, T. Suga, A. Tagliabue, and P. Williamson, 2019, 'Changing Ocean, Marine Ecosystems, and Dependent Communities. In: IPCC Special Report on the Ocean and Cryosphere in a Changing Climate [H.-O. Pörtner, D.C. Roberts, V. Masson-Delmotte, P. Zhai, M. Tignor, E. Poloczanska, K. Mintenbeck, A. Alegría, M. Nicolai, A. Okem, J. Petzold, B. Rama, N.M. Weyer (eds.)]. *'Cambridge University Press, Cambridge, UK and New York, NY, USA*, 447-587.

Bjørnsen, P. K. and Kuparinen, J., 1991, 'Determination of bacterioplankton biomass, net production and growth efficiency in the Southern Ocean'. *Marine Ecology Progress Series*, 71, 185–194.

Blain, S., Quéguiner, B., Armand, L., et al., 2007, 'Effect of natural iron fertilization on carbon sequestration in the Southern Ocean', *Nature*, 446, 1070–1074.

Bonnain, C., Breitbart, M., Buck, K. N., 2016, 'The Ferrojan Horse hypothesis: iron-virus interactions in the ocean', *Frontiers in Marine Science*,3, 82.

Boyd, P., Watson, A., Law, C. et al., 2000, 'A mesoscale phytoplankton bloom in the polar Southern Ocean stimulated by iron fertilization', *Nature,* 407, 695–702.

Boyd, P. W., 2002, 'Environmental factors controlling phytoplankton processes in the Southern Ocean', *Journal of Phycology*, 38, 844–861.

Boyd, P. W., C. S. Law, D. A. Hutchins, E. R. Abraham, P. L. Croot, M. Ellwood, R. D. Frew, et al., 2005, 'FeCycle: attempting an iron biogeochemical budget from a mesoscale SF6 tracer experiment in unperturbed low iron waters', *Global Biogeochemical Cycles*, 19, GB4S20.

Boyd, P. W. and Trull, T., 2007, 'Understanding the export of biogenic particles in oceanic waters: is there consensus?', *Progress in Oceanography,* 72, 276–312.

Boyd, P. W., Jickells, T., Law, C. S., Blain, S., Boyle, E. A., Buesseler, K. O., Coale, K. H., Cullen, J. J., debar, H. J. W., Follows, M., Harvey, M., Lancelot, C., Levasseur, M., et al., 2007, 'Mesoscale Iron Enrichment Experiments 1993–2005: Synthesis and Future Directions', *Science,* 315, 612.

Boyd, P. W., Ibisanmi, E., Sander, S. G., Hunter, K. A., Jackson, G. A., 2010, 'Remineralization of upper ocean particles: Implications for iron biogeochemistry', *Limnology and Oceanography*, 55, 1271–1288.

Boyd, P. W., and Ellwood, M. J., 2010, 'The biogeochemical cycle of iron in the ocean', *Nature Geoscience*, 3, 675–682.

Boyd, P. W., Strzepek, R., Chiswell, S., Chang, H., DeBruyn, J. M., Ellwood, M., Keenan, S., King, A. L., Maas, E. W., Nodder, S., Sander, S. G., Sutton, P., Twining, B. S., Wilhelm, S. W., Hutchins, D. A., 2012, 'Microbial control of diatom bloom dynamics in the open ocean', *Geophysical Research Letters,* 39, L18601.

Boyd, P. W., Strzepek, R., Ellwood, M. J., Hutchins, D. A., Nodder, S. D., Twining, B. S., Wilhelm, S. W., 2015, 'Why are biotic iron pools uniform across high- and low-iron pelagic ecosystems?', *Global Biogeochemical Cycles*, 29, 1028–1043.

Boyd, P. W., Ellwood, M. J., Tagliabue, A., Twining, B. S., 2017, 'Biotic and abiotic retention, recycling and remineralization of metals in the ocean', *Nature Geoscience*, 10.

Boyd, P. W., Claustre, H., Levy, M., Siegel, D. A., Weber, T., 2019, 'Multi-faceted particle pumps drive carbon sequestration in the ocean', *Nature*, vol. 568, no. 7752, pp. 327-335.

Boysen-Ennen, E., Hagen, W., Hubold, G., Piatkowski, U., 1991, 'Zooplankton biomass in the ice-covered Weddell Sea, Antarctica', *Marine Biology*, 111, 227-235.

Bowie, A. R., Lannuzel, D., Remenyi, T., Wagener, T., Lam, P. J., Trull, P. W., et al., 2009, 'Biogeochemical iron budgets of the Southern Ocean south of Australia: decoupling of iron and nutrient cycles in the subantarctic zone by the summertime supply'. *Global Biogeochemical Cycles,* 23, 1–14.

Bowie, A. R., van der Merwe, P., Quéroué, F., Trull, T., Fourquez, M., Planchon, F., et al., 2015, 'Iron budgets for three distinct biogeochemical sites around the Kerguelen archipelago (Southern Ocean) during the natural fertilisation study, KEOPS-2', *Biogeoscience,* 12, 4421–4445.

Braun, V., and Killmann, H., 1999, 'Bacterial solutions to the iron-supply problem', *Trends in Biochemical Sciences*, 24, 104-109.

Bressac, M., Guieu, C., Ellwood, M. J., Tagliabue, A., Wagener, T., Laurenceau-Cornec, E. C., Whitby, H., Sarthou, G., Boyd, P. W., 2019, 'Resupply of mesopelagic dissolved iron controlled by particulate iron composition', *Nature geoscience',* 12, 995-1000.

Brown, L., Sanders, R., Savidge, G., Lucas, C. H., 2003, 'The uptake of silica during the spring bloom in the Northeast Atlantic Ocean', *Limnology and Oceanography*, 48, 1831–1845.

Browning, T. J., Achterberg, E. P., Rapp, I., Engel, A., Bertrand, E. M., Tagliabue, A., Moore, C. M., 2017, 'Nutrient co-limitation at the boundary of an oceanic gyre', *Nature* 551, 242–246.

Bruland, K., W and Lohan, M., C, 2003, 'Controls of Trace Metals in Seawater', *Treatise on Geochemistry*, 6, 23-47.

Brzezinski, M. A., 1985, 'The Si:C:N Ratio Of Marine Diatoms: Interspecific Variability and the Effect of Some Environmental Variables', *Journal of Phycology*, 21, 347–357.

Brzezinski, M. A., Nelson, D. M. Franck, V. M., Sigmon, D. E., 2000. 'Silicon dynamics within an intense diatom bloom at the Antarctic Polar Front along 170°W longitude'. *Deep Sea Research II*, 48, 3997-4018.

Buchanan, P.J., Aumont, O., Bopp, L., 2021, 'Impact of intensifying nitrogen limitation on ocean net primary production is fingerprinted by nitrogen isotopes.' *Nature Communication*, 12, 6214.

Buesseler, K. O. and Boyd, P. W., 2009, 'Shedding light on processes that control particle export and flux attenuation in the twilight zone of the open ocean', *Limnology and Oceanography,* 54, 1210-1232.

Burd, A. B., Hansell, D. A., Steinberg, D. K., Anderson, T. R., Arístegui, J., 2010, 'Assessing the apparent imbalance between geochemical and biochemical indicators of meso- and bathypelagic biological activity: What the @$#! is wrong with present calculations of carbon budgets?', *Deep Sea Research II*, 57, 1557–1571.

Caprara, S., Buck, K. N., Gerringa, L. J. A., Rijkenberg, M. J. A., Monticelli, D., 2016, 'A Compilation of Iron Speciation Data for Open Oceanic Waters', *Frontiers in Marine Science,* 3, 221.

Cappellen, P., and Qui, L., 1997, 'Biogenic silica dissolution of the Southern Ocean: II. Kinetics', *Deep Sea Research II,* 44, 1129-1149.

Cavan, E.L., Henson, S.A., Belcher, A., Sanders, R., 2017a, 'Role of zooplankton in determining the efficiency of the biological carbon pump', *Biogeosciences*, 14, 177–186.

Cavan, E. L., Trimmer, M., Shelley, F., Sanders, R., 2017b, 'Remineralization of particulate organic carbon in an ocean oxygen minimum zone', *Nature Communica*tions, 8, 14847.

Cavan, E. L., Henson, S. A., Boyd, P. W., 2019a, 'The Sensitivity of Subsurface Microbes to Ocean Warming Accentuates Future Declines in Particulate Carbon Export', *Frontiers in Ecology and Evolution*, 6, 230.

Cavan, E. L, Laurenceau-Cornec, E. C., Bressac, M., Boyd, P. W., 2019b, 'Exploring the ecology of the mesopelagic biological pump', *Progress in Oceanography,* 176, 102125.

Chavez, F. P. and Toggweiler, J. R., 1995, 'Physical estimates of global new production: the upwelling contribution', *Upwelling in the Ocean: Modern Processes and Ancient Records*, Wiley, Chichester, 313-320.

Cerovečki, I., Talley, L. D., Mazloff, M. R., Maze, G., 2013, 'Subantarctic mode water formation, destruction and export in the eddy-permitting Southern Ocean state estimate', *Journal of Physical Oceanography*, 43, 1485–1511.

Chever F., Bucciarelli, E., Sarthous, G., Speich, S., Arhan, M., Penven, P., Tagliabue, A., 2010 'Physical speciation of iron in the Atlantic sector of the Southern Ocean along a transect from the Subtropical domain to the Weddell Sea gyre'. *Journal of Geophysical Research,* 115, C10059.

Chisholm, S. W. and Morel, F. M. M., 1991, 'What controls phytoplankton production in nutrient-rich areas of the open sea?', *Limnology and Oceanography*, 36, 8.

Cho, B. C. and Azam, F., 1998, 'Major role of bacteria in biogeochemical fluxes in the ocean's interior', *Nature*, 332, 441–443.

Church, M., J., Hutchins, D. A., Ducklow, H., W., 2000, 'Limitation of Bacterial Growth by Dissolved Organic Matter and Iron in the Southern Ocean', *Applied and Environmental Microbiology,* 455-466.

Chróst, R. J., 1991. 'Microbial Enzymes in Aquatic Environments'. *Springer-Verlag*, New York.

Cole, J. J., Findlay, S., Pace, M. L., 1988, 'Bacterial production in fresh and saltwater ecosystems: a cross system overview', *Marine Ecology Progress Series*, 43, 1–10.

Conway, T. M. and John, S. G., 2014, 'Quantification of dissolved iron sources to the North Atlantic Ocean', *Nature,* 511, 212-215.

Cram, J. A., Chow, C. E. T., Sachdeva, R., Needham, D. M., Parada, A. E., Steele, J. A., 2015, 'Seasonal and interannual variability of the marine bacterioplankton community throughout the water column over ten years'. *ISME Journal*, 9, 563–58.

Cutter, G., Andersson, P., Codispoti, L., Croot, P., Francois, R., Lohan, M.C., Obata, H., Rutgers vd Loeff, M., 2010, 'Sampling and sample-handling protocols for GEOTRACES cruises'.

Cutter, G., Casciotti, K., Croot, P., Geibert, W., Heimbürger, L.E., Lohan, M., Planquette, H., 2017, 'Sampling and Sample-handling Protocols for GEOTRACES Cruises'. Version 3, http://www.geotraces.org/images/Cookbook.pdf

Dang, H., and Lovell, C.R., 2016, 'Microbial surface colonization and biofilm development in marine environments', *Microbiology and Molecular Biology Review*, 80, 91–138.

Davis, C. E. and Mahaffey, C., 2017, 'Elevated alkaline phosphatase activity in a phosphate replete environment: Influence of sinking particles', *Limnology and Oceanography*, 62, 2389-2403.

De Baar, H. J. W., 1994, 'Von Liebig's Law of the Minimum and plankton ecology (1899-1991)'. *Progress in Oceanography*, 33, 347-386.

De Baar, H. J. W., De Jong, J. T. M., Bakker, D. C. E., Löscher, B. M., Veth, C., Bathmann, U., Smetacek, V., 1995, 'Importance of iron for plankton blooms and carbon dioxide drawdown in the Southern Ocean', *Nature,* 373, 412–415.

De Baar, H. J. W. and De Jong, J. T. M., 2001, 'Distributions, sources and sinks of iron in seawater', *Biogeochemistry of Iron in Seawater*, Wiley, New York, 123-253.

Del Giorgio, P. A., and Cole, J. J., 1998, 'Bacterial growth efficiency in natural aquatic systems', *Annual Review of Ecology, Evolution and Systematics,* 29, 503-541.

Denman, K. L., and Penam M. A., 2000, 'The dynamic ocean carbon cycle: A midterm synthesis of the Joint Global Ocean Flux Study, in Beyond JGOFS, edited by R. B. Hanson, H. W. Ducklow, and J. G. Field', *Cambridge University Press*, New York, 469–490.

Devol, A. H., and Hartnett, H. E. 2001. 'Role of the oxygen-deficient zone in transfer of organic carbon to the deep ocean', *Limnology and Oceanography*, 46, 1684–1690.

Ducklow, H. W. and Carlson, C. A., 1992, 'Oceanic bacterial production', *Advanced Microbial Ecology*, 12, 113-181.

Ducklow, H. W., Kirchman, D. L., Quinby, H. L., Carlson, C. A., Dam, H. G., 1993, 'Stocks and dynamics of bacterioplankton carbon during the spring bloom in the eastern northern Atlantic Ocean', *Deep Sea Research II,* 40, 245–263.

Ducklow, H., 2000, 'Bacterial production and biomass in the oceans'. *Microbial Ecology of the Oceans,* 1, 85–120.

Ducklow, H., W., Steinberg, D. K., Bursseler, K. O., 2001, 'Upper Ocean Carbon Export and the Biological Pump', *Oceanography,* 14, 50-58.

Dugdale, R. C. and Goering, J. J, 1967, 'Uptake of new and regenerated forms of nitrogen in primary productivity', *Limnology and Oceanography*, 12, 196-206.

Duret, M. T., Lampitt, R. S., Lam, P., 2019, 'Prokaryotic niche partitioning between suspended and sinking marine particles', *Environmental Microbiology Reports*, 11, 386–400.

Durkin, C. A., Estapa, M., L., Buesseler, K. O., 2015, 'Observations of carbon export by small sinking particles in the upper mesopelagic', *Marine Chemistry*, 175, 72-81.

Eckhardt, U., and Buckhout, T. J., 1998, 'Iron assimilation in Chlamydomonas reinhardtii involves ferric reduction and is similar to Strategy I higher plants', *Journal of Experimental Botany*, 49, 1219–1226.

Eppley, R., W. and Peterson, B., J., 1979, 'Particulate organic matter flux and planktonic new production in the deep ocean', *Nature*, 282, 677–680.

Falkowski, P. G., 1997, 'Evolution of the nitrogen cycle and its influence on the biological sequestration of CO_2 in the ocean', *Nature*, 387, 272–275.

Fourquez, M., Obernosterer, I., Davies, D. M., Trull, T. W., Blain, S., 2015, 'Microbial iron uptake in the naturally fertilized waters in the vicinity of the Kerguelen Islands: Phytoplankton–bacteria interactions', *Biogeosciences*, 12, 1893–1906.

Fourquez, M., Bressac, M., Deppeler, S. L., Ellwood, M., Obernosterer, I., Trull, T. W., Boyd, P. W., 2020, 'Microbial competition in the Subpolar Southern Ocean: An Fe–C Co-limitation experiment', *Frontiers in Marine Science*, 6, 776.

Frew, R. D., Hutchins, D. A., Nodder, S., Sanudo-Wilhelmy, S., Tovar-Sanchez, A., Leblanc, K., Hare, CE., Boyd, P.W., 2006, 'Particulate iron dynamics during FeCycle in subantarctic waters southeast of New Zealand', *Global Biogeochemical Cycles*, 20, GB1S93.

Fukuda, R., Ogawa, H., Nagata, T., Koike, I., 1998, 'Direct Determination of Carbon and Nitrogen Contents of Natural Bacterial Assemblages in Marine Environments', *Applied and Environmental Microbiology,* 64, 3352-3358.

Ganesh, S., Parris, D. J., DeLong, E. F., Stewart, F. J., 2014, 'Metagenomic analysis of size-fractionated pico-plankton in a marine oxygen minimum zone', *ISME Journal*, 8,187–211.

Gao, X., Bowler, C., Kazamia, E., 2021, 'Iron metabolism strategies in diatoms', *Journal of Experimental Botany,* 72, 2165-2180.

Gehlen, M., Bopp, L., Emprin, N., Aumont, O., Heinze, C., Ragueneau, O., 2006, 'Reconciling surface ocean productivity, export fluxes and sediment composition in a global biogeochemical ocean model', *Biogeoscience Discussion*, 3, 803–836.

Geider. R., J and La Roche, J., 2002, 'Redfield revisited: variability of C:N:P in marine microalgae and its biochemical basis', *European Journal of Phycology*, 37, 1-17.

Giering, S., Sanders, R., Lampitt, R., Anderson, T., Tamburini, C., Boutrif, M., Zubkov, M., Marsay, C. M., Henson, S. A., Saw, K., Cook, K., Mayor, D. J., 2014, 'Reconciliation of the carbon budget in the ocean's twilight zone', *Nature* 507, 480–483.

Giovannoni, S. J., 2017, 'Sar11 bacteria: The most abundant plankton in the oceans.' *Annual Review of Marine Science*, 9(1), 231-255.

Gledhill, M. and Buck, K. N., 2012, 'The organic complexation of iron in the marine environment: a review', *Frontiers in Microbiology,* 3, 69.

Goldberg, E., D, 1954, 'Marine Geochemistry 1. Chemical Scavengers of the Sea.', *The Journal of Geology,* 62, 249-265.

Goldman, S. J., Lammers, P. J., Berman, M. S., Sanders-Loehr, J., 1983, 'Siderophore-mediated iron uptake in different strains of Anabaena sp', *PMCID,* 156, 1144-1150.

Greene, R. M., Geider, R. J., Kolber, Z., Falkowski, P. G., 1992, 'Iron-induced changes in light harvesting and photochemical energy-conversion processes in eukaryotic marine-algae', *Plant Physiology*, 100, 565–575.

Grossart, H. P., Tang, K. W., Kiørboe, T., Ploug, H., 2007, 'Comparison of cell-specific activity between free-living and attached bacteria using isolates and natural assemblages', *FEMS Microbiology Letters,* 266, 194–200.

Guidi, L., Chaffron, S., Bittner, L., Eveillard, D., Larhlimi, A., Roux, S., 2016, 'Plankton networks driving carbon export in the oligotrophic ocean', *Nature*, 532, 465–470.

Haake, B. and Ittekkot, V., 1990, 'Die Wind-getriebene "biologische Pumpe" und der Kohlenstoffentzug im Ozean', *Naturwissenschaften*, 77, 75-79.

Hamm, C. E., 2002, 'Interactive aggregation and sedimentation of diatoms and clay-sized lithogenic material'*, Limnology and Oceanography*, 47, 1790-1795.

Hansell, D. A, 2013, 'Recalcitrant dissolved organic carbon fractions', *Annual Review Marine Science*, 5, 421–45.

Hargrave, B. T., 1972, 'Aerobic decomposition of sediment and detritus as a function of particle surface area and organic content', *Limnology and Oceanography*, 17, 583–586.

Harpole, W. S., Ngai, J. T., Cleland, E. E., Seabloom, E. W., Borer, E. T., Bracken, M. E. S., Elser, J. J., Gruner, D. S., Hillebrand, H., Shurin, J. B., Smith, J. E., 2011, 'Nutrient co-limitation of primary producer communities', *Ecology Letters*, 14, 852–862.

Hassler, C. S., Slaveykova, V. I., Wilkinson, K. J., 2004, 'Discrimination between intra and extracellular metals using chemical extractions.' *Limnology and Oceanography*, 237-347.

Hassler, C., Cabanes, D. J. E, Blanco-Ameijeiras, S., Sanders, S. G., Benner, R., 2020, 'The role of labile and refractory ligands in the global ocean iron cycle: closing the loop', *Marine and Freshwater Research*, 71, 311-320.

Hecky, R. E., Mopper, K., Kilham, P., Degens, E. T., 1973, 'The amino acid and sugar composition of diatom cell walls', *Marine Biology*, 19, 323-331.

Henson, S. A., Sanders, R., and Madsen, E. 2012. 'Global patterns in efficiency of particulate organic carbon export and transfer to the deep ocean.' *Global Biogeochemical Cycles*. 26, GB1028.

Hinz, D. J., Nielsdottir, M. C., Korb, R. E., Whitehouse, M. J., Poulton, A. J., Moore, C. M., Achterberg, E. P., Bibby, T.S., 2012, 'Responses of microplankton community structure to iron addition in the Scotia Sea', *Deep Sea Research II*, 59–60, 36–46.

Hoffmann, L. J., Peeken, I., Lochte, K., Assmy, P., Veldhuis, M., 2006, 'Different reactions of Southern Ocean phytoplankton size classes to iron fertilization', *Limnology and Oceanography*, 51, 3, 1217-1229.

Hogle, S. L., Thrash, J. C., Dupont, C. L., Barbeau, K. A., 2016, 'Trace Metal Acquisition by Marine Heterotrophic Bacterioplankton with Contrasting Trophic Strategies', *Applied and Environmental Microbiology,* 82, 1613-1624.

Holeton, C. L., Ne´de´lec, F., Sanders, R., Brown, L., Moore, C. M., Stevens, D. P., Heywood, K. J., Stat ham, P. J., Lucas, C. H., 2005, 'Physiological state of phytoplankton communities in the southwest Atlantic sector of the Southern Ocean, as measured by fast repetition rate fluorometry', *Polar Biology*, 29, 44 – 52.

Holte, J., Talley, L. D., Gilson, J., Roemmich, D., 2017, 'An Argo mixed layer climatology and database', *Geophysical Research Letters*, 44, 5618–5626.

Hooker, S B., Rees, N. W., Aiken, J., 2000, 'An objective methodology for identifying oceanic provinces', *Progress in Oceanography*, 45, 313-318.

Hopkins, T. L., 1985, 'The zooplankton community of Croker Passage, Antarctic Peninsula', *Polar Biology*, 4, 161-170.

Hopkins, T. L., and Torres, J. J. 1989, 'Midwater food web in the vicinity of a marginal ice zone in the western Weddell Sea', *Deep Sea Research*, 36, 543560.

Hopkins, T. L., Lancraft, T. M., Torres, J. J., Donnelly, J., 1993, 'Community structure and trophic ecology of zooplankton in the Scotia Sea marginal ice zone in winter', *Deep Sea Research*, 40, 81-105.

Hopkinson, B. M. and Barbeau, K. A., 2008, 'Interactive influences of iron and light limitation on phytoplankton at subsurface chlorophyll maxima in the eastern North Pacific', *Limnology and Oceanography*, 53, 1303–1318.

Hou, L., Liang, Q., Wang, F., 2020, 'Mechanisms that control the adsorption–desorption behavior of phosphate on magnetite nanoparticles: the role of particle size and surface chemistry characteristics', *Royal Society of Chemistry,* 10, 2378-2388.

Hudson, R. J. M. and Morel, F. M. M., 1989, 'Distinguishing between extra- and intracellular iron in marine phytoplankton', *Limnology and Oceanography*, 34, 1113-1120.

Hutchings, L., van der Lingen, C., Shannon, L., Crawford, R., Verheye, H. M. S., Bartholomae, C., van der Plas, A., Louw, D., Kreiner, A., Ostrowski, M., Fidel, Q., Barlow, R., Lamont, T., Coetzee, J., Shillington, F., Veitch, J., Currie, J., Monteiro, P., 2009, 'The Benguela Current: an ecosystem of four components', *Progress in Oceanography*. 83, 1–4, 80-96.

Hutchins, D. A., 1995, 'Iron and the marine phytoplankton community', *Phycology Research*, 11, 1–49.

Hutchins, D. A. and Bruland, K. W., 1998, 'Iron-limited diatom growth and Si:N uptake ratios in a coastal upwelling regime', *Nature*, 393, 561-564.

Hutchins D. A., Witter A. E., Butler A. E., Luther G. W., 1999, 'Competition among marine phytoplankton for different chelated iron species', *Nature,* 400, 858.

IPCC, 2021: Climate Change 2021: The Physical Science Basis. Contribution of Working Group I to the Sixth Assessment Report of the Intergovernmental Panel on Climate Change [Masson-Delmotte, V., P. Zhai, A. Pirani, S.L. Connors, C. Péan, S. Berger, N. Caud, Y. Chen, L. Goldfarb, M.I. Gomis, M. Huang, K. Leitzell, E. Lonnoy, J.B.R. Matthews, T.K. Maycock, T. Waterfield, O. Yelekçi, R. Yu, and B. Zhou (eds.)]. Cambridge University Press. In Press.

Ito, T., Follows, M. J., Boyle, E. A., 2004. 'Is AOU a good measure of respiration in the oceans?', *Geophysical Research Letters,* 31, 17.

Jain, A., Meena, R. M., Naik, R. K., Gomes, J., Bandekar, M., Bhat, M., Mesquita, A., Ramaiah, N., 2015, 'Response of polar front phytoplankton and bacterial community to micronutrient amendments', *Deep Sea Research II*, 118, 197-208.

Janssen, D. J., Rickli, J., Abbott, A. N., Ellwood, M. J., Twining, B. S., Ohnemus, D. C., Nasemann, P., Gilliard, D., Jaccard, S. L., 2021, 'Release from biogenic particles, benthic fluxes, and deep water circulation control Cr and δ^{53}Cr distributions in the ocean interior', *Earth and Planetary Science Letters,* 574, 117163.

Johnson, K. S., Gordon, R. M., Coale, K. H., 1997, 'What controls dissolved iron concentrations in the world ocean?', *Marine Chemistry*, 57, 137-161.

Karl, D., Michaels, A., Bergman, B., Capone, D., Carpenter, E., Letelier, R., Lipschultz, F., Paerl, H., Sigman, D., Stal, L., 2002, 'Dinitrogen fixation in the world's oceans', *Biogeochemistry,* 57/58, 47–98.

Kagaya, S., Maeba, E., Inoue, Y., Kamichatani, W., Kajiwara, T., Yanai, H., Saito, M., Tohda, K., 2009, 'A solid phase extraction using a chelate resin immobilizing carboxymethylated pentaethylenehexamine for separation and preconcentration of trace elements in water samples', *Talanta*, 79, 146-152.

Kamatani, A., Ejiri, N., Treguer, P., 1988, 'The dissolution kinetics of diatom ooze from the Antarctic area', *Deep Sea Research I*, 35, 1195-1203.

Kazamia, E., Sutak, R., Paz-Ypres, J., Dorrell, R. G., et al., 2018, 'Endocytosis-mediated siderophore uptake as a strategy for Fe acquisition in diatoms', *Science Advances,* 4, 5.

Klaas, C. and Archer, D. E., 2002, 'Association of sinking organic matter with various types of mineral ballast in the deep sea: Implications for the rain ratio', *Global Biogeochemical Cycles*, 16, 1116.

Kirchman, D., K'nees, E., Hodson, R., 1985, 'Leucine Incorporation and Its Potential as a Measure of Protein Synthesis by Bacteria in Natural Aquatic Systems', *Applied and Environmental Microbiology*, 49, 599-607.

Kirchman, D., 2008, 'Introduction and Overview', *Microbial Ecology of the Oceans*, Second Edition 1. 1-26 (John Wiley & Sons).

Kirkwood, D. S., 1989, 'Simultaneous determination of selected nutrients in seawater', ICES CM 29, Int. Counc. for the Explor. of the Sea, Copenhagen.

Klunder, M. B., Laan, P., Middag, R., De Baar, H. J. W., van Ooijen, J. C., 2011, 'Dissolved iron in the Southern Ocean (Atlantic sector)', *Deep Sea Research II*, 58, 2678-2694.

Klunder, M. B., Laan, P., Middag, R., De Baar, H. J. W., Bakker, K., 2012, 'Dissolved iron in the Arctic Ocean: Important role of hydrothermal sources, shelf input and scavenging removal', *Journal of Geophysical Research,* 117, C4.

Kolber, Z. S., Prášil, O., Falkowski, P. G., 1998, 'Measurements of variable chlorophyll fluorescence using fast repetition rate techniques: defining methodology and experimental protocols', *Biochimica et Biophysica Acta*, 1367, 88-106.

Korb, R. E., Whitehouse, M. J., Atkinson, A., Thorpe, S., E., 2008, 'Magnitude and maintenance of the phytoplankton bloom at South Georgia: A naturally iron-replete environment', *Marine Ecology Progress Series*, 368, 75–91.

Korb, R. E., Whitehouse, M. J., Gordon, M., Ward, P., Poulton, A. J., 2010. 'Summer microplankton community structure across the Scotia Sea: implications for biological carbon export'. *Biogeosciences,* 7, 343– 356.

Korb, R. E., Whitehouse, M. J., Ward, P., Gordon, M., Venables, H. J, 2012, 'Regional and seasonal differences in microplankton biomass, productivity and structure across the Scotia Sea and implications to the export of biogenic carbon', *Deep Sea Research II*, 59–60, 67-77.

Kraemer, S.M., 2004, 'Iron Oxide Dissolution and Solubility in the Presence of Siderophores', *Aquatic Sciences*, 66, 3-18.

Krause, J. W., and Lomas, M. W., 2020, 'Understanding Diatoms' Past and Future Biogeochemical Role in High-Latitude Seas'. *Geophysical Research Letters*, 47, e2019.

Kustka, A. B., Sanudo-Wilhelmy, A., Carpenter, E. J., 2003, 'Iron requirements for dinitrogen- and ammonium-supported growth in cultures of Trichodesmium (IMS 101): Comparison with nitrogen fixation rates and iron:carbon ratios of field populations, *Limnology and Oceanography,* 48, 1869-1884.

Kwon, E. Y., Primeau, F., Sarmiento, J. L., 2009, 'The impact of remineralization depth on the air-sea carbon balance'. *Nature Geoscience,* 2, 630–635.

Lamborg, C. H., Buesseler, K. O., Lam, P. J., 2008, 'Sinking fluxes of minor and trace elements in the North Pacific Ocean measured during the VERTIGO program', *Deep Sea Research II: Topical Studies in Oceanography*, 55, 1564-1577.

Lampe, R. H., Mann, E. L., Cohen, N. R., Till, C. P., Thamatrakoln, K., Brzezinski, M. A., Bruland, K. W., Twining, B. S., Marchetti, A., 2018. 'Different iron storage strategies among bloom-forming diatoms', *Proceedings of the National Academy of Sciences,* 10-1073.

Landa, M., Blain, S., Christaki, U., Monchy, S., Obernosterer, I., 2016, 'Shifts in bacterial community composition associated with increased carbon cycling in a mosaic of phytoplankton blooms'. *ISME Journal*, 10, 39–50.

Landa, M., Blain, S., Harmand, J., Monchy, S., Rapaport, A., Obernosterer, I., 2018, 'Major changes in the composition of a Southern Ocean bacterial community in response to diatom-derived dissolved organic matter', *FEMS Microbiology Ecology*, 94, 4.

Lauro, F. M., McDougald, D, Thomas, T., Williams, T. J., Egan, S., Rice, S., Demeare, M. Z., et al., 2009, 'The genomic basis of trophic strategy in marine bacteria', *Proceedings of the National Academy of Science,* 106, 15527–33.

Laws, E. A., Falkowski, P. G., Smith, W. O., Ducklow, H., McCarthy, J. J, 2000, 'Temperature effects on export production in the open ocean', *Global Biogeochemical Cycles*, 14, 1231–1246.

Liu, Y., Debeljak, P., Rembauville, M., Blain, S., Obernosterer, I., 2019, 'Diatoms shape the biogeography of heterotrophic prokaryotes in early spring in the Southern Ocean', *Environmental Microbiology*, 24, 1452-1465.

Longhurst, A.R. and Harrison, W.G., 1989. 'The Biological Pump: Profiles of Plankton Production and Consumption in the Upper Ocean'*, Progress in Oceanography*, 22, 47-123.

Longhurst, A. R., 1991, 'Role of the marine biosphere in the global carbon-cycle', *Limnology and Oceanography*, 36, 1507 – 1526.

Loucaides, S., Van Cappelle, P., Behrends, T., 2008, 'Dissolution of biogenic silica from land to ocean: role of salinity and pH', *Limnology and Oceanography*, 53, 1614-1621.

Lønborg, C., Martínez-García, S., Teira, E., Álvarez-Salgado, X., 2011, 'Bacterial carbon demand and growth efficiency in a coastal upwelling system', *Aquatic Microbial Ecology,* 63, 183–191.

Luna, G. M., Chiggiato, J., Quero, G. M., Schroeder, K., Bongiorni, L., Kalenitchenko, D., Galand, P. E., 2016, 'Dense water plumes modulate richness and productivity of deep sea microbes', *Environmental Microbiology*, 18, 4537–4548.

Mackey, K. R., Post, A. F., McIlvin, M. R., Cutter, G. A., John, S. G., Saito, M. A., 2015, 'Divergent responses of Atlantic coastal and oceanic Synechococcus to iron limitation', *Proceedings in National Academy of Science*, 112, 9944–9949.

Maldonado, M.T., and Price, N. M., 2001, 'Reduction and transport of organically bound iron by Thalassiosira oceanica (Bacillariophyceae)', *Journal of Phycology*, 37, 298-310.

Marie, D., Partensky, F., Jacquet, S., Vaulot, D, 1997, 'Enumeration and cell cycle analysis of natural populations of marine picoplankton by flow cytometry using the nucleic acid stain SYBR Green I', *Applied and Environmental Microbiology,* 63, 168- 193.

Marsay, C. M., Sanders, R. J., Henson, S. A., Pabortsava, K., Achterberg, E. P., Lampitt, R., 2015, 'Attenuation of sinking particulate organic carbon flux through the mesopelagic ocean'. *Proceedings of the National Academy of Sciences,* 112, 1089–109.

Martin, J., Knauer, G., Karl, D., Broenkow, W., 1987, 'VERTEX: carbon cycling in the Northeast Pacific', *Deep Sea Research*, 34, 267– 285.

Martin, J. H., 1990, 'Glacial-interglacial CO2 change: the iron hypothesis.' *Paleoceanography* 5, 1–13.

Martin, P., Lampitt, R. S., Perry, M., Sanders, R., Lee, C., D'Asaroc, E., 2011, 'Export and mesopelagic particle flux during a North Atlantic spring diatom bloom', *Deep Sea Research I*, 58, 4, 338-349.

Martiny, A. C., Pham, C. T. A., Primeau, F. W., Vrugt, J. A., Moore, J. K., Levin., S. A., Lomas, M. W., 2013, 'Strong latitudinal patterns in the elemental ratios of marine plankton and organic matter', *Nature Geoscience,* 6, 279-283.

Mayor, D. J., Sanders, R., Giering, S. L. C., Anderson, T. R., 2014. 'Microbial gardening in the ocean's twilight zone'. *BioEssays*, 36, 1132–1137.

McQuaid, J. B., Kustka, A. B., Oborník, M., Horák, A., McCrow, J. P., Karas, B. J., et al., 2018, 'Carbonate-sensitive phytotransferrin controls high-affinity iron uptake in diatoms', *Nature,* 555, 534–537.

Mestre, M., Ruiz-González, C., Logares, R., Duarte, C. M., Gasol, J. M., Sala, M. M., 2018, 'Sinking particles promote vertical connectivity in the ocean microbiome'. *Proceedings of the National Academy of Sciences,* 115, E6799.

Mills, M. M., C. Ridame, M. Davey, J. La Roche, R. J. Geider. 2004. 'Iron and phosphorus co-limit nitrogen fixation in the eastern tropical North Atlantic'. *Nature,* 429: 292–294.

Mills, M. M., Moore, C. M., Langlois, R., Milne, A., Achterberg, E., Nachtigall, K., Lochte, K., Geider, R. J., La Roche, J., 2008, 'Nitrogen and phosphorus co-limitation of bacterial productivity and growth in the oligotrophic subtropical North Atlantic', *Limnology and Oceanography,* 53, 824-834.

Milne, A., Landing, W., Bizimis, M., Morton, P., 2010, 'Determination of Mn, Fe, Co, Ni, Cu, Zn, Cd and Pb in seawater using high resolution magnetic sector inductively coupled mass spectrometry (HR-ICP-MS)', *Analytica Chimica Acta*, 665, 200-207.

Mohrholz, V., Bartholomae, C. H., van der Plas, A. K., Lass, H.U., 2008, 'The seasonal variability of the northern Benguela under current and its relation to the oxygen budget on the shelf', *Continental Shelf Research*, 28, 424–441.

Moore, C. M., Lucas, M. I., Sanders, R., Davidson, R., 2005, 'Basin-scale variability of phytoplankton bio-optical characteristics in relation to bloom state and community structure in the Northeast Atlantic', *Deep Sea Research I: Oceanographic Research Papers*, 52, 401-419.

Moore, C. M., Seeyave, S., Hickman, A. E., Allen, J. T., Lucas, M. I., Planquette, H., Pollard, R. T., Poulton, A. J., 2007a, 'Iron–light interactions during the CROZet natural iron bloom and EXport experiment (CROZEX) I: Phytoplankton growth and photophysiology', *Deep Sea Research II: Topical Studies in Oceanography*, 54, 18–20, 2045-2065.

Moore, C. M., Hickman, A. E., Poulton, A. J., Seeyave, S., Lucas, M. I., 2007b, 'Iron–light interactions during the CROZet natural iron bloom and EXport experiment (CROZEX): II—Taxonomic responses and elemental stoichiometry', *Deep Sea Research II: Topical Studies in Oceanography*, 54, 18–20, 2066-2084.

Moore, C. M., Mills, M. M., Arrigo, K. R., et al, 2013, 'Processes and patterns of oceanic nutrient limitation', *Nature Geoscience,* 6, 701-710.

Morel, F. M. M., Milligan, A. J., Saito, M. A., 2003, 'Marine Bioinorganic Chemistry: The Role of Trace Metals in the Oceanic Cycles of Major Nutrients, *Treatise on Geochemistry*, 6, 113-143.

Morel, F., M., M., Kustka, A., B., Shaked, Y., 2008, 'The role of unchelated Fe in the iron nutrition of phytoplankton', *Limnology and Oceanography*, 53, 1, 400-404.

Moriceau, B., Garvey, M., Ragueneau, O., Passow U., 2007, 'Evidence for reduced biogenic silica dissolution rates in diatom aggregates', *Marine Ecology Progress Series,* 333, 129-142.

Moriceau, B., Iversen, M., H., Gallinari, M., Evertsen, A. J., Le Goff, M., Beker, B., Boutorh, J., Corvaisier, R., Coffineau, N., Donval, A., Giering, S. L. C., Koski, M., Lambert, C., Lampitt, R. S., Le Mercier, A., Masson, A., Stibor, H., Stockenreiter, M., De La Rocha, CL., 2018, 'Copepods Boost the Production but Reduce the Carbon Export Efficiency by Diatoms', *Frontiers in Marine Science,* 5, 82.

Morrissey, J., and Bowler, C., 2012, 'Iron utilization in marine cyanobacteria and eukaryotic algae', *Frontiers in Microbiology,* 3, 43.

Muggli, D. L., Lecourt, M., Harrison, P. J., 1996, 'Effects of iron and nitrogen source on the sinking rate, physiology and metal composition of an oceanic diatom from the subarctic Pacific', *Marine Ecology Progress Series*, 132, 215-227.

Myklestad, S. M., 2000, 'Dissolved organic carbon from phytoplankton'. *Marine Chemistry*, Wangersky, P.J. (ed). Berlin, Heidelberg, Springer, 111–148.

Nakano, S., 1996, 'Bacterial response to extracellular dissolved organic carbon released from healthy and senescent Fragilaria crotonensis (Bacillariophyceae) in experimental systems', *Hydrobiologia,* 339, 47–55.

Nelson, D. M., Goering, J. J., Kilham, S. S., Guillard, R. R. L., 1976, 'Kinetics and silicic acid uptake and rates of silica dissolution in marine diatom Thalassiosira pseudonana', *Journal of Phycology,* 12, 246-252.

Nelson D. M. and Tréguer, P., 1992, 'Role of silicon as a limiting nutrient to Antarctic diatoms: evidence from kinetic studies in the Ross Sea ice-edge zone', *Marine Ecology Progress Series*, 80, 255-264.

Nielsdottir, M. C., Bibby, T. S., Moore, C. M., Hinza, D. J., Sanders, R., Whitehouse, M., Korb, R., Achterberg, E. P., 2012, 'Seasonal and spatial dynamics of iron availability in the Scotia Sea', *Marine Chemistry,* 30-31, 62-72.

Nishioka J., Takeda, S., de Baar, H. J. W., Croot, P. L., Boye, M., Laan, P., Timmermans, K. R., 2005, 'Changes in the concentration of iron in different size fractions during an iron enrichment experiment in the open Southern Ocean'. *Marine Chemistry,* 95, 51.

Noble, A. E., Moran, D. M., Allen, A. E., Saito, M. A., 2013, 'Dissolved and particulate trace metal micronutrients under the McMurdo Sound seasonal sea ice: basal sea ice communities as a capacitor for iron', *Frontiers in Chemistry*, 1. 25.

Obata, H., Karatani, H., and E. Nakayama, 1993, 'Automated determination of iron in seawater by chelating resin concentration and chemiluminescence detection', *Analytical Chemistry*, 65, 1524-1528.

Obernosterer, I., Christaki, U., Lefevre, D., Catala, P., Van Wambeke, F., Lebaron, P., 2008, 'Rapid bacterial mineralization of organic carbon produced during a phytoplankton bloom induced by natural iron fertilization in the Southern Ocean', *Deep Sea Research II*, 55, 777-789.

Obernosterer, I., Fourquez, M., Blain, S., 2015, 'Fe and C co-limitation of heterotrophic bacteria in the naturally fertilized region off the Kerguelen Islands', *Biogeosciences,* 12, 1983-1992.

Ogle, S. E., Tamsitt, V., Josey, S. A., Gille, S. T., Cerovecki, I., Talley, L. D., Weller, R. A., 2018, 'Episodic Southern Ocean heat loss and its mixed layer impacts revealed by the farthest south multiyear surface flux mooring', *Geophysical Research Letters*, 45, 5002–5010.

Olson, R. J., Zettler, E. R., DuRand, M. D., 1993, 'Phytoplankton analysis using flow cytometry'. *Handbook of Methods in Aquatic Microbial Ecology*, 22, 175-186.

Orsi, A. H., Whitworth III, T., Nowlin Jr. W., D., 1995, 'On the meridional extent and fronts of the Antarctic Circumpolar Current', *Deep Sea Research I*, 42, 641–673.

Paasche, E. and Brutak, S., 1994, 'Enhanced calcification in the coccolithophorid Emiliania huxleyi (Haptophyceae) under phosphorus limitation', *Phycologia*, 33, 324-330.

Pakulski, J. D., Coffin, R. B., Kelley, C. A., Holder, S. L., Downer, R., Aas, P., Lyons, M. M., Jeffrey, W. H., 1996, 'Iron stimulation of Antarctic bacteria', *Nature*, 383, 133–134.

Passow, U., French, M. A., Robert, M., 2011, 'Biological controls on dissolution of diatom frustules during their descent to the deep ocean: Lessons learned from controlled laboratory experiments', *Deep Sea Research I,* 58, 1147-1157.

Passow, U., Engel, A., Ploug, H., 2003, 'The role of aggregation for the dissolution of diatom frustules', *FEMS Microbiology Ecology*, 46, 247-255**.**

Passow, U. and Carlson, C., 2012, 'The biological pump in a high CO_2 world', *Marine Ecology Progress Series,* 470, 249-271.

Patrick, S and Holding, A. J., 1985, 'The effect of bacteria on the solubilization of silica in diatom frustules', *Journal of Applied Bacteriology*, 59, 7-16.

Pedro´s-Alio´, C., Caldero´n-Paz, J., I., Guixa-Boixereu, N., Estrada, M., Gasol, J. M., 1999, 'Bacterioplankton and phytoplankton biomass and production during summer stratification in the northwestern Mediterranean Sea', *Deep Sea Research,* 46, 985–1019.

Peers, G. and Price, N. M., 2006, 'Copper-containing plastocyanin used for electron transport by an oceanic diatom', *Nature*, 441, 341–344.

Pham, L. D., A., Aumont, O., Ratnarajah, L., Tagliabue, A., 2021,'Examinging the interaction between free-living bacteria and iron in the global ocean', *ESSOAr,* 52.

Planquette, H., Statham, P. J., Fones, G., R., Charette, M. A., Moore, C. M., Salter, I., Ne´de´lec, F. H., Taylor, S. L., French, M., Baker, A. R., Mahowald, N., Jickells, T. D., 2007, 'Dissolved iron in the vicinity of the Crozet Islands, Southern Ocean', *Deep Sea Research II*, 18-20, 1999-2019.

Pollard, R., Tréguer, P., Read, J., 2006, 'Quantifying nutrient supply to the Southern Ocean', *Journal of Geophysical Research*, 111, C05011.

Pollard, R., Sanders, R., Lucas, M., Statham, P., 2007, 'The Crozet Natural Iron Bloom and Export Experiment (CROZEX)', *Deep Sea Research II*, 54, 1905–1914.

Pollard, R., Salter, I., Sanders, R. *et al.,* 2009, 'Southern Ocean deep-water carbon export enhanced by natural iron fertilization'. *Nature,* 457**,** 577–580.

Ragueneau, O., Schultes, S., Bidle, K., Claquin, P., Moriceau, B., 2006, 'Si and C interactions in the world ocean: importance of ecological processes and implications for the role of diatoms in the biological pump', *Global Biogeochemical Cycles,* 20, GB4S02.

Raiswell, R. and Canfield, D. E., 2012, 'The Iron Biogeochemical Cycle Past and Present', *Geochemical Perspectives*, 1, 1.

Ramaswamy, V., Nair, R. R., Manganini, S., Haake, B., Ittekkot, V., 1991, 'Lithogenic fluxes to the deep Arabian Sea measured by sediment traps', *Deep Sea Research*, 38, 169-184.

Rapp, I., Schlosser, C., Rusiecka, D., Gledhill, M., Achterberg, E. P., 2017, 'Automated preconcentration of Fe, Zn, Cu, Ni, Cd, Pb, Co, and Mn in seawater with analysis using high-resolution sector field inductively-coupled plasma mass spectrometry', *Analytica Chimica Acta*, 976, 1-13.

Ratnarajah, L., Blain, S., Boyd, P. W., Fourquez, M., Obernosterer, I., Tagliabue, A., 2021, 'Resource Colimitation Drives Competition Between Phytoplankton and Bacteria in the Southern Ocean', *Geophysical Research Letters,* 48, 1.

Redfield, A.C., 1934, 'On the Proportions of Organic Derivatives in Sea Water and Their Relation to the Composition of Plankton'. *James Johnstone Memorial Volume, University Press of Liverpool*, 176-192.

Resing, J. A., Sedwick, P. N., German, C. R., Jenkins, W. J., Moffett, J. W., Sohst, B. M., Tagliabue, A., 2015, 'Basin-scale transport of hydrothermal dissolved metals across the South Pacific Ocean', *Nature,* 523, 200-203.

Richert, I., Yager, P. L., Dinasquet, J., Logares, R., Riemann, L., Wendeberg, A., Bertilsson, S., Scofield, D. G., 2019, 'Summer comes to the Southern Ocean: how phytoplankton shape bacterioplankton communities far into the deep dark sea', *Ecosphere*, 10, e02641.

Richier, S., Achterberg, E. P., Dumousseaud, C., Poulton, A. J., Suggett, D. J., Tyrrell, T., Zubkov, M. V., Moore, C. M., 2014, 'Phytoplankton responses and associated carbon cycling during shipboard carbonate chemistry manipulation experiments conducted around Northwest European shelf seas', *Biogeosciences,* 11, 4733-4752.

Rigby, S. J., Williams, R. G., Achterberg, E. P., Tagliabue, A., 2020, 'Resource Availability and Entrainment Are Driven by Offsets Between Nutriclines and Winter Mixed-Layer Depth', *Global Geochemical Cycles,* 34, 7.

Robinson, J., Popova, E. E., Srokosz, M. A., Yool, A., 2016. 'A tale of three islands: Downstream natural iron fertilization in the Southern Ocean', *Journal of Geophysical Research: Oceans*, 121, 3350–3371.

Saito, M. A., Geopfert, T. J., Ritt, J. T., 2008, 'Some thoughts on the concept of colimitation: Three definitions and the importance of bioavailability', *Limnology and Oceanography*, 53, 276-290.

Saito, M. A., Noble, A. E., Tagliabue, A., Goepfert, T. J., Lamborg, C. H., Jenkins, W. J., 2013, 'Slow-spreading submarine ridges in the South Atlantic as a significant oceanic iron source', *National Geosciences*, 6, 775–779.

Sanders, R., Morris, P.J., Stinchcombe, M., Seeyave, S., Venables, H.J., Lucas, M.I., 2007, 'New production and the f-ratio around the Crozet Plateau in austral summer 2004–5 diagnosed from seasonal changes in inorganic nutrient levels'. *Deep Sea Research II*, 54, 2191-2207.

Sanders, R. J., Henson, S. A., Martin, A. P., Anderson, T. R., et al., 2016, 'Controls over Ocean Mesopelagic Interior Carbon Storage (COMICS): Fieldwork, Synthesis, and Modelling Efforts.' *Frontiers of Marine Science*, 3, 136.

Sarmiento, J. L., and Gruber, N., 2002, 'Anthropogenic carbon sinks', *Physics Today*, 55, 30–36.

Sarmiento, J. L., Gruber, N., Brzezinski, M., Dunne, J. P., 2004, 'High latitude controls of thermocline nutrients and low latitude biological productivity'*, Nature*, 427, 56 – 60.

Sarthou, G., Vincent, D., Christaki, U., Obernosterer, I., Timmermans, K. R., Brussaard, C. P. D., 2008, 'The fate of biogenic iron during a phytoplankton bloom induced by natural fertilisation: impact of copepod grazing', *Deep Sea Research II,* 55, 734–751.

Satinsky, B. M., Crump, B. C., Smith, C. B., Sharma, S., Zielinski, B. L., Doherty, M., et al., 2014, 'Microspatial gene expression patterns in the Amazon River plume', *Proceedings in National Academy of Science*, 111, 11085–11090.

Schlosser, C., Schmidt, K., Aquilina, A., Homoky, W. B., Castrillejo, M., Mills, R. A., Patey, M. D., Fielding, S., Atkinson, A., Achterberg, E. P., 2018, 'Mechanisms of dissolved and labile particulate iron supply to shelf waters and phytoplankton blooms off South Georgia, Southern Ocean', *Biogeosciences*, 15, 4973–4993.

Shaked, Y., Kustka, A. B., Morel, F. M. M., 2005, 'A general kinetic model for iron acquisition by eukaryotic phytoplankton', *Limnology and Oceanography*, 50, 872-882.

Shaked Y. and Lis H., 2012, 'Disassembling iron availability to phytoplankton', *Frontiers in Microbiology*, 3, 123.

Sigman, D. M. and Hain, M. P., 2012, 'The Biological Productivity of the Ocean', *Nature Education,* 3, 6.

Smetacek, V. S., 1985, 'Role of sinking in diatom life-history cycles: Ecological, evolutionary and geological significance', *Marine Biology*, 84, 239–251.

Smetacek, V., Klaas, C., Strass, V. H., Assmy, P., Montresor, M., Cisewski, B., et al., 2012, 'Deep Carbon export from a Southern Ocean Iron-Fertilized Diatom Bloom', *Nature,* 487, 313–319.

Smith, D. C., Simon, M., Alldredge, A. L., Azam, F., 1992, 'Intense hydrolytic enzyme activity on marine aggregates and implications for rapid particle dissolution', *Nature*, 359, 139–142.

Sondergaard, M. and Schierup, H., 1982, 'Release of extracellular organic carbon during a diatom bloom in Lake Mossö: molecular weight fractionation', *Freshwater Biology*, 12, 313–320.

Soria-Dengg, S., Reissbrodt, R., Horstmann, U., 2001, 'Siderophores in marine coastal waters and their relevance for iron uptake by phytoplankton: experiments with the diatom *Phaeodactylum tricornutum*', *Marine Ecology Progress Series,* 220, 73-82.

Steinberg, D. K., and Landry, M. R., 2017, 'Zooplankton and the Ocean Carbon Cycle', *Annual Review of Marine Science,* 9, 413–44.

Steinberg, D. K., Carlson, C. A., Bates, N. R., Goldthwait, S Aa., Madin, L. P., Michaels, A.F., 2000, 'Zooplankton vertical migration and the active transport of dissolved organic and inorganic carbon in the Sargasso Sea', *Deep Sea Research I,* 47, 137–158.

Strzepek, R. F., Maldonado M. T., Hunter K. A., Frew, R. D., Boyd, P. W., 2011, 'Adaptive strategies by Southern Ocean phytoplankton to lessen iron limitation: Uptake of organically complexed iron and reduced cellular iron requirements', *Limnology and Oceanography*, 56.

Strzepek, R. F., Hunter, K. A., Frew, R. D., Harrison, P. J., Boyd, P. W., 2012, 'Iron–light interactions differ in Southern Ocean phytoplankton'*, Limnology and Oceanography*, 57, 1182–1200.

Sunda, W. G., 2012, 'Feedback interactions between trace metal nutrients and phytoplankton in the ocean', *Frontiers in Microbiology,* 3, 204.

Sunda, W. G. and Huntsman, S. A., 1995, 'Iron uptake and growth limitation in oceanic and coastal phytoplankton'. *Marine Chemistry,* 50, 189-206.

Sundquist, E. T. and Visser, K., 2003, 'The Geologic History of the Carbon Cycle', *Biogeochemistry*, 8, 425-472.

Sutak, R., Camadro, J., Lesuisse, E., 2020, 'Iron Uptake Mechanisms in Marine Phytoplankton', *Frontiers in Microbiology,* 11, 2831.

Tagliabue, A., Sallée, J. B., Bowie, A. R., Lévy, M., Swart, S., Boyd, P. W, 2014, 'Surface-water iron supplies in the Southern Ocean sustained by deep winter mixing', *Nature Geoscience*, 7, 314–320.

Tagliabue, A., Aumont, O., DeAth, R., Dunne, J. P., Dutkiewicz, S., Galbraith, et al., 2016, 'How well do global ocean biogeochemistry models simulate dissolved iron distributions?' *Global Biogeochemical Cycles*, 30(2), 149-174.

Tagliabue, A., Bowie, A. R., Boyd, P. W., Buck, K. N., Johnson, K. S., Saito, M. A., 2017, 'The integral role of iron in ocean biogeochemistry', *Nature Review*, 543, 51-59.

Tagliabue, A., Bowie, A. R., DeVries, T., Ellwood, M.J., Landing, W. M., Milne, A., Ohnemus, D. C., Twining, B. S., Boyd, P. W., 2019, 'The interplay between regeneration and scavenging fluxes drives ocean iron cycling', *Nature Communications,* 10, 4960.

Tang, D. & Morel, F. M. M., 2006, 'Distinguishing between cellular and Fe-oxide associated trace elements in phytoplankton'. *Marine Chemistry,* 98, 18-30.

Taylor, S. R., 1964, 'Abundance of chemical elements in the continental crust: a new table' *Geochimica Et Cosmochimica Acta*, 28, 1273-1285.

Thomalla, S. J., Waldron, H., N., Lucas, M. I., Read, J. F., Ansorge, I. J., Pakhomov, E., 2011, 'Phytoplankton distribution and nitrogen dynamics in the southwest indian subtropical gyre and Southern Ocean waters', *Ocean Science,* 7, 113-127.

Tortell, P. D., Maldonado, M. T., Granger, J., Price, N. M., 1999, 'Marine bacteria and biogeochemical cycling of iron in the oceans', *FEMS Microbiology and Ecology*, 29, 1–11.

Tovar-Sanchez, A., Sanudo-Wilhelmy, S. A., Garcia-Vargas, M., Weaver, R. S., Popels, L. C., Hutchins, D. A., 2003, 'A trace metal celan reagent to remove surface-bound iron from marine phytoplankton.' *Marine Chemistry,* 82, 91-99.

Tréguer, P. and van Bennekom, A. J., 1991, 'The annual production of biogenic silica in the Antarctic Ocean', *Marine Chemistry*, 35, 477-488.

Trowbridge, J., Weller, R., Kelley, D., Dever, E., Plueddemann, A., Barth, J. A., Kawka, O., 2019, 'The Ocean Observatories Initiative', *Frontiers in Marine Science,* 6, 74.

Twining, B. S. and Baines, S. B., 2013, 'The Trace Metal Composition of Marine Phytoplankton', *Annual Reviews Marine Science,* 5, 191–215.

Twining, B. S., Nodder, S. D., King, A. L., Hutchins, D. A., LeCleir, G. R., DeBruyn, J. M., Maas, E. W., Vogt, S., Wilhelm, S. W., Boyd, P. W., 2014, 'Differential remineralization of major and trace elements in sinking diatom', *Limnology and Oceanography*, 59, 689–704.

Twining, B. S., Rauschenberg, S., Morton, P. L., Vogt, S., 2015, 'Metal contents of phytoplankton and labile particulate material in the North Atlantic Ocean,' *Progress in Oceanography,* 137, 261-283.

Volk, T., and Hoffert, M. I., 1985, 'Ocean carbon pumps: analysis of relative strengths and efficiencies in ocean-driven atmospheric CO_2 changes'. *The Carbon Cycle and Atmospheric CO_2: Natural variations Archaean to Present, Geophysical Monographs*, 32, 99–110.

Waide, R. B., Willig, M. R., Steiner, C. F., Mittelbach, G., Gough, L., Dodson, S., I., Juday, G. P., Parmenter, R., 1999, 'The relationship between productivity and species richness', *Annual Reviews of Ecology and Systematics*, 30, 257–300.

Weber, T. and Deutsch, C., 2014, 'Local versus basin-scale limitation of marine nitrogen fixation', *Proceedings of the National Academy of Science*, 111, 8741–8746.

Weber, T., Cram, J. A., Leung, S. W., DeVries, T., Deutsch, C., 2016, 'Deep ocean nutrients imply large latitudinal variation in particle transfer efficiency', *Proceedings of the National Academy of Science*, 113, 8606-8611.

Weber, T., Tagliabue, A., DeVries, T., 2018, 'Biological uptake and reversible scavenging of zinc in the global ocean', *Science*, 361, 72 - 76.

Welschmeyer, N., A., 1994, 'Fluorometric analysis of chlorophyll a in the presence of chlorophyll b and phaeopigments', *Limnology and Oceanography*, 39, 1985-1992.

Wells, M. L., and Mayer, L. M., 1991, 'Variations in the chemical lability of iron in estuarine, coastal and shelf waters and its implications for phytoplankton', *Marine Chemistry*, 32, 195 – 210.

Wenley, J., Currie, K., Lockwood, S., Thomson, B., Baltar, F., Morales, S. E., 2021, 'Seasonal Prokaryotic Community Linkages Between Surface and Deep Ocean Water', *Frontiers in Marine Science*, 8, 777.

Wilson, S., Ruhl, H., Smith, K., 2013, 'Zooplankton fecal pellet flux in the abyssal northeast Pacific? A 15 year time-series study', Limnology and Oceanography, 58, 881–892.

Zehr, J. P. and Ward, B. B., 2002, 'Nitrogen cycling in the ocean: New perspectives on processes and paradigms', Applied Environmental Microbiology, 68, 1015-1024.

Zubkov, M. V., Fuchs, B. M., Burkill, P. H., Amann, R., 2001, 'Comparison of cellular and biomass specific activities of dominant bacterioplankton groups in stratified waters of the Celtic Sea', *Applied and Environmental Microbiology*, 67, 5210-5218.